The Cenozoic Magmatism of East Africa: Part III – Rifting of the Craton

Tyrone O. Rooney

Dept. of Earth and Environmental Sciences, Michigan State University, East Lansing, MI 48823, USA

Abstract

Magmatic activity in the Tanzania Craton-influenced regions of the East African Rift System (EARS) exhibits clear evidence of derivation from a variety of metasomatic sources. These metasomatic sources, which may span a range of ages, have likely been preserved within the lithospheric mantle. The influence of these metasomes on the composition of the rift magmas represents the single greatest heterogeneity in the composition of erupted lavas within the EARS. The earliest widespread magmatic event in the craton-influenced regions of the EARS south of Lake Turkana is the Samburu Phase (ca. 20-17 Ma), which manifests as alkaline volcanics derived from the lithospheric mantle. This phase represents the initial destabilization of the continental lithosphere as a precursor of rift development. The Flood Phonolite Phase (ca. 16 – 12 Ma) was most pronounced in regions south of those impacted by the prior Samburu Phase, and likely represent the continued southward expansion of lithospheric destabilization. The Mid-Miocene Resurgence Phase (ca. 12 – 9 Ma) is poorly represented in the Southern Kenya Rift, though magmatic activity is recorded in the western branch of the EARS at Kivu during this time. In contrast, the Early Rift Development Phase (ca. 9 – 4 Ma) is particularly well-represented in the Kenya Rift. Large-scale magmatic events include: commencement of activity in the Northern Tanzania Divergence (NTD) and Mt. Kenya, Rungwe Volcanic Province, and the

Southern Kenya Rift. The Stratoid Phase (ca. 4 Ma – 0.5 Ma) commences with significant magmatic events at ca. 3 to 2.5 Ma within the Southern Kenya Rift and NTD. This phase manifests as basalts and trachytes that flood the newly formed graben in the Southern Kenya Rift. This phase also correlates with the main phase of magmatism in the NTD, the commencement of volcanism at Virunga, and the intermediate shield phase in the Rungwe Volcanic Province. The Axial Phase (0.5 Ma to present) is defined by narrow axial grabens in the Kenya Rift with central volcanoes and interposing basaltic cinder cones. In the less mature regions of the EARS, alkaline volcanoes dominate. Three distinct pulses of magmatism and extension initiated in Turkana commencing at ca. 23 Ma, 12 Ma, and 4 Ma; the consistent temporal lag in magmatic activity in the Southern EARS following each pulse reveals the southward expansion of these extensional events. Lavas at any given location within the rift exhibit a consistent temporal sequence characterized by a shift from Type II lavas (lithospheric mantle derived) to Type IV lavas (hybrid lithospheric mantle – sub-lithosphere derived) to Type III lavas (sub-lithosphere derived), requiring a progressive change in the reservoirs contributing to rift magmatism from lithospheric to sub-lithospheric. When examined in aggregate these data paint a picture of progressive rift development and attendant lithospheric thinning, mediated by pulses of extension originating in Turkana.

Keywords: Rift, magmatism, East Africa, Kenya, Tanzania, Craton, Ethiopia, East African Rift System

1. Introduction

Magmatism in the Southern Kenya Rift and western branch of the East African Rift System (EARS) is fundamentally controlled by the presence of the Tanzania craton (Fig. 1). The most significant heterogeneity in the observed composition of rift volcanics relates to whether a lava erupted within the shadow of the craton or within the mobile belt (Hyndman et al., 2005; Rogers, 2006; Foley, 2008). The primary observation from lavas erupted along the entire Kenya Rift is

that that there is a latitudinal variability such that lavas erupted in the Southern Kenya Rift typically exhibit enrichment in more incompatible elements and are isotopically distinct in comparison to lavas erupted in the northern Kenya Rift. Lavas erupting within the Tanzania craton-influenced regions of the EARS exhibit clear evidence of derivation from a variety of metasomatic sources that have likely been preserved within the lithospheric mantle of the craton. The formation of such metasomes results from the interaction between sub-lithospheric derived melts that percolate through the solid lithospheric mantle and react through chromatographic processes to form diverse compositional domains within the thick cratonic lithospheric mantle (e.g., Pilet et al., 2011). The antiquity of the craton equally plays a role – significant fractionation of parent and daughter isotopes facilitated by chromatographic processes can, over time, yield extreme ratios in commonly used radiogenic isotope tracers. Magmas that are derived either through direct melts of such metasomes or from sub-lithospheric magmas that interact with them enroute to the surface, will inherit the unusual geochemical characteristics preserved within the metasomes.

It is thus apparent that the common conception of the continental lithospheric mantle as a barren depleted residue with limited compositional diversity is inadequate. Rift lavas are messengers from the complex continental lithospheric mantle that is present within the craton, and allow us to probe a currently overlooked geochemical reservoir in its own right – one with the potential for long-term storage of important geochemical species (e.g., CO_2: Brune et al., 2017). Destabilization of the Tanzania craton during the evolution of rifting in East Africa has resulted in lava compositions in the regions surrounding the Tanzania craton that are among the most diverse in existence, and provide insight into the myriad magmatic processes that may result in melt generation in continental rift environments.

In the previous contribution (Part II)(Rooney, 2020a) I showed that three distinct pulses of magmatism and extension initiated in the Turkana Depression commencing at ca. 23 Ma, 12

Ma, and 4 Ma, consistent with other regional synthesis studies (Macgregor, 2015; Purcell, 2018). In this contribution I show that the consistent temporal lag in magmatic activity in the southern EARS following each pulse reveals the southward expansion of these extensional events. Lavas within the rift exhibit a consistent temporal sequence characterized by a shift from Type II lava (lithospheric mantle derived), to a newly defined Type IV lava (a hybrid type that is defined by mixing of melts derived from the lithospheric mantle and sub-lithospheric domains), to Type III lava (sub-lithosphere derived), requiring a progressive change in the reservoirs contributing to rift magmatism from lithospheric to sub-lithospheric over time (Table 1). When examined in aggregate, these data paint a picture of progressive rift development and attendant lithospheric thinning, mediated by pulses of extension originating in Turkana and expanding outward to other parts of the southern East African Rift System.

2. Background and Regional Context

2.1 Evidence on craton extent derived from Xenoliths

Within studies of the East African Rift, the influence of the Tanzania craton on both the magmatic products and rift development has long been acknowledged (e.g., McConnell, 1967; Harris, 1969). However, the boundary of the craton remains somewhat ambiguous, and is dependent on the definition used to define the limits of the craton (Fig. 1). Xenoliths have provided an unusually direct method by which the community has been able to constrain the composition of the lithospheric mantle associated with the Tanzania craton, and recognize that it is distinct from xenolith suites recovered further north. Lee and Rudnick (1999) established a compositionally stratified cratonic lithosphere from a xenolith suite in the Northern Tanzania Divergence, while Chesley et al. (1999) demonstrated Archean Re-depletion ages for these same samples. These studies and those from Rudnick et al. (1998), Aulbach et al. (2008) and others have equally demonstrated that this stratified Archean mantle is currently in the process

of being overprinted metasomatically by modern rift lavas. Metasomes manifest as veins of phlogopite, amphibole, pyroxenes, and carbonate (Lee et al., 2000; Mattsson et al., 2013). The most pronounced expression of metasomatic xenoliths come from the current northern limit of the western branch of the EARS (Katwe-Kikirongo and Bunyaruguru), where mica-rich compositions are common and olivine-rich compositions are much rarer (Lloyd et al., 1991). These xenolith studies provide compelling evidence of a layered lithospheric mantle with metasomatic overprint yielding easily fusible lithologies.

2.2 Evidence on Craton Extent derived from Lavas

While xenolith studies are a useful probe of the Tanzanian craton's lithospheric mantle, these suites are only available in a select number of locales. Thus, lavas erupted within the rift provide better spatial constraints as to the influence of the Tanzania craton and its boundaries. Purcell (2018) present the current surface distribution of crustal rocks attributed to the Tanzania Craton, but there is complex crustal geometry associated with the orogenic belts surrounding the craton. Thus, rocks that appear at the surface may not be reflective of whether the entire lithospheric column at that location has mobile belt or craton characteristics. Foley et al. (2012) convincingly demonstrate that the surface-defined boundary of the Tanzania craton is inadequate, and instead presents a revised estimate of the limits within which lavas may influenced by the craton (despite seemingly being erupted onto crust mapped as part of the mobile belt). These studies have also produced clear spatial patterns wherein lavas become more alkalic with proximity to the craton (basalt -> nephelinite/ melilitite -> alkali picrite -> kimberlite) (Foley et al., 2012). In short, existing work has demonstrated that easily-fusible metasomatic lithologies (identified in xenolith suites) form an important source reservoir to lavas in rift sectors impacted by the Tanzania craton (Foley et al., 2012).

2.3 Evidence on Craton Extent derived from Geophysics

The extent of the Tanzania craton and behavior of the upper mantle beneath the craton is further constrained with evidence derived from seismic exploration of the rift. Teleseismic tomographic studies show a lithospheric keel beneath the Tanzania craton of at least 200 km (though possibly as deep as 350 km), consistent with other Archean cratons (Ritsema et al., 1998). However, the Tanzania craton exhibits much lower seismic wavespeeds beginning at ~130 km depth, which have been attributed to both thermal erosion of the lithosphere relating to the presence of hot mantle beneath the craton, and melt infiltration into the cratonic root (Weeraratne et al., 2003; Adams et al., 2012, 2018; Wölbern et al., 2012; O'Donnell et al., 2013). In regions more directly impacted by rift development, however, the thickness of the lithosphere is significantly perturbed by thermal (and possibly mechanical) erosion to ~60 km (Tiberi et al., 2018). These seismic data thus support the geochemical observations of melt infiltration and thermal destabilization of the continental lithospheric mantle.

2.4 Upper Mantle Conditions and Melt Generation

Beneath the Tanzania craton, anomalous mantle conditions such as elevated mantle temperature have been detected (e.g., Grijalva et al., 2018). These observations are likely related to plume material rising around the craton root (Nyblade et al., 2000; Park and Nyblade, 2006). These data are consistent with geochemical evidence of elevated mantle potential temperatures in lavas erupted around the Tanzania craton (Rooney et al., 2012b). Anomalous upper mantle conditions caused by deep mantle upwelling are supported by evidence of a perturbation of the mantle transition zone in the region (Owens et al., 2000; Huerta et al., 2009) – suggestive of a thermal anomaly rising from the African Low Large Shear Velocity Province (LLSVP) (Mulibo and Nyblade, 2013). A deep mantle origin for this material is consistent with evidence of elevated $^{3}He/^{4}He$ in some lavas in the region (Hilton et al., 2011; Halldórsson et al., 2014).

Lavas erupted to the surface within the East African Rift thus represent complex mixtures of lithospheric and sub-lithospheric reservoirs, some of which may be derived from the deep mantle. The potential mechanisms by which these different reservoirs contribute to erupted lavas are equally complex. The is wide diversity in lithologies present within the lithospheric mantle (e.g. carbonated veins, mica or amphibole rich lithologies, pyroxenites - Lloyd et al., 1991; Lee et al., 2000; Chakrabarti et al., 2009b; Mattsson et al., 2013), and within the upwelling plume (pyroxenites of various types – e.g. Herzberg, 2011), which likely results in differential melting on the basis fusibility (e.g., Stracke and Bourdon, 2009). Furthermore, the potential detachment and mixing of lithospheric lithologies into the upper mantle may equally impact both the melt composition and melting mechanism (e.g., Rogers et al., 2006; Furman et al., 2014). It is therefore apparent that while there is clear influence from these various reservoirs on rift lavas, establishing the precise mechanisms by which these reservoirs may have contributed can be challenging.

2.5 Combined Magmatic and Structural Context for the EARS

In the previous contribution to this series (Part II)(Rooney, 2020a), I described how existing regional studies (Macgregor, 2015; Purcell, 2018) provided constraints as to the development of the Turkana Depression and the recognition of distinct phases of tectonic activity at: 22 – 17 Ma, 13 – 10 Ma, and 5 – 3 Ma, which correlated with the recognized magmatic pulses in Turkana at ca. 20-23 Ma, 12 Ma, and 4 Ma. I argue these pulses have profound importance for the development of the EARS in southern Kenya, as both McGregor and Purcell describe Turkana as a nexus of extension, from which rifting has propagated to the north and south during multiple periods in the past 20 Ma. Within this contribution I show that following each of these defined pulses, a significant period of magmatism follows in the Southern Kenya Rift: the 16 – 12 Ma Flood Phonolites; the 9 to 4 Ma Early Rift Development Phase, typified by large volumes of basalts and more evolved magmatic products; the 4 – 0.5 Ma Stratoid Phase, during

which activity commenced at ca. 3 – 2.5 Ma in the Southern Kenya Rift, later than in Turkana (Table 2).

These three temporally offset magmatic events broadly correlate with evidence of extension in the Southern Kenya Rift: (1) At ca. 22 – 17 Ma, Purcell (2018) describes half graben formation in the Baringo region (bounding the northern and Southern Kenya Rift), consistent with the formation of distinct sedimentary deposits in this area during this period (Morley et al., 1999). Further south, however, there is no evidence for any topographic expression of rifting; the Flood Phonolites appear to have been emplaced as a sheet rather than into a developing basin (Wichura et al., 2011; Macgregor, 2015; Purcell, 2018). Thus, while large scale magmatism has clearly occurred during this period, we lack any clear surface expression of rifting (Le Gall et al., 2008). (2) During the Early Rift Development Phase (9 to 4 Ma), there is a significant advance in the surface expression of the rift as far south as the border with Tanzania (Le Gall et al., 2008; Purcell, 2018). Full graben morphology had developed ca. 4 Ma within the central part of the Kenya Rift (Baker, 1987). (3) From 5 Ma to present, faulting impacted the NTD, which developed a series of dispersed grabens (Le Gall et al., 2008), while the border between the Southern Kenya rift and NTD experienced reactivation of preexisting transverse structures (Muirhead and Kattenhorn, 2018). Collectively, these observations define a coherent narrative of pulses of extension and associated magmatism initiating in Turkana and migrating outward in three distinct phases during the evolution of the EARS in this region.

The western branch of the EARS is defined by asymmetric en-echelon basins bounded on one side by border faults and on the opposing side (commonly) by a monocline or ramp (Ebinger, 1989b). South and southwest of the Tanzania craton, these basins may reactivate earlier Karoo extensional faults (Nyblade and Brazier, 2002). Thus, the development of the rift basins within the western branch of the EARS should be considered in the context of the preexisting rift architecture – e.g., in the Rungwe Volcanic Province, rifting during the Mesozoic

has impacted modern rift development (Purcell, 2018). The early manifestation of volcanism in the Rungwe Volcanic Province (26 Ma: Roberts et al., 2012) may therefore indicate some degree of lithospheric perturbation at this time. However, this activity is limited to that basin. A more widespread phase of activity within the Rungwe Volcanic Province at ca. 17 Ma (Mesko et al., 2014) and Kivu ca. 20 Ma (Pouclet et al., 2016) is coincident with the pulse of extension migrating southward from the Turkana Depression. However the development of new rift basins in the western branch is not thought have occurred until after ca. 12 Ma (Ebinger, 1989b; Cohen et al., 1993; Macgregor, 2015; Purcell, 2018). in the Rungwe Volcanic Province, this phase of rifting begins ca. 8.6 Ma (Ebinger et al., 1993b), while the border fault is thought to have formed in Kivu by ca. 10 Ma (Ebinger, 1989a). The formation of the Lake Tanganyika rift is also estimated to be 9 – 12 Ma (Cohen et al., 1993). While the surface expression of rifting within the western branch does not occur until after 12 Ma, the occurrence of magmatism contemporaneous with the earlier phase of extension defined in the eastern branch (ca. 22 – 17 Ma), is suggestive of an initial stage of lithospheric instability predating surface deformation. The subsequent development of magmatic provinces in the western branch is strongly linked with the rifting process, as most of the volcanically active regions occur at highly faulted accommodation zones between that separate individual rift basins (Ebinger, 1989b).

3. South and South-Central Kenya Rift

This section provides a systematic overview of events within the South and South-Central Kenya Rift. These regions, which are in proximity to the craton, exhibit differences in the composition and timing of magmatic events in comparison to magmatism further north (see Part II) (Rooney, 2020a). Importantly, while the boundary of the Tanzania craton remains ambiguous (see discussion in section 2), the lithosphere traversed by the rift in this region (Mesoproterozoic and older) is temporally distinct from that further north (Neoproterozoic) (Fig. 1). A summary of

the six different magmatic phases, their distribution, and the characteristics of constituent lavas is presented in Table 2. Information on the sources of geochemical data and the grouping of these data is presented in the Background Datasets.

3.1 The Samburu Phase (20-16 Ma) – Basaltic Shield and Alkaline Volcanism

3.1.1 Distribution of magmatism

The Samburu Phase most obviously manifests as a period of significant basaltic volcanism. Indeed, throughout the rift that traverses mobile belt lithosphere, this phase is synonymous with low basaltic shields and fissural flows (Fig. 2) (See Part II) (Rooney, 2020a). However, in magmatic regions that developed upon cratonic lithosphere, there is a significant dichotomy in the composition of the magmatic products. Highly alkaline, silica under-saturated volcanism becomes the norm for products erupted on cratonic lithosphere during the Samburu Phase (e.g., Baker, 1987; Simonetti and Bell, 1995). While the Samburu Phase represents the first instance of this lithosphere-based compositional dichotomy in erupted magmatic products, such divisions persist throughout the Cenozoic development of the rift. It is difficult to assess the mass contribution from the convecting mantle and lithospheric mantle to the generation of such magmas, but one observation is secure – to produce these alkaline magmas, phases such as amphibole and phlogopite must contribute to melt generation. The origin and age of domains containing such phases remains a subject of active discussion (Rosenthal et al., 2009; Castillo et al., 2014; Hudgins et al., 2015; Rooney et al., 2017; Nelson et al., 2019).

The Samburu phase is linked with the Early Miocene Resurgence (ca. 23 Ma), which is a notable period of magmatic activity throughout the northern portion of the East African Rift system (e.g., Rooney, 2017). Indeed, the Samburu Phase represents a continuation of the Early Miocene Resurgence event and is described in more detail in Part II (Rooney, 2020a). During the Samburu phase, existing rift basins in Turkana deepened, and rifting expanded away from Turkana, both to the north and south (Macgregor, 2015; Purcell, 2018). Notably, the Kenya Rift

expanded southward to the Baringo area, manifesting as half grabens (Purcell, 2018). The surface distribution of the Samburu Phase basalts generally coincides with the rift development within lithosphere of the Mobile Belt. The existence of contemporaneous alkaline volcanism in the Nyanza Rift, and in Eastern Uganda suggests that this phase also records the early interaction between the developing rift and the Tanzania craton. The first manifestation of volcanism in the Kivu region (western branch), which occurs during this phase of activity (Pouclet et al., 2016), may suggest that this extensional event is widespread south of Turkana. It is thus apparent that the Samburu Phase of magmatic activity is intimately linked with the expansion of rifting and extension away from the Turkana region into mid to Southern Kenya, and the early stages of cratonic destabilization, despite the lack of any obvious surface expression of extension in the more distal regions.

Within the south central Kenya Rift, the Samburu Basalt occurs in the very north around Lake Bogoria (Hackman, 1988), however, the supposed southern continuation of this unit as the ‘Simbara Basalts’ (Smith, 1994) is unclear. Baker et al. (1971) report an age of 5.5 Ma (± 1), however Smith (1994) point out that the region from which this sample was taken corresponds to the Sirrma basalts and assigns the Simbara basalts to an older phase. Further work is needed in order to constrain the volcanic stratigraphy in this region but for now I classify the Simbara basalts as part of the earlier basaltic shield phase.

Within the Nyanza (formerly Kavirondo) rift and in Eastern Uganda, activity during this phase consisted of nephelinite, melilitite, and carbonatite, largely associated with Kisingiri volcano (and surrounding carbonatite vents), Tinderet volcano (Van Couvering and Miller, 1969; Bishop et al., 1969; Le Bas and Rubie, 1977; Deans and Roberts, 1984; Bestland et al., 1995) Mt. Elgon (King et al., 1972; Simonetti and Bell, 1995), Napak (King et al., 1972; Simonetti and Bell, 1993), Moroto (King et al., 1972), and other smaller centers. These volcanic centers form a roughly north-south alignment, with Tinderet displaced to the east. The erupted rock types,

which are almost universally highly alkaline and silica-under saturated, are a remarkably similar assemblage to modern volcanism in the NTD. For example, one of the most unusual lava types found in the modern NTD is natrocarbonatite; remnants of this rare lava type are also found in the Nyanza rift (Deans and Roberts, 1984). This volcanic region is built upon the Tanzania craton (Foley et al., 2012), and thus the observation of a similar sequence of rocks within the initial stages of magmatism from two rifts that ingress upon the Tanzanian craton may reveal a commonality in processes.

The time period over which Kisingiri was active has remained unclear. Le Bas and Rubie (1977) suggested an extended ~10 Ma period of magmatism from ca. 20 to 10 Ma, however Drake et al. (1988) suggested a restricted period of activity of a few hundred thousand years at 17.8 Ma. More recent work suggests that the earliest activity may be at ca. 20 Ma and last until 17 Ma (Geraads et al., 2016) but the detailed geochronologic data has yet to be published. The interested reader is referred to the very detailed description of magmatic activity of Kisingiri described in Le Bas and Rubie (1977). Magmatic activity at Tinderet occurs over a wide time period that extends into the Pliocene, but the carbonatite occurrences noted above are found associated with the Koru Beds that are dated at ~19.55 Ma ± 0.3 (Bishop et al., 1969).

In Eastern Uganda, magmatic activity is centered on Mt. Elgon, Napak, and Moroto. These volcanoes have been significantly eroded, with original basal diameters ranging from 35 km for Moroto to 100 km for Mt. Elgon (King et al., 1972). The edifices are constructed dominantly of nephelinite and melilite pyroclastics, though lavas dominate Moroto (King et al., 1972). These volcanoes have been re-dated using high-precision $^{40}Ar/^{39}Ar$ techniques because of the importance of the volcanic deposits to paleo-anthropology studies. Mt. Elgon, has been dated on the basis of a nephelinite flow over basement near the Bukwa fossil site at 19.0 Ma (± 1.0 $^{40}Ar/^{39}Ar$) (Cote et al., 2018). Lavas over the fossil site yield a similar age. Moroto has been dated on the basis of a lava flow overlying a fossiliferous horizon that lies on basement at 20.61 Ma (± 0.05 $^{40}Ar/^{39}Ar$) (Gebo et al., 1997). The volcanics at Napak have been dated at ca. 20 Ma

using $^{40}Ar/^{39}Ar$ techniques, however this data is from a 2006 abstract (Maclatchy et al., 2006), though it is referenced to in Cote et al., (2018) as the most reliable age for Napak. (Note, that as in prior parts of the synthesis series, radiogenic dates that are based on the $^{40}Ar/^{39}Ar$ technique are explicitly notated, where no such notation is evident the date is from K-Ar techniques. The errors provided are those of the original publication).

3.1.2 Geochemical Composition of the Samburu Phase Lavas

The majority of basaltic lavas erupted during the Samburu phase are in the north, and north central Kenya Rift. Limited instances of basaltic volcanism are evident in the south-central Kenya rift, and typically alkaline silicate rocks (and carbonatites) occur throughout Uganda, away from the axis of the modern rift. The limited analyses of the Samburu Phase basalts in this region exhibit somewhat enriched values of Zr and Nb in comparison to more recent Stratoid and Axial Phase basalts within the rift (Fig. 3). There is a similarity in terms of REE and other incompatible trace element variation between the Samburu phase and the subsequent Flood Phonolite phase (Fig. 4; 5). Samburu Phase lavas generally exhibit a weak Type II lava pattern with a pronounced negative Zr-Hf anomaly (see fuller discussion on this fingerprint in discussion of the Rungwe Volcanic Province in the western branch), suggesting a derivation from a lithospheric metasome (Fig. 5).

The Samburu Phase edifices of Elgon and Napak (Uganda) have undergone some major element and isotopic analyses (though trace elements are typically lacking). In comparison to the modern activity in the Toro Ankole region of Uganda (at the northern tip of the western branch of the EARS – see discussion later), these lavas follow evolution pathways that exhibit significantly less enriched values of incompatible trace elements (Fig. 6). There are no clear variations between MgO and $^{87}Sr/^{86}Sr$ or $^{143}Nd/^{144}Nd$ isotopes. However, both Elgon and Napak extend over a wide range of $^{87}Sr/^{86}Sr$ - $^{143}Nd/^{144}Nd$ isotopic compositions (Fig. 6). Pb

isotope ratios for these units extend to much more radiogenic values than that found in the Toro Ankole Volcanic Province, but also exhibit a significant range in values. It should be noted that melt/mineral isotopic disequilibrium has been observed in these systems that has been interpreted as melts undergoing isotopic change during melt evolution (Simonetti and Bell, 1993), consistent with open system behavior (Simonetti and Bell, 1994).

Carbonatite volcanoes lack sufficient trace element data to yield a primitive mantle normalized pattern. However, isotopic data is available. Carbonatite lavas in eastern Uganda collectively plot over a large range of compositions in $^{143}Nd/^{144}Nd$ vs $^{87}Sr/^{86}Sr$ (Fig. 7). In terms of Pb isotopes, the Eastern Ugandan carbonatites are consistently among the most radiogenic in both $^{206}Pb/^{204}Pb$ and $^{208}Pb/^{204}Pb$ (Fig. 7). Simonetti & Bell (1994) suggest models to explain these data by either a HIMU-like melt interacting with lower crustal granulites, or mixing between melts derived from “isotopically heterogeneous mantle” that are then mixed at shallower levels in the crust (Simonetti and Bell, 1995). I should note that in the isotopic figures presented throughout this contribution, I utilize a common set of geochemical endmembers to facilitate ease of comparison among figures. These endmembers or reservoirs may not impact all lavas within the rift, and indeed the Pan-African Lithosphere component (PA) is not directly relevant to lavas influenced by the Tanzania craton. Where appropriate, I have added endmembers that have been identified by others in some figures. I further note that the endmembers are currently marked as a single point but in reality, the endmembers occupy a space within these figures.

For the Nyanza Rift, most of the eruptive material during this period was carbonatite. As with eastern Uganda, there is a lack of trace element data available, but there is a significant volume of isotopic information. These data (grouped as Homa Bay but cover the Nyanza Rift) cover an array of compositions that extend to much less radiogenic values of Pb isotopes in comparison to the equivalent materials erupted in Eastern Uganda (Fig. 7). The isotopic

compositions overlap with that from Oldoinyo Lengai and lie along the East Africa Carbonatite Line (Bell and Blenkinsop, 1987), discussed in part V of the synthesis series (Rooney, 2020c).

Considering the trace element evidence that Samburu Phase lavas exhibit a signature consistent with an origin from a metasome in the lithospheric mantle, and the particularly radiogenic Pb data that is consistent with a lithospheric origin (e.g., Rooney et al., 2014), in aggregate, these data suggest that the Samburu phase lavas in the study region result from destabilization of the continental lithospheric mantle. It is proposed that small volume melts of mantle metasomes result in the highly alkaline lavas typical during this phase.

3.2 Flood Phonolite Phase (16 to 12 Ma)

3.2.1 Distribution and chronology of Flood Phonolite Lavas

The Flood Phonolite phase in Kenya results in the widespread eruption of a diverse array of phonolite magmas throughout the region, with a temporal focus ca. 13 to 11 Ma (Smith, 1994). These flood phonolites formed vast platforms that extended over much of the Southern Kenya Rift (Fig. 2), and were eventually dissected by subsequent rifting (Purcell, 2018). It is important to consider the spatial and temporal context of this event; it follows the Samburu phase, which dominantly impacted the regions directly south of the Turkana Depression (Table 2). The Flood Phonolite phase, in contrast, dominantly impacts the Southern Kenya Rift and is considered related to the southward expansion of rifting, but predates the surface expression of rifting (Macgregor, 2015; Purcell, 2018). Unlike prior studies that have linked the Flood Phonolites with the 13 – 10 Ma rifting event centered on Lake Turkana, I argue that the origin of the Flood Phonolite phase is linked in space and time with the preceding Samburu Phase: it is the southward manifestation of a pulse of extension that commenced in Turkana ca. 23 Ma. Support for this revised model comes from the newer high precision dating that show the flood phonolites (>13.7 Ma)(Truckle, 1977) predate the basaltic pulse in Turkana (which tend to date <13 Ma, though higher precision dating is needed) – See discussion in Part II (Rooney, 2020a).

While it is possible that there is a synchronous pulse throughout the rift at ca. 13 Ma, no magmatic activity is recorded in the north central Kenya Rift at this time. Thus, while future revision is possible with new dating, the extant evidence point towards a pulsing of extension and associated magmatism. In this region, the Flood Phonolite phase is followed by a pronounced hiatus in magmatism, during which a new phase of extension and associated magmatism had begun in Turkana.

During the Flood Phonolite phase magmatic activity within the Nyanza rift paralleled that within the adjacent Kenya rift with dominantly phonolite eruptions (Timboroa formation and Kericho phonolites) that appear to have migrated eastward over time (Jones and Lippard, 1979). Jones and Lippard (1979) note the continuation of phonolites, phonolitic tuffs and basanites at the intersection of the Kenya and Nyanza rift until ca. 7.5 Ma. Similarly, within the South-Central Kenya Rift this period is represented by Flood Phonolites. North of the junction with the Nyanza rift, the initial Flood Phonolites on the western rift margin are typically called Uasin Gishu Phonolites (see Part II)(Rooney, 2020a), though to the south the unit is termed the Kericho Phonolite (Jones and Lippard, 1979). The Kericho Phonolites are temporally well-constrained at 13.7 Ma (± 0.3 $^{40}Ar/^{39}Ar$) within the Nyanza rift owing to the Fort Ternan fossil fauna that they enclose (Pickford et al., 2006). On the eastern plateau, the Kapiti Phonolite is temporally equivalent (12.9 Ma ± 0.7 to 13.4 Ma) (Baker et al., 1971), and is thought to be the oldest lava in the Nairobi area (Saggerson, 1991).

The oldest unit in the Southern Kenya Rift is the Lisudwa Formation (15.2 – 12 Ma with no error provided: Crossley, 1979). These rocks are dominantly melanephelinites from an isolated center along the western rift margin. The Plateau Phonolites are also represented in the Southern Kenya rift (and adjacent regions) as the Kapiti Phonolite (see description in south central Kenya Rift above), and the Yatta Phonolite (13.2 Ma: Baker et al., 1971). The Southern

Kenya rift represents the southern boundary of the Flood Phonolite phase (Lippard, 1973; Smith, 1994), and thus volumes are modest within the region.

The Flood Phonolite phase is clearly well-developed within the Southern Kenya Rift (Fig. 2), and the temporal evidence presented above is suggestive that this event is the southern manifestation of the earlier Samburu phase. The later time of initiation of magmatism reflects the progressive southward migration of strain, while the compositional heterogeneity results from the interaction of the rift and resulting rift magmas with the thicker cratonic lithosphere. While appealing in its simplicity, this assertion is not yet supported with geochemical analytical data and requires further research.

3.2.2 Geochemical Composition of the Flood Phonolite Phase Lavas

Given the large volume of Flood Phonolite lavas erupted in Southern Kenya, it is remarkable that there is so little published data available. Indeed, the extant dataset is dominantly the basaltic materials co-erupted with the phonolite lavas (Fig. 3). These lavas are similar to the Samburu Phase lavas (Fig. 4; 5), exhibiting a Type II lava signature suggesting a derivation from a mantle metasome. The similarity in the lava compositions between these two phases of activity supports the notion that the Flood Phonolite Phase may be the southern continuation of a pulse of magmatic activity that commenced in Turkana during the Early Miocene and propagated southward. The single Pb isotope analysis of one of these basalts plots at radiogenic $^{206}Pb/^{204}Pb$ values that could suggest a plume input, but has unradiogenic values of $^{143}Nd/^{144}Nd$ that instead requires lithospheric influence (Fig. 8). With a single data point it is not possible to constrain the role of the continental crust, however some understanding of such contamination can be gleaned from modern magmatic activity where crustal influence will result in coupled variations towards radiogenic $^{87}Sr/^{86}Sr$ and unradiogenic $^{143}Nd/^{144}Nd$. This is not observed for the Flood Phonolite Phase sample, which instead plots on the same trend as some of the Stratoid Phase lavas – i.e. towards unradiogenic $^{143}Nd/^{144}Nd$ but at only modestly

radiogenic values of $^{87}Sr/^{86}Sr$ (Fig. 8). A subset of these Stratoid Phase lavas also exhibit a Type II lava pattern (Fig. 5). When examined together these data point towards a lithospheric mantle metasome that melted to form the primary magma. This metasome is distinct from those found further north in exhibiting markedly unradiogenic $^{143}Nd/^{144}Nd$ (consistent with a cratonic lithospheric mantle), but also with similarly radiogenic $^{206}Pb/^{204}Pb$.

3.3 Mid-Miocene Resurgence Phase (12 to 9 Ma)

Within the Turkana and Ethiopian sectors of the East African Rift System there is a pronounced period of magmatic activity focused upon the Turkana Basin and the margins of the Afar Depression (see parts II and IV of the synthesis)(Rooney, 2020a, 2020b). This Mid-Miocene Resurgence phase reflects the recommencement of significant basaltic volcanism in those regions. This phase is tectonically important as it coincides with the formation of the northern Main Ethiopian Rift, and significant changes to the regions that were accommodating strain in the Turkana Depression (Purcell, 2018). In terms of the focus of this contribution, the Mid-Miocene Resurgence phase represents a renewed pulse of extension originating in the Turkana Depression. Volcanism associated with this event is largely absent within the Southern Kenya Rift. Smaller-scale volcanism is evident where phonolites continued to erupt sporadically. Where detailed work has been undertaken in the north-central Kenya Rift, this phase is represented by sedimentary formations (e.g., Hautot et al., 2000). These observations provide further support to a model whereby extension during this interval was focused further to the north. However, as with the Samburu and subsequent Flood Phonolite phases, a renewed period of activity follows in the more southern reaches of the Kenya Rift.

3.4 Early Rift Development Phase (9 to 4 Ma)

3.4.1 Distribution and chronology of Early Rift Development Phase Lavas

This period is critically important in this region, manifesting as significant volcanic activity and associated rift development (Fig. 9). Notably, large-scale bimodal volcanism becomes established within the region. This phase of activity parallels similar rift development within central Ethiopia, yet no significant volcanic units are recorded in Turkana during this phase. These observations support the developing model of a temporal and spatial southward migration of strain from Turkana. Thus, the Early Rift Development phase is linked with the earlier Mid-Miocene resurgence phase that was centered on Turkana. It is important to note that there is a strong spatial control to magmatism during this period whereby lavas are restricted to the Kerio Basin, distinct from the later phases of activity that occur further to the east (Fig. 9).

In the north-central Kenya Rift, the initial stages of this period are marked by a significant eruption ca. 9 Ma – the Ewalel Phonolite. The Ewalel Phonolite is subsequently tilted and eroded as rifting begins within the region (Mugisha et al., 1997). Along the western rift margin near the Nyanza rift junction, are the Timboroa Phonolites (8.9 Ma ± 0.2 to 9.4 Ma ± 0.3) (Jones and Lippard, 1979), which are thought equivalent to the Ewalel Phonolite to the north, indicating a continuity of this early phase of extension-related magmatism within the Southern Kenya Rift. Following the eruption of the widespread phonolites throughout the Kenya rift, a distinct shift in magmatic character (towards explosive eruptions) and composition (towards trachytes) is observed. This transition in the composition of evolved magmatic products is coincident with an important shift in the composition of mafic rift magmas (see geochemistry below).

This new phase of explosive magmatic activity was initially thought to have commenced ca. 6 Ma and was centered on the Naivasha area (Olkaria – see Axial Phase) of the south-central Kenya Rift, with deposits extending in a 90 km radius (Smith 1994). Recent examination of high precision $^{40}Ar/^{39}Ar$ dating of distal ash flow tuffs near Mt. Kenya suggest that these explosive eruptions actually began much earlier and travelled much further (150 km) than that

previously envisioned (Claessens et al., 2016). Within the south and south-central Kenya Rift, large-scale explosive volcanic eruptions dominated the stratigraphy during the early part of this period. Near Mt. Kenya a series of pantelleritic distal ash flows have been dated from 8.13 Ma (± 0.08 $^{40}Ar/^{39}Ar$) to 6.36 Ma (± 0.03 $^{40}Ar/^{39}Ar$), which may be related to the undated Athi tuffs that dominate the sequence within the Southern Kenya Rift near Nairobi (Saggerson, 1991; Claessens et al., 2016), and are temporally correlated with the Mpesida Pyroclastics further north (Kingston et al., 2002). The Mau Tuffs near the western rift border commence between 6.0 Ma (± 0.2) and 5.8 Ma (± 0.2), but their termination is poorly constrained as it is not a single event but a series of volcanic eruptions (Jones and Lippard, 1979; Leat, 1991). This large-scale explosive period may have terminated with the widespread 3.4 to 3.7 Ma Kinangop Tuffs (Baker et al., 1988), though tuffs from the modern central volcanoes continue to be deposited in the rift until recent times (e.g., Leat, 1991).

A distinct new phase of effusive activity commenced ca. 6.5 Ma with the eruption of widespread basalts and trachytes. Thus, this period sees the co-existence of large-scale 'flood' trachyte flows with the massive pyroclastic eruptions. This new event is critically important in the development of this sector of the rift as it corresponds with the initial development of Mt. Kenya and also heralds the first magmatic activity within the NTD, starting at Essimingor at 5.9 Ma (Mana et al., 2012) (see section on NTD). In the south-central Kenya Rift, the Kapkut Trachyte has been linked with the Kabarnet Trachyte to the north (6.37 Ma: Kingston et al., 2002) and covers an area of 250 km^2 (Jones and Lippard, 1979). Elsewhere, lava flows are grouped as the 'Satima Series', which is comprised of the Thompson's Falls Phonolite (6.2 Ma ± 0.5 to 6.7 Ma ±0.5) (Baker et al., 1971) and Laikipian Basalts that lie under the Mt. Kenya volcanics. Other compilations omit the Satima Series and instead note a Thompson's Falls Formation to include phonolites, trachytes and trachytic tuffs, and the overlying Pliocene basalts of various names (Hackman, 1988). The Turasha Basalts are poorly temporally constrained (McCall, 1967;

MacDonald et al., 2001), but are assigned to this phase as they underlie tuffs that are thought to correlate with the boundary between this phase and the subsequent Stratoid Phase.

In contrast with the magmatism further north, where this time period was coincident with a shift towards more trachytic lavas, in the Southern Kenya Rift phonolites continued erupting along the eastern margin of the rift. The Kandizi and Nairobi Phonolites are not well-dated, and the existing information has suggested two ages for the Nairobi Phonolite of 5.2 and 10.4 Ma (Saggerson, 1991). For this compilation I prefer the younger date as the Nairobi phonolites are seen to overlie the Athi Tuffs, though it is possible that there are two phonolites within this single unit (Saggerson, 1991). Further geochronological constraints are needed as to the ages of these phonolites. The Lengitoto Trachytes (5 to 6.9 Ma) and Endosapia Trachytes (3.2 – 5.1 Ma) were the next major magmatic events, and erupted into the evolving rift basin (Crossley, 1979). At the very southernmost limit of the rift, volcanic centers began to form, with the earliest volcanic activity recorded at Ol Esayeti (5.85 Ma) and Olorgesailie (5.83 Ma) (Saggerson, 1991). In summation, within the Southern Kenya Rift, there are proliferation of unit names describing individual trachytic flows ca. 5 – 6 Ma. They are amalgamated here as the Early Rift Development Series.

During this period, construction of the massive 5200m Mt. Kenya volcanic complex began on the eastern rift shoulder. Recent investigation of the base of the complex has revealed that the construction of the edifice began between about 5.45 Ma (± 0.06 $^{40}Ar/^{39}Ar$) with a ‘trachytic andesite’ (Mahaney et al., 2011), or 5.78 Ma (± 0.05 $^{40}Ar/^{39}Ar$), with the Gachoka Phonolite overlying basement (Veldkamp et al., 2012). It should be noted that Baker (1967) suggests the earliest magmatic activity on Mt. Kenya are olivine alkali basalts and andesites that underlie the phonolites, implying that magmatic activity may have commenced slightly earlier than the dates noted above. The majority of the main phase of activity that constructed the Mt. Kenya edifice were basalts, phonolites, kenytes, and trachytes (Baker, 1967; Price et al.,

1985). Baker (1967) noted that the volcanism on Mt. Kenya was divided into that derived from the main vent and those from satellite vents. Subsequent magmatism on Mt. Kenya spans an array of dates from 4.89 Ma (±0.21 $^{40}Ar/^{39}Ar$) to 2.81 Ma (± 0.34 $^{40}Ar/^{39}Ar$), with the main body of the volcano thought to have been constructed by at least 4.22 Ma (Veldkamp et al., 2012). Note the late (post 0.8 Ma) Thiba basalts on Mt. Kenya are described with the Nyambeni Hills.

Within the Nyanza Rift, magmatic activity during this period was limited due to the migration of magmatic activity towards the west (Jones and Lippard, 1979). However, a basanite from the summit of Tinderet volcano has been dated at 5.6 Ma (± 1.3) (Baker et al., 1971). In addition, carbonatite and silica-undersaturated magmatism is recorded at Homa Mountain and the Ruri Hills that largely parallels in compositional range of magmas erupted at the earlier Kisingiri volcano (Le Bas and Rubie, 1977). The best age constraints for activity in these volcanoes comes from the clastic record where the Rawi Formation (3.110 – 2.581 Ma) and overlying Homa agglomerates contains material from Homa Mountain (Ditchfield et al., 1999), though magmatic activity here may have continued to 1 Ma (Le Bas and Rubie, 1977).

3.4.2 Geochemical Characteristics of Early Rift Development Lavas

Lavas of the Early Rift Development phase typically plot at very enriched values of CaO/Al_2O_3, Zr, and Nb for a given MgO, consistent with similar characteristics during the previous phases of activity, but distinct from the latter phases (Fig. 3). Despite these similarities, lavas from this phase do not show the typical Type II pattern (Table 1) and instead resemble the Type IV magma category that is more common in Turkana (see Part II) (Fig. 5) (Rooney, 2020a). Type IV magmas result from the mixing of melts derived from Type II and III magmas and are thus a mix of material derived from a lithospheric mantle metasome and a sub-lithospheric reservoir. The volume of isotopic data is limited, but the extant data could be explained by a mix of the

Afar plume component, and a lithospheric mantle metasome endmember – the hypothesized source of the prior Phases of magmatic activity (i.e., radiogenic $^{206}Pb/^{204}Pb$) (Fig. 8). This very tentative hypothesis that the Early Rift Development phase exhibits both lithospheric mantle metasome and sub-lithospheric melts has important implications for the development of magmatism as rifting evolves – the magmatic system has matured to the point where, for the first time in this region, sub-lithospheric derived materials are erupting to the surface. As noted earlier in this section, this phase also correlates with the transition from phonolite to trachyte lavas within the region. When combined, these observations suggest the decrease in alkali content of the primitive magmas, which is caused by the dilution of metasome-derived magmas with those derived from sub-lithospheric reservoirs, may influence the composition of the resulting evolved magma suites.

3.5 The Stratoid Phase (ca. 4 Ma to 0.5 Ma)

3.5.1 Distribution and chronology of Early Rift Development Phase Lavas

The initiation of this magmatic phase at ca. 4 Ma is defined primarily by the recommencement of volcanism following a long magmatic hiatus within the Turkana Depression. Elsewhere within the rift (such as within the south and south-central Kenya Rift) magmatic activity had not been subject to this hiatus, thus the precise assignment of units to the Stratoid phase can be ambiguous within these regions, and might call into question the utility of creating such a time period! However, previous studies have placed a division in the development of the rift at ca. 4 Ma, coincident with the transition towards full graben morphology (Baker, 1987; Baker et al., 1988). Moreover, the thick flows that develop subsequent to 4 Ma fill the evolving rift graben in a manner similar to contemporaneous flows within the Main Ethiopian Rift (e.g., Bofa Stratoid

Series). There thus remains a compelling rationale for formation of this temporal division throughout the eastern branch of the East African Rift.

As with the prior events that initially manifested in Turkana, there is limited expression of this phase during its early stages in the southern EARS. There is a decrease in massive phreatomagmatic eruptions following the ca. 3.5 Ma Kinangop Tuffs. The Kirikiti Basalts (2.5 to 3.1 Ma) filled the rift valley floor to a depth of 550m (Crossley, 1979), with the subsequent eruption (locally) of the Singaraini Basalts (2.31 – 2.33 Ma). Within the south-central Kenya Rift, the most volumetrically significant unit in this region are the 400m thick Limuru Trachytes (1.96 Ma ± 0.04) (Baker et al., 1988), which occupies an area of ca. 1400 km^2, though it should be noted that these trachytes are regarded as a composite unit and that individual flows are much smaller in volume than the Flood (Plateau) Phonolite event (Leat, 1991). Smaller volume events are also common during this period. In the Nairobi region, the prevalence of trachytes (of various names – see Saggerson, 1991) has resulted in an upper and lower trachyte division. In the Southern Kenya Rift, the Limuru Trachyte is overlain by the Ol Keju Nero Basalts ca. 1.9 to 1.65 Ma, which are conformably overlain by the Ol Tepesi Basalts (1.65 to 1.4 Ma). The rift valley floor was then flooded with a trachyte – the Plateau Trachyte (Baker and Mitchell, 1976; Baker et al., 1988) or Magadi Trachyte (Crossley, 1979; Crossley and Knight, 1981). This fissural event is dated to 0.93 Ma (± 0.06) to 1.17 Ma (± 0.04) by Baker and Mitchell (1976), though Baker et al., (1988) suggests a range of 0.8 to 1.4 Ma, citing the original 1976 paper. Smaller trachytes, phonolites, and basalts erupted along the rift margins throughout this period (Guth, 2013). It is notable that this period, which is contemporaneous with similar activity in the Main Ethiopian Rift at this time (Bofa Stratoid Series), is equally complex and is typified by thick basaltic and trachytic flows interbedded with volcanoclastic sediments. The similarity in composition of these units means, that from a geochemical perspective, it is suggested that all basaltic and trachytic units of the rift floor erupted during this period be amalgamated into an

unitary name – the Southern Kenya Rift Stratoid Series, a mirror of the Bofa Stratoid Series within the Main Ethiopian Rift (See Part II) (Rooney, 2020a).

In addition to these flood trachyte events, a series of volcanic centers developed within the Southern Kenya rift and along the rift margin: Ol Esayeti, Ngong, Olorgesailie, Lenderut, Oldoinyo Sambu and Shombole (Le Roex et al., 2001; Dawson, 2008) (Fig. 9). The initial phases of Ol Esayeti and Olorgesailie extend to be as old as ~ 5 to 7 Ma (Baker et al., 1988; Saggerson, 1991), though most of the volcanoes exhibit ages that range from ca. 2 to 3 Ma (Baker et al., 1988). There is a general lack of precise geochronology from these centers but trachytes from Olorgesailie, which underlie the fossiliferous Olorgesailie Formation, yield ages of 2.874 Ma (+/ 0.112 $^{40}Ar/^{39}Ar$) (Deino and Potts, 1990). The age range of these volcanoes, which lie just north of the NTD, thus correlate with the Main Phase of activity recorded in the NTD (Mana et al., 2015). As a whole, magmatism during this phase of activity migrated from the Kerio basin during the Early Rift Development Phase to the Baringo basin during the Stratoid Phase (Fig. 9).

3.5.2 Geochemical Characteristics of the Stratoid Phase

During this phase of magmatic activity, there exists a compositional dichotomy between lavas erupted into the rift basin and those associated with the volcanic edifices along the rift margin (e.g., Shombole), though some overlap exists (e.g., Le Roex et al., 2001). In figures where distinct populations are evident, these rift margin lavas plot at high TiO_2, Zr, Nb for a given MgO and are remarkably similar to the Early Rift Development phase lavas (Fig. 3). There is significant REE slope in these rift margin lavas; $(Tb/Yb)_{CN}$ in the rift marginal lavas have values > 2, and exhibit consistently elevated La/Yb in comparison to the rift basin lavas that manifests as a crossing REE pattern between the two groups (Fig. 3; 4). The source of this deviation is the

predominance of Type IV lavas along the rift margins, and first occurrence of Type III lavas in the rift basin (Fig. 5).

This dichotomy is also evident in terms of isotopic values – lavas from the rift floor display a consistently restricted isotopic range that is radiogenic in terms of $^{143}Nd/^{144}Nd$ but at about the same value of $^{87}Sr/^{86}Sr$ in comparison to the widely variable rift margin lavas (Fig. 8). The rift margin lavas extend to an unusual isotopic space in comparison to the rest of the samples from the region and require contribution from the cratonic lithosphere given the unradiogenic values of $^{143}Nd/^{144}Nd$. Considering the Type IV trace element pattern exhibited by these lavas, a metasomatic origin for this lithospheric component is probable. Le Roex et al. (2001) noted that Lenderut volcano, in particular, exhibited another unusual characteristic – very unradiogenic Pb isotope values (Fig. 8), and postulated either a lower crustal assimilant or lithospheric metasome. The unradiogenic values of $^{207}Pb/^{204}Pb$ exhibited by these lavas is inconsistent with the extant data on crustal granulite xenoliths in this region that exhibit much more radiogenic $^{207}Pb/^{204}Pb$ at a given $^{206}Pb/^{204}Pb$ (Cohen et al., 1984). The metasomatic model is thus preferred and the array seen may relate to mixing between magmas derived from this metasome and sub-lithosphere Type III lavas. This presents an unusual observation, however, in that the lithospheric component that melted to form these lavas has unusually unradiogenic Pb isotopes in comparison to that typically inferred from other lavas. Further work on these and other lavas is necessary to fully resolve these observations.

3.6 Magmatic Activity on the Rift Floor and Eastern Plateau (0.5 to Present)

3.6.1 Distribution and chronology of Rift Floor and Eastern Plateau Lavas

Within the south-central Kenya Rift, activity during this period has been termed the ‘Central Kenya Peralkaline Province’ by MacDonald and Scaillet (2006), and is comprised of five recent

volcanoes: Menengai, Eburru, Olkaria, Longonot, and Suswa (Fig. 10). This region is an important geothermal energy producing domain and consequently has been the focus of significant study over the past 30 years. Detailed accounts of the stratigraphy, geochronology, and petrology of units from this region are presented by Clarke (1990). The most complete geochemical information for the region is presented by MacDonald and Scaillet (2006) and Marshall (2009). The interested reader is directed to these works for a more complete presentation of magmatic activity in this region. A wider-scale overview is presented by Rogers et al., (2000).

Menengai volcano is predominantly constructed of peralkaline trachytes that is thought to have commenced at 0.18 Ma (± 0.01) (Leat, 1984 citing a personal communication from J.G. Mitchell). Menengai has generated significant volume of tuffs during its lifetime and some form important marker horizons, such as the 35.62 ka (± 0.26 $^{40}Ar/^{39}Ar$) Menengai Tuff (Blegen et al., 2016). Eburru volcano is largely constructed of pantellerite flows and pyroclastics which commenced < 0.45 Ma (Clarke, 1990). The Olkaria volcanic complex (also Naivasha in older literature), is a significant multi-center complex dominated by comendiditic lavas and pyroclastics (MacDonald and Scaillet, 2006). The complex is much younger than the others discussed thus far and is thought to have commenced ca. 20 ka (Marshall et al., 2009). Longonot volcano dominantly produced pyroclastic rocks during its earlier phase with more recent trachyte lavas forming the cone and summit (MacDonald and Scaillet, 2006). The age of this volcano is poorly constrained and is thought to be less than 0.4 Ma (Clarke, 1990). Suswa volcano is the most southern of the modern volcanoes within the Kenya rift, north of the quite distinct activity in the NTD. Volcanic activity at Suswa is estimated to have commenced ca. 0.240 Ma (± 0.01) (Baker et al., 1988). Magmatic activity at Suswa is initially a silica-saturated peralkaline composition but transitions to a later phase that is dominated by phonolites (White et

al., 2012). Within the Southern Kenya Rift, activity during this time period is largely limited to Suswa volcano (Baker et al., 1988; Guth, 2013).

While earlier phases of magmatic activity along the eastern rift margins were generally contiguous with activity within the rift itself, during this period magmatic activity began to exhibit distinctive differences depending on where lavas were erupted. In particular, the evolution of a chains of basaltic cinder cones and fissures resulted in the significant accumulation of basalts along the eastern rift shoulder during this period. The Chyulu Hills are a NW-SE aligned field of primitive alkaline lavas covering ca. 2840km^2 (Späth et al., 2001) (Fig. 10). It is divided into an older North Chyulu Hills, where the earliest activity recorded is 2.01 Ma (± 0.09 ^{40}Ar/^{39}Ar) (Chualaowanich et al., 2014). Rocks within this older portion of the volcanic field are named the Sultan Hamad/Emali/Simba units (basanites, nephelinites, and basalts) and the Nguu and Ngatatema lavas (basanite-alkali basalt). The Southern Chyulu Hills are considered Holocene, and consist of basanites, alkali basalts, hawaiites, and the Mzima transitional basalts (Späth et al., 2001; Le Gall et al., 2008). The alignment of the volcanic vents is thought related to the influence of the Aswa shear zone; the reactivation of such basement fabrics are thought particularly important in domains that have remained relatively intact and cold during rift evolution (Le Gall et al., 2008).

The Nyambeni (Nyambene) Hills volcanic series, which is directly adjacent to Mt. Kenya, have been divided into a lower series (basalts) and an upper series with a significant textural and compositional heterogeneity (basalts, phonolites and tephrites) (Mason, 1955). This 1000m thick section of basalts has been recently dated at between 1.64 Ma (± 0.5 ^{40}Ar/^{39}Ar) and 0.30 Ma (Opdyke et al., 2010). A date of 4.42 Ma (± 1.06 ^{40}Ar/^{39}Ar) has also been reported by Opdyke et al. (2010) in an area mapped as part of the Nyambeni volcanics, however the boundary between the Mt. Kenya flows and Nyambeni volcanics is not well constrained (Mason, 1955) and this sample may also be derived from flows emanating from Mt. Kenya. The volcanic

vents are interpreted to young to the northeast within this NE-SW orientated field (Mason, 1955) that covers more than 4000 km^2 (Guth, 2013). Contemporaneous with the basaltic magmatism in the Nyambeni Hills, Mt. Kenya experienced a volcanic reactivation with the eruption of the Thiba Basalts (Baker, 1967) between 0.797 Ma (± 0.023 $^{40}Ar/^{39}Ar$) and 0.45 Ma ± 0.17 (Opdyke et al., 2010; Veldkamp et al., 2012). The Thiba basalts, which have a wide array of textures, cover ca. 1300 km^2 and are derived from a series of parasitic vents on Mt. Kenya (Baker, 1967).

3.6.2 Geochemical Characteristics of Modern Rift Lavas

Lavas from the modern Southern Kenya rift provide an excellent opportunity to examine the impact of crustal assimilation and magma hybridization (see MacDonald and Scaillet, 2006; Marshall et al., 2009 for a much more detailed view). As with most discussions that focus on silicic magmatic eruptions, the most pronounced controversies focus on whether evolved lavas are produced through crustal anatexis (i.e. no significant mass contribution from mantle melts), or assimilation and fractional crystallization processes (AFC). Initial studies focused on this region suggested the anatexis model on the basis of crustal isotopic signatures in the lavas and the existence of a Daly Gap (e.g., Clarke, 1990). More recent geochemical work has shown that the origin of the silicic magmas is more likely related to complex AFC processes and that the Daly Gap evident in lava suites throughout the East African Rift is instead evidence for the development of magma mushes from which melts can be extracted once they have reached a critical locking point (e.g., Bachmann and Bergantz, 2008; Rooney et al., 2012a). Clear fractional crystallization trends are evident for TiO_2 whereby lavas from the Axial Phase join lavas from the Stratoid Phase in increasing in concentration of TiO_2 to about 5 wt. % MgO, and thereafter falling due to Fe-Ti oxide fractionation (Fig. 3). However, another group of such samples crosses this evolutionary space directly and is suggestive of magma mixing, as has been noted by previous authors (Marshall et al., 2009). The extant work has suggested a complex series of multi-level mush and magma chambers that are fed by basaltic dikes

(Marshall et al., 2009) – a condition also proposed for lavas erupted in the Main Ethiopian Rift (see Part II) (Rooney, 2020a).

Lavas from the Axial Phase track the same compositional evolutionary trends as the prior Stratoid phase lavas from the rift floor (Fig. 3). It is therefore unsurprising that the Axial lavas all exhibit the sub-lithospherically derived Type III lava pattern (consistent with the rift flood Stratoid Phase lavas) (Fig. 5). Some complexity in primitive mantle and chondrite normalized patterns is the result of mixing with more evolved lavas (Fig. 4; 5). Isotopically, these lavas tend to exhibit a greater degree of crustal assimilation in comparison to the earlier Stratoid Phase, extending to very unradiogenic $^{143}Nd/^{144}Nd$ and radiogenic $^{87}Sr/^{86}Sr$ (Fig. 8). The Pb isotope composition of this crustal endmember is unlike the northern portions of the rift in that it is has both radiogenic $^{206}Pb/^{204}Pb$ and very radiogenic $^{207}Pb/^{204}Pb$, forming a vertical array in Pb isotope space (Fig. 8). In short, there appears to be limited variation in $^{206}Pb/^{204}Pb$ between the parental liquid entering into the crustal mush zones, but this crustal component is apparent in the other isotopic ratios.

When examined as a sequence from the initial stages of volcanism to the modern Axial activity, basaltic lavas display a consistent message – an initial metasomatic signature, an intermediate mixed metasomatic – sub-lithospheric signal, and a modern sub-lithospheric signature. While such an observation is clearly consistent with the temporal evolution of a rift, the magmas are providing an additional constraint to the story, demonstrating early lithospheric destabilization to form alkaline lavas.

4. Northern Tanzania Divergence

Despite some temporal similarities with magmatic activity within the Southern Kenya Rift, activity within the NTD follows a slightly different evolutionary trend, which justifies addressing

this region independently. Whereas magmatism to the north in Kenya has been a mixture of rift-wide magmatic events and large central volcanoes, activity in the NTD is typically limited to the large edifices and intervolcano cinder cones (Dawson, 2008) (Fig. 10). Recent compilations of the stratigraphy (Dawson, 2008) and new geochronologic constraints (Mana et al., 2015) have substantially clarified the evolution of this region and the interested reader is directed to these papers for more detail. Older papers suggest a division of the magmatic events into a pre-rift and post-rift phase at 1.2 Ma (Dawson, 2008), though more recent work has suggest a more complex four-fold magmatic evolution (Mana et al., 2015). Mana et al. (2015) and Le Gall et al. (2008) recognize the progressive evolution of the magmatic centers in time and space. Mana et al. (2015) show that volcanism in the NTD is focused on two parallel trends that become progressively younger to the east. A) Essimingor to Kilimanjaro Trend (Essimingor; Burko; Tarosero; Monduli; Meru; Shira/Kibio/Mawenzi on Kilimanjaro); B) Sadiman to Gelai trend (Sadiman, Lemagrut, Engelosin, Oldeani, Ngorongoro, Olmoti, Loolmalasin, Embagai, Kerimasi, Ketumbeine, Mosonik, Oldoinyo Lengai, Gelai). Le Gall et al. (2008) notes the correlation between the migration of magmatism and strain as the rift evolves. In the interests of continuity with the activity further north within the rift, I have opted to retain the nomenclature for the different phases and place NTD magmatic activity within that framework. For studies that examine the NTD in isolation, this division may not capture the diversity of events within the area, however from an EARS-wide perspective it is necessary to discuss the events in the NTD within the broader framework.

4.1 Early Rift Development Phase

Unlike activity to the north, volcanism within the NTD appears focused on distinct edifices (as opposed to fissural flows), thus discussion within this section focuses upon individual edifices. The Early Rift Development phase (9 – 4 Ma) was defined on the basis of magmatic activity within the north and north central Kenya Rift and the Main Ethiopian Rift, however this phase

also marks the first magmatic activity within the NTD. Volcanoes during the initial stages of magmatic activity (pre 1.2 Ma) have been classified by Dawson (2008) as ‘older extrusives’, and exhibit a commonality that magmatic products from these volcanoes during this period were typically Si-saturated to transitional, following the alkali-basalt evolutionary trend. There were some exceptions, however, and Si-undersaturated products were observed as early products of some of the older extrusives volcanoes (Dawson, 2008). Mana et al. (2015) identified a temporal relationship between the occurrences of these Si-undersaturated lavas and created a new early magmatic phase commencing ca. 5.9 Ma. This phase was restricted to Sadiman and Essimingor, though it is possible that early activity at Lemagrut volcano (adjacent to Sadiman), which is also highly silica-undersaturated, is part of this early phase. This period is referred to as Phase 1 by Mana et al. (2015) and lasts from ca. 5.9 to 2.9 Ma.

Phase 1 lavas within the NTD exhibit a wide range of compositions that spans the compositional endmembers defined by the moderately incompatible trace element depleted phases 2/3, and the incompatible element enriched phase 4 (Fig. 11; 12; 13). It is notable that the enriched endmember is restricted to Essimingor volcano, which exhibits some lavas that have characteristics consistent with melting of a lithospheric metasome – namely enriched TiO_2, CaO/Al_2O_3, Nb, and isotopic values that trend towards the HIMU endmember (Fig. 14;15). In contrast, lavas from Lemagrut are far less enriched in incompatible trace elements and have a composition consistent with a mix between material derived from the CLM component (Furman & Graham 1999) and a crustal endmember (Fig. 15) (note the CLM component is defined as a specific isotopic reservoir and should not be confused with the more general term – SCLM). While $(Tb/Yb)_{CN}$ values for Essimingor are elevated (up to 3.75) in comparison to Lemagrut (>2.5), the Type II magma patterns exhibited by both suites (Fig. 13), requires caution in any interpretation for differing depths of melt generation due to the likely metasomatic origin of the source rocks to both lava suites. Lavas at Sadiman and Engelosin have experienced significant

magmatic differentiation and fall along clear crustal assimilation trends evident as unradiogenic $^{143}Nd/^{144}Nd$ and radiogenic $^{87}Sr/^{86}Sr$ with decreasing MgO (Fig. 15).

4.2 Stratoid Phase

Following the small-scale ultra-alkaline activity that defined the earlier initial phase, the NTD underwent what has been described as the main phase of activity from 2.9 to 0.5 Ma. This period incorporates Stage 2 (2.6 – 1.8 Ma) and 3 (1.65 to 0.75 Ma) of Mana et al. (2015). When the Si-undersaturated volcanoes are removed from the 'older extrusives' group of Dawson (2008), what remains are a large volume of transitional to marginally Si-undersaturated lavas. The following volcanoes form this group: Elanairobi, Olmoti, Loolmalasin, Ngorongoro, Oldeani, Tarosero, Monduli, Ketumbeine, Gelai, Shira & Mawenzi on Kilimanjaro, and Mosonik. It should be noted that the commencement of magmatism during this main phase of activity temporally lags the defined bounds of the Stratoid phase, which was determined on the basis of magmatic activity in Turkana. Given the southward expansion of rifting discussed within this contribution, the temporal lag is unsurprising.

It is not always possible to assign lavas definitively to the four fold division established by Mana et al. (2015), thus hybrid groupings of phases are necessary when discussing magmatic activity from this phase. Phases 1 to 2 (where lavas could not be assigned definitively to either period) and Phase 2 to 3 exhibit largely similar major element, trace element, and isotopic characteristics (Fig. 11; 12; 13; 14). It is important to note that these periods represent the most volumetrically significant magmatic phase within the NTD (e.g., Mana et al., 2015), and thus high degrees of melting are not unexpected. Accordingly, lavas from these periods exhibit a relative depletion in incompatible trace elements in comparison to some Phase 1 and all Phase 4 lavas (Fig. 11), where the volume of magmatism was significantly less. Despite the decrease in incompatible trace element enrichment, lavas from these phases of magmatism exhibit the same Type II magma patterns suggesting similar source lithologies to the other

phases of magmatism in the region or the influence of a particularly trace element enriched lithology in a two component melting model. $(Tb/Yb)_{CN}$ values during this phase extend to much lower values than during Phase 1 and 4 (Fig. 11), as has been noted by prior authors (Mana et al., 2015). Lavas from these periods do not exhibit the same extreme radiogenic $^{206}Pb/^{204}Pb$ values common to Phase 1 and 4, and instead form arrays towards less radiogenic compositions (Fig. 14).

While individual volcanoes typically follow relatively tight arrays during these phases of magmatic activity (Fig. 16), the evolved compositions of Tarosero and Ngorongoro provide insight into potential crustal assimilants. Most lava suites during this phase of activity exhibit strong correlation between $^{143}Nd/^{144}Nd$ and MgO, forming linear arrays anchored in the most primitive lavas erupted (Fig. 15). The patterns at Monduli, Ketumbeine, and the Mawenzi and Shira phase of Kilimanjaro typify this relationship and show a progressive decrease in $^{143}Nd/^{144}Nd$ with melt evolution, but lack a sympathetic co-variation in $^{87}Sr/^{86}Sr$ (Fig. 16; 17). With continued melt evolution, the influence of a radiogenic $^{87}Sr/^{86}Sr$ component becomes evident, as seen in the Ngorongoro lavas (Fig. 16). Evolved lavas from Tarosero similarly exhibit the influence of a radiogenic $^{87}Sr/^{86}Sr$ crustal assimilant but the composition of this component differs significantly to that influencing the other volcanoes. Specifically, the $^{143}Nd/^{144}Nd$ of this crustal assimilant is more radiogenic in terms of $^{143}Nd/^{144}Nd$, and has extremely radiogenic values of $^{208}Pb/^{204}Pb$ (Fig. 16). Regardless of the precise composition of any assimilant, the most primitive samples in the region all converge on a single value of $^{87}Sr/^{86}Sr$ ~0.7035 and $^{143}Nd/^{144}Nd$ of 0.5127-0.5128 (Fig. 16).

Pb isotope ratios form no coherent trend versus MgO (not shown) and complicate the seemingly simple story of crustal assimilation from an isotopically relatively homogenous parental magma. Instead, it is increasingly evident that primitive lavas in this portion of the rift form a linear array in $^{206}Pb/^{204}Pb$-$^{208}Pb/^{204}Pb$ with no convergence to a unitary value on the basis

of MgO. Such observations might reflect early contamination of the parental lavas, however, the vector of assimilation contradicts this model. Crustal assimilation results in lavas leaving the afore mentioned array, usually along a particular vector. The strong crustal influence in more evolved lavas in Tanzania provides an opportunity to visualize this process (Fig. 18). It is clear that more evolved lavas tend to leave the array defined by the primitive lavas and trend towards a contaminant resembling the Pan-African Lithosphere (PAL) component in Pb isotope space (Fig. 18).

Paslick et al. (1995) suggested that magmatism within the NTD was derived from the sub-continental lithospheric mantle on the basis of the unusual occurrence of radiogenic, HIMU-like Pb isotope compositions that were combined with relatively radiogenic values of $^{87}Sr/^{86}Sr$. This model invoked a ca. 2 Ga underplated plume as the source for magmatism in the region. This model has been subsequently refined to suggest an origin from a amphibole-phlogopite-garnet metasome within the sub-continental lithospheric mantle (Nonnotte et al., 2011; Mana et al., 2012; Mattsson et al., 2013), consistent with recovered xenoliths in the region (e.g., Dawson and Smith, 1988; Rudnick et al., 1993; Lee et al., 2000; Dawson, 2008). Despite the general agreement as to an origin within the sub-continental lithospheric mantle, the origin of the metasomatizing agent remains unclear. The current state of knowledge is that the metasomatic agent that could either be an ancient event, the interaction of more recent plume-derived melts with the lithospheric mantle, or both (Nonnotte et al., 2011; Mana et al., 2015).

4.3 Axial Phase - Recent NTD (0.5 Ma to Present)

Within the NTD, this time period (termed Stage 4 by Mana et al. 2015) is typified by ultrabasic and ultra-alkaline volcanic activity. Typical rock types are nephelinite, carbonatite, phonolite, melilite, and ankaramite. Unlike regions to the north, where magmatic activity typically occurs within an axial graben, the less mature rifting in the NTD results in dispersed magmatism that is spatially restricted and occurs at: Meru, Oldoinyo Lengai, Kerimasi, Burko, Kwaraha, Hanang,

and Kibo on Kilimanjaro. Stage 4 magmatism within the NTD (0.5 Ma to present) is notably more enriched in incompatible trace elements and extends to far more mafic compositions than the prior magmatic periods (Fig. 11). Consistent with these observations, lavas from Stage 4 plot at the enriched end of the Zr/Nb-La/Yb plot (Fig. 11). Similar to the enriched lavas from Stage 1 that erupted on Essimingor, Stage 4 lavas exhibit fractionated MREE/HREE values as seen as elevated values of $(Tb/Yb)_{CN}$ (Fig. 11). However, the Type II magma pattern (Fig. 13) suggests an origin from a metasomatically-influenced source for these lavas and caution is advised in the interpretation of the cause of this fractionation. When individual volcanic units are examined in detail, there is significant overlap between most of the volcanoes in major and trace element composition (Fig. 17). Lavas exhibit progressive crustal contamination towards a radiogenic $^{87}Sr/^{86}Sr$ and unradiogenic $^{143}Nd/^{144}Nd$ endmember (Fig. 17). An exception to this are the Kibo lavas of Kilimanjaro, which exhibit no clear evidence of any crustal assimilation despite the low MgO values inherent to that lava suite (Fig. 17). Pb isotopes form a somewhat tighter array in comparison to earlier magma series (Fig. 14), extending from dominantly radiogenic values at volcanoes such as Burko towards significantly less radiogenic values at Oldoinyo Lengai and Meru (Fig. 17). See the previous section for fuller description of the origin of magmatism in the NTD.

The vast majority of data from carbonatite rocks within the rift at this time are centered on the magmatic edifice of Oldoinyo Lengai. Carbonatite lavas from Oldoinyo Lengai exhibit distinctive compositions in terms of being natrocarbonatites but also in terms of their trace element characteristics. Specifically, extreme depletions in Th, Ta, Zr, Hf, and Ti are diagnostic of this carbonatite (Fig. 19). Eruptions at Oldoinyo Lengai are not solely carbonatite and can have mixed magmas. During the 2007/8 eruption hybrid compositions were generated and a silicate magma with carbonatite contributions was erupted (Bosshard-Stadlin et al., 2014). This hybrid material does not fall along the typical evolution pathways common in the rift and, for

example, plots at very high CaO/Al_2O_3 at relatively low MgO values (Fig. 17). The hybrid magma roughly follows a similar pattern to the carbonatite in terms of primitive mantle normalized values but the anomalies are much more muted (Fig. 19). Some rare calciocarbonatites found at Oldoinyo Lengai have compositions far more enriched in trace elements than either the natrocarbonatite or silicate phases (Keller et al., 2006). These calciocarbonatites are low temperature alteration products resulting from trace element enrichment and mineral breakdown from a natrocarbonatite protolith and should not be confused with primary carbonatite magma (Keller et al., 2006). A fuller discussion of carbonatite lava genesis is described in Part V of this synthesis (Rooney, 2020c).

5 THE WESTERN BRANCH

5.1 Rungwe Volcanic Province

This volcanic province lies at the intersection of the Malawi (Nyasa) Rift, Rukwa Rift, and Usangu Basin and occupies approximately 1500 km^2 (Ebinger et al., 1989, 1997; Fontijn et al., 2012). Lavas erupted in this province differ from the others in the western branch in that they are not ultra-potassic, or ultra-sodic (Furman, 1995). The relationship between the modern tectonic structure in the region and magmatism remains controversial (Roberts et al., 2012; Mesko et al., 2014). Indeed, geophysical evidence is consistent with thermal weakening of the lithosphere (and associated volcanism) preceding rift-related fault development (Grijalva et al., 2018). This model is consistent with geochemical evidence in Rungwe Volcanic Province lavas of slightly younger magmatism showing elevated mantle temperatures (Rooney et al., 2012b), compositional characteristics of erupted lavas requiring a metasomatized lithospheric mantle source (Furman, 1995), and primordial helium and neon isotopes (Hilton et al., 2011; Halldórsson et al., 2014), which together indicate the influence of the African Superplume on the

continental lithospheric mantle. Thus, the existing evidence suggests that volcanism may be associated with thermal destabilization of the continental lithospheric mantle by the African Superplume – a process which is thought to have continued throughout the development of the province.

Early work by Harkin (1960) still provides an important basis for modern observations, and a very detailed and review of the Rungwe Volcanic Province has been published by Fontijn et al. (2012); the interested reader is advised to consult that publication for more in-depth discussion of the magmatism of the region. In the following discussion I follow the nomenclature of Fontijn et al. (2012), who collated the existing age dates and stratigraphic constraints to demonstrate three periods of magmatic activity in the late Cenozoic. To these three periods we add an earlier period from 26 Ma to 17 Ma, during which time very alkaline magmas were erupted. These earlier events have been noted by Fontijn et al. (2012), but are not strictly connected with the Rungwe Volcanic Province, which began developing at ca. 9 Ma. I have attempted to place existing data within this temporal framework (Fig. 20), however ambiguities in location information have likely resulted in inaccuracies in the assignments. In particular, most existing work has classified samples on the basis of the edifice from which they were taken, however as of the writing of this document, the region is undergoing significant geophysical, and geochemical investigation that will likely yield further insights into the region in the near future.

5.1.1 Phase 1 - Limited Alkaline Volcanism 26-17 Ma

Roberts et al. (2012) present clear evidence using multiple dating methods of a temporally well-constrained carbonatite eruption in the region at 26 Ma. The eruption of this tuff was argued to be synchronous with rift development and uplift (Roberts et al., 2012). However, the eruption of

this tuff appears to have been isolated event, as no further volcanism is recorded in the region until ca. 19 Ma (Rasskazov et al., 1999, 2003; Mesko et al., 2014). Isolated carbonatite volcanoes are common in the region, and have erupted as a result of lithospheric disturbance since at least the Neoproterozoic (Boniface, 2017) – e.g., the 165.7 Ma (± 1.3) Panda Hill carbonatite, and the 154.2 Ma (± 0.9) Mbalizi carbonatite (Mesko et al., 2014). This phase of activity, lasting from 17.6-18.51 Ma (errors not provided; Mesko et al., 2014) or 17.3 Ma (± 0.3 $^{40}Ar/^{39}Ar$) to 18.6 Ma (± 1 $^{40}Ar/^{39}Ar$) (Rasskazov et al., 2003), is also dominated by alkaline magmas but in contrast to the 26 Ma episode, the actual volcanic centers have been identified. During this phase, phonolite domes occur within the Usangu Basin (Fontijn et al., 2012; Mesko et al., 2014) and a single mafic flow is evident on the uplifted Mbeya block. The Kiwira Series, previously considered part of the older extrusives (e.g., Harkin, 1960) have yielded an age of 18.56 Ma (± 1.03 $^{40}Ar/^{39}Ar$) (Ivanov et al., 1999), and thus are now attributed to Phase 1. It should also be noted that the lava flow along the Kiwira River itself (once considered one of the oldest flows in the region on the basis of morphology) has been dated to 0.04 Ma (± 0.02 $^{40}Ar/^{39}Ar$) (Ivanov et al., 1999). Such unexpected temporal relationships attest to the complexity of categorizing lavas in the province.

5.1.2 Phase 2 - Early Rungwe Volcanic Province volcanism. (9.2 to 5.45 Ma)

Volcanism within the Rungwe Volcanic Province proper differs to that of the earlier phase in that it is intimately linked with faulting (Ebinger et al., 1997), and shows distinct cycles of activity that initiate with effusive basaltic and phonolitic flows, with later pyroclastic events (Fontijn et al., 2010a, 2011, 2012). The earliest phase of activity within the Rungwe Volcanic Province is bounded by the 9.2 Ma (± 0.4) Usangu trachytic dome and the 5.45 Ma (± 0.21) Mbaka older basalts (Ebinger et al., 1989; Ivanov et al., 1999; Fontijn et al., 2012). Volcanoclastic rocks are common in the Rungwe Volcanic Province (Fontijn et al., 2010a, 2010b, 2013) and important

markers such as the Songwe Tuffs are widespread (Ebinger et al., 1989, 1993a). In addition, widely erupted basaltic and phonolitic units occur during this period that include the 7.43 Ma ± 0.19 Alton basalts and phonolites, and the 5.52 Ma (± 0.03 $^{40}Ar/^{39}Ar$) Masukulu phonolites (Ebinger et al., 1993a).

5.1.3 Phase 3 – Intermediate Rungwe Volcanic Province volcanism (3.04 to 1.34 Ma)

The intermediate phase of magmatic activity in the Rungwe Volcanic Province is bounded by the 3.04 Ma (± 0.04 $^{40}Ar/^{39}Ar$) Mbeya olivine basalt and the 1.34 Ma (± 0.02 $^{40}Ar/^{39}Ar$) Tukuyu phonolite (Ebinger et al., 1989; Fontijn et al., 2012). This Phase saw significant magmatic activity centered on the Tukuyu shield volcano and the Porotos Mountains (early Ngozi volcano). This period of activity can be difficult to distinguish from the more recent Rungwe Volcanic Province volcanism and prior work has assigned the Ngozi and Tukuyu volcanoes to the more recent phase of volcanic activity. However, the compilation of age dates by Fontijn et al. (2012) clearly show that the Tukuyu shield predates the modern volcanic episode (1.34 Ma ± 0.02 to 2.25 Ma ± 0.07) (Ebinger et al., 1989; Ivanov et al., 1999). The recognition that the Tukuyu shield belongs to an earlier phase of magmatic activity may help explain geochemical observations of an abrupt boundary in lava composition between the basanite lavas of Tukuyu and the adjacent (and younger) nephelinite lavas of Kyejo (Furman 1995). Katete volcano is tentatively assigned to this period based on a single date of 2.35 Ma (± 0.04) (Ebinger et al., 1989), though little further information is available. Ngozi volcano is typically considered a recent volcanic center due to the young explosive volcanism associated with the 0.010 – 0.012 Ma Kitulo pumice and more recent Ngozi tuff (Fontijn et al., 2010b). However, other than the modern caldera, the edifice of Ngozi is itself indistinct and is typically described as the Porotos

(Poroto) Range that connects Ngozi and Katete volcanoes. An age date of 2.2 Ma (± 0.2) (Ebinger et al., 1989) has been obtained from the Porotos Range, which implies that it should be classified as an intermediate age (and by extension, the main body of the Ngozi edifice). It should be noted, however, that the northern side of the Porotos Range exhibits a significant volume of volcanism that is attributed to stage 4 (Fontijn et al., 2012). It is thus unclear how to categorize lavas that have been assigned to the Porotos Range or Ngozi volcano without further specific location or geochronologic information.

5.1.4 Phase 4 – Recent Rungwe Volcanic Province volcanism (0.57 Ma to Present)

The final phase of magmatic activity in the region is constrained by the 0.57 Ma (± 0.01 $^{40}Ar/^{39}Ar$) Porotos/Usangu olivine basalt and the ca. 1800 AD eruption from the Sarabwe and Fiteko parasitic cones on the flanks of Kyejo (Harkin, 1960; Ebinger et al., 1989; Fontijn et al., 2012). Magmatic activity during this Phase is dominated by Rungwe Volcano, the Kyejo (Kiejo) complex, Ngozi volcano, and the northern reaches of the Porotos Range (Fontijn et al., 2012). A recent chain of cinder cones (0.10 Ma ± 0.11) (Ebinger et al., 1989) is aligned with the Mbaka fault, and the major volcanic edifices exhibit frequent parasitic volcanism along fissure zones (Ebinger et al., 1989). Similarly young activity is seen in the northwest along the Mbeya Range Fault. This fault-related cone activity extends to the basin floor, where small edifices are common and aligned with faults (Furman, 1995). A wide range of compositions were erupted during this cycle extending from picrites at Rungwe and Mbaka, to phonolitic to trachytic tuffs derived from Rungwe and Ngozi volcano (Fontijn et al., 2010b, 2013).

5.1.5 Geochemical Variation within the Rungwe Volcanic Province

Lavas within the Rungwe Volcanic Province have been divided into the four temporal phases previously identified. There is complete overlap between the units from a geochemical perspective. Notable differences include a wide range of magma evolution during Phase 4 at Rungwe (Fig. 21), though this likely reflects sampling bias. Similarity between the Phases extends both to REE patterns (Fig. 22) and primitive mantle normalized patterns (Fig. 23). Rungwe lavas all exhibit Type III lava patterns but are notable for both a more pronounced negative K anomaly than normally seen in Type III and a profound negative anomaly in both Zr and Hf (Fig. 23). The magnitude of this negative K and Zr-Hf anomaly increases during Phase 3 and 4 magmatism (Fig. 21; 23).

Furman (1995) showed that the source within the Rungwe Volcanic Province likely contained an array of metasomatic phases including – amphibole, zircon, ilmenite, and phlogopite. These phases likely controlled the incompatible trace element behavior and the unusual fractionation patterns observed. Apatite, which was raised as a possible metasomatic phase by Furman (1995) was further explored by Ivanov et al. (1998) in terms of the pronounced negative Zr-Hf anomaly. Ivanov et al. (1998) describes the possible origin of this signature in terms of: liquid immiscibility, accessory ore minerals, mixing of carbonatite and silicate melts, melting of metasomatized mantle. Ivanov et al. (1998) reasons that the signature is most likely related to melting of metasomatized mantle and that the negative Zr-Hf anomaly related to the presence of apatite in the metasomatic source. This assertion is consistent with observations that the rocks which display the most pronounced Zr-Hf anomalies also are the most enriched in P, and that the anomaly decreases in parallel to the P content of lavas from the Rungwe Volcanic Province. Similar geochemical characteristics are evident in Pliocene-Quaternary metasomatically influenced lavas from the Bale Mountains on the Eastern Ethiopian plateau (Nelson et al., 2019), strengthening a potential metasomatic origin for this signature. It remains a question as to why rocks from the Rungwe Volcanic Province, given the hypothesis

that they are a mix of lithospheric metasome and sub-lithospheric domains, do not exhibit a Type IV lava signature; this may suggest compositional differences between the metasome sampled here and those from parts of the Eastern Branch of the EARS.

Excluding one sample exhibiting evidence of crustal assimilation, the remaining Rungwe Volcanic Province samples do not show any systematic variation with MgO (Fig. 21), suggesting limited control on the isotopic ratios from incorporation of the continental crust. This is consistent with the limited variation in in $^{143}Nd/^{144}Nd$ (0.5124-0.5126) and $^{87}Sr/^{86}Sr$ isotopes (~0.7045-7055) (Fig. 24). Despite this limited variation in terms of Sr and Nd isotopes, Pb isotopes exhibit a significant range from $^{206}Pb/^{204}Pb$ of 18 to 20, forming a linear array (Fig. 24). The one sample exhibiting crustal contamination is deflected towards the PAL endmember. These Pb isotope characteristics are consistent with observations from the Northern Tanzania Divergence where crustal assimilation drove compositions towards a component similar to the PAL endmember in Pb isotope space, and that primitive magmas exhibited a range of Pb isotope values with limited co-variation in Sr and Nd isotopes. It should be noted that Os isotopes from the Rungwe Volcanic Province have exhibited characteristics consistent with small amounts of crustal assimilation, though the volumes may be too small to detect in other isotopic systems (Nelson et al., 2012).

Previous work in the region has resulted in the necessity of at least three endmembers in order to describe the isotopic variations (Furman and Graham, 1994; Ivanov et al., 1998). These three components are described as: (1) Metasomatized amphibole- and apatite-bearing mantle with $^{87}Sr/^{86}Sr$ of 0.7048-0.7052, and a distinctive negative Zr-Hf anomaly. Ivanov et al. (1998) link this component with the third component mentioned by Furman and Graham (1994) as having less radiogenic Pb isotopes. This metasome may have originated within the Usangu belt during the Early Proterozoic. (2) A Modern component with $^{87}Sr/^{86}Sr$ of 0.7045 and $^{206}Pb/^{204}Pb > 18.9$, displaying no Zr-Hf anomaly. This component may be related to a more

recent metasomatism of the lithospheric mantle, as the lack of correlation between Rb/Sr, 1/Sr and Sr isotopes does not suggest significant radiogenic ingrowth. This component is seen only in the south of the province. (3) Ancient Rb-enriched mantle (containing mica) with $^{87}Sr/^{86}Sr$ of 0.7056, unradiogenic $^{206}Pb/^{204}Pb$ and more radiogenic $^{208}Pb/^{204}Pb$, again with no Zr-Hf anomaly. This component is restricted to lavas from the northern part of the Rungwe Volcanic Province and it is assumed is associated with the Tanzania craton, which lies further to the north. Furman and Graham (1994) suggest an origin within either an enriched lithosphere or crust.

More recent work has provided new insights into the possible mantle endmembers contributing to magmatism within the Rungwe Volcanic Province. Hilton et al. (2011) presented $^{3}He/^{4}He$ isotopic data showing the presence of significantly elevated values in lavas of all ages within the Rungwe Volcanic Province. Such an observation requires a mantle plume contributes to magmatism, but the manner by which this contribution is made remains unclear. Castillo et al. (2014) present a model whereby magmatism within the Rungwe Volcanic Province is the result of binary mixing between a new plume component titled 'V' and the continental lithosphere, which has been fluxed by the same component over an extended period. The 'V' component is defined as having high $^{3}He/^{4}He$, $^{143}Nd/^{144}Nd = 0.5127$, $^{87}Sr/^{86}Sr = 0.7045$, $^{206}Pb/^{204}Pb = 19.4$, $^{207}Pb/^{204}Pb$ ~15.65 (Fig. 24). The suggested mixing between the continental lithosphere and 'V' component in terms of $^{143}Nd/^{144}Nd$ and $^{87}Sr/^{86}Sr$ does encompass the data *as a whole* within the Rungwe Volcanic Province, however, samples that should have greatest hypothesized contribution from 'V' (i.e. those displaying the highest $^{3}He/^{4}He > 14$ and most radiogenic $^{206}Pb/^{204}Pb > 19.8$) plot at the lithospheric end of the array ($^{143}Nd/^{144}Nd = 0.512447$-$0.51247$ and $^{87}Sr/^{86}Sr = 0.70518 – 0.70559$) (Fig. 24). These same samples also exhibit very radiogenic $^{207}Pb/^{204}Pb$ values (15.716-15.743), indicating that the Pb (in addition to the Sr and Nd) budget of these lavas is not controlled by contributions from the hypothesized 'V' component (Fig. 24), and instead suggest that lithospheric mantle associated with the Tanzania craton may be

influencing the isotopic compositions in these samples, consistent with their location in the northern part of the Rungwe Volcanic Province (c.f. Ivanov et al., 1998). These observations present difficulties for a simple binary mixing solution. Further discussion of the 'V' component is presented in Part V of the synthesis series (Rooney, 2020c).

The observations of complex relationships between the different isotopic systems could potentially reflect a role for differential melting of domains within the lithospheric mantle. The existing (limited) data show that more silica-undersaturated samples exhibit more radiogenic values of $^{206}Pb/^{204}Pb$ within the Rungwe Volcanic Province (Fig. 24) and might suggest a linkage between lithology and isotopic signatures – significantly more work will be needed to explore these observations. While the precise mechanisms by which the melting occurs in the lithospheric mantle are unclear, a modified version of the original three component models suggested by Furman and Graham (1994) and Ivanov et al. (1998) may resolve the isotopic observations. This model would permit a larger range in Pb isotopes within endmember 3, which would now extend to much more radiogenic Pb isotopic values (consistent with the samples discussed in the prior paragraph). Endmember 2, which was noted by Furman and Graham (1994) to have $^{3}He/^{4}He$ ~9 (above normal SCLM) would now extend to 15. Thus, Endmember 2, which was considered by Ivanov et al. (1998) to reflect a relatively recent metasomatic input into the lithosphere, would now represent modern plume additions to the lithospheric mantle. Lavas erupted within the Rungwe Volcanic Province might be derived from a mix of these three components.

5.2 The Virunga and Kivu Volcanic Provinces

The Virunga and Kivu (sometimes referred to as South Kivu) volcanic provinces occur to the north and south respectively of Lake Kivu within the western branch of the EARS (Fig. 25).

These provinces are frequently discussed as individual entities given the spatial and compositional differences between them. However, given the temporal similarities in the origin of magmatism, I have grouped the provinces together. The interested reader is referred to the recent review articles by Pouclet et al. (2016) and Barette et al. (2017) for a more detailed account of the structural and geochemical variations within the region. In a broad sense, both the Kivu and Virunga provinces occur in accommodation zones between basins in the rift. The Kivu province manifests as the rift steps westward from the Rusizi Basin in the south, to the Kivu Basin in the north. The majority of magmatic activity within the Kivu province occurs near this accommodation zone in the southern portion of the Kivu Basin, though some lavas extend into the Bugarama graben of the Rusizi Basin (Ebinger et al., 1993a). The Virunga Volcanic Province is located where there is a step in the rift basin to the east. On the basis of the recent geochronological compilation by Pouclet et al. (2016), magmatism in the region can be divided into three distinct periods: An early phase at ca. 21-20 Ma, an intermediate phase at ca. 13 to 4 Ma, and Modern magmatic events (2.6 Ma to present).

5.2.1 The Early Phase (20 to 21 Ma)

Establishing the timing of the earliest magmatic activity in the region had remained somewhat controversial given the ambiguities with the dating methods that have been used in prior studies. K-Ar dates within the western branch of the EARS from earlier publications have generally been subject to extensive debate due to the unusually old ages reported. This has resulted in some skepticism at claims of magmatism commencing earlier than ca. 12 Ma (Bellon and Pouclet, 1980). There is, however, mounting evidence of an early phase in magmatic activity in the western branch. I have previously described the ca. 18-19 Ma activity within the Rungwe Volcanic Province in terms of small alkaline flows and plugs that appeared disconnected from the surface expression of the rifting event; a similar event appears to have occurred within the Kivu-Virunga region. Pouclet et al. (2016) report two ages from nephelinites

occurring as an isolated flow on N. Idjwi Island at 20.97 Ma (± 0.56) and 19.98 Ma (± 1.00), a significant revision of the initial age reported at 28 Ma (± 1.4) (Bellon & Pouclet 1980). An equivalent unit is thought to occur within the Numbi region along the western margin of the rift, though little else is known about this outcrop (Pouclet et al., 2016).

5.2.2 The Intermediate Phase (13 to 4 Ma)

This phase of activity is characterized by synchronous eruptions of largely olivine- and tholeiitic-basalts throughout the region, though more evolved alkaline-series rocks also present (Pouclet et al., 2016). The earliest activity north of Lake Kivu is at Bishusha (12.6 Ma ± 0.7) (Bellon and Pouclet, 1980) and Tongo (11.8 Ma ± 0.8), which have been described as evolved end-members of the basanite-series (Pouclet et al., 2016). Magmatic activity continued here until 8.9 Ma ± 0.5 (Bellon and Pouclet, 1980), whereafter no magmatic events are recorded until the commencement of the modern Virunga Volcanic Province at 2.6 Ma

South of Lake Kivu, magmatic activity commenced at Bugarama at 10.63 Ma (± 0.53) (Pouclet et al., 2016) and consisted of largely tholeiitic flows. Magmatic activity then continued uninterrupted until 4.06 Ma (± 0.21) (Pasteels et al., 1989), primarily consisting of tholeiitic and alkaline basalts (Pouclet et al., 2016). Many authors have further subdivided this intermediate phase with a break at ca. 7.5 Ma corresponding to rift development (Ebinger, 1989b; Furman and Graham, 1999). Magmas erupting prior to 7.5 Ma were focused along faults, while magmas subsequent to this period were centralized in the rift basin. Auchapt et al. (1987) also describes the temporal evolution in terms of increasing alkalinity – i.e. from quartz-normative tholeiites, to olivine-normative tholeiites, to finally alkali basalts and basanites. In this contribution, I do not use this subdivision as it is difficult to ascribe all lavas in the region to a specific period. Furthermore, this subdivision has not been used in some previous geochemical investigations (e.g., Furman and Graham, 1999). There is, however, a spatial division in rocks from this period – the Bukavu and Mwenga-Kamituga provinces (e.g., Auchapt et al., 1987). Despite parallels

between the types of rocks erupted in both provinces, lavas of the Mwenga-Kamituga province are typically more enriched in the more incompatible trace elements (with the exception of Rb), in comparison to lavas from the Bukavu province (Auchapt et al., 1987). In the Bukavu province, lavas exhibit among the least radiogenic $^{87}Sr/^{86}Sr$ and most radiogenic values of $^{143}Nd/^{144}Nd$ in the western branch, suggesting that in addition to metasomatized lithospheric mantle, contributions from sub-lithospheric reservoirs are also required (Furman and Graham, 1999). In contrast, relatively little is known about the isotopic characteristics of the Mwenga-Kamituga province.

5.2.4 Modern Magmatic Events (2.6 to Recent)

Virunga Volcanic Province

Magmatic activity in the modern Virunga Volcanic Province is thought to commence ca. 2.6 Ma with eruptions at Mikeno volcano (Guibert et al., 1975). This date is, however, an outlier for the province as a whole, and thus the specific timing of the initiation of magmatism is not well constrained. Few radiogenic dates exist within the Virunga Volcanic Province, and these existing dates return ages less than 0.2 Ma (Sabinyo), but typically younger than 0.1 Ma (all other edifices) (De Mulder et al., 1986; Rogers et al., 1998; Barette et al., 2017). Existing geochronological evidence would therefore suggest that majority of the Virunga Volcanic Province has developed over the past 100,000 years.

The Virunga Volcanic Province is distinctive in comparison to the other areas within the region in that magmas are potassic (shoshonitic: Hudgins et al., 2015). This has resulted in some complexity in naming protocols for the lavas; the mostly commonly used scheme is modified from the IUGS system by applying the same names but a “K” prefix – e.g. K-hawaiite (e.g., Rogers et al., 1998; Pouclet et al., 2016). Leucite is a common phase in many of the

lavas, denoting shallow fractionation conditions (Sack et al., 1987). The origin of the particularly unusual compositions is almost universally ascribed to mantle metasomes containing amphibole and phlogopite within the lithospheric mantle.

While some authors have ascribed a direct mantle plume origin for Nyiragongo lavas (Chakrabarti et al., 2009a), the isotopic composition of these lavas are inconsistent with “C”-like plume-derived lavas deduced elsewhere in the rift in terms of Sr-Nd-Pb isotopes, and He isotopes (Rooney et al., 2012b; Halldórsson et al., 2014) – see Part V (Rooney, 2020c). Furthermore, the proposed carbonatite-influenced source for Nyiragongo may be related to an earlier metasomatic event (Condomines et al., 2015). Potential recent plume-derived metasomatism may, however, play a role in partially overprinting existing mantle metasomes.

Magmatic activity is dominated by the development of large central volcanoes. These edifices (Nyamuragira, Nyiragongo, Mikeno, Karisimbi, Bisoke (Visoke), Sabinyo, Gahinga (Mgahinga), and Muhabura (Muhavura)), are cut by faults and exhibit abundant parasitic cones that are frequently aligned. Cinder cones may occur in the regions between the edifices (e.g., abundant cones between Bisoke and Sabinyo) or on the rift floor distant from any central volcano (e.g. Bufumbira volcanic field). The Virunga Volcanic Province is divided by the N-S trending Virunga fault, which separates the current active volcanoes of Nyamuragira and Nyiragongo in the Albert Rift, from the slightly older edifices to the east (Platz et al., 2004), with the exception of the 1957 eruption of Bisoke. The volcanoes that lie outside the Albert Rift are sometimes collectively referred to as ‘Bufumbira’, however I use the term “Bufumbira volcanic field” following Hudgins et al. (2015) who describe it as field of ~40 cinder cones with basanitic to trachy-andesitic compositions.

Nyamuragira. This volcano is among the most active in the world, having produced at least 16 effusive eruptions between 1980 and 2010 (Head et al., 2011). Compositionally, the volcano dominantly produces lavas in the magma series that extends from olivine basanites through

phonolites, and is distinctly less alkaline than neighboring Nyiragongo (Aoki and Kurasawa, 1984; Barette et al., 2017). Over the past century, lava compositions have been relatively similar, averaging 4-6 % MgO, with some lower MgO (<4%) values in the 1970s and an extremely primitive lava (MgO = 13.5%) erupting in 1912 (Aoki et al., 1985; Head et al., 2011)(Aoki et al., 1985; Head et al., 2011). Studies of melt inclusions constrain the magma chamber beneath Nyamuragira to be between 3 and 5 km depth (Head et al., 2011). Further INSAR investigations of the volcano have revealed that, in addition to the ca. 4 km shallow reservoir, a deeper ca. 25 km magma chamber may feed eruptions more distal to the caldera, and the shallow magma chamber beneath the edifice (Wauthier et al., 2013).

Nyiragongo. This edifice exhibits particularly alkaline, Si-undersaturated lavas that generally follow a melilite lava series (Barette et al., 2017). The volcano is a composite structure comprising of the parasitic Baruta, and Shaheru cones with the youngest - Nyiragongo cone dominant (Demant et al., 1994). The early flows of the volcano are not exposed, and the frequent activity make it probable that only Holocene aged materials are exposed (Demant et al., 1994). Flows from the volcano can be areally very extensive (e.g., 1977 flows) but only be centimeters thick (Demant et al., 1994). Much of the petrographic variation is derived from the flotation of feldspathoids (Demant et al., 1994). Indeed, extensive fractionation of leucite and subordinate nepheline within the volcano edifice itself has been proposed as the primary mechanism driving magma variability (Hertogen et al., 1985; Platz et al., 2004), though instances of crustal assimilation have also been noted (Chakrabarti et al., 2009a). As with most volcanoes in the province, there are abundant small parasitic cones – the most pronounced of which are termed the “Rushayo chain”, a collection of about 20 cones orientated in a northeast trend (Demant et al., 1994). The Rushayo chain erupts olivine melilites, which has been proposed as composition of the primitive lavas that fractionate to form the main lavas series at Nyiragongo (Platz et al., 2004). Rare alkali olivine basalts have also been noted (Platz et al.,

2004). Many authors have remarked at the compositional distinction between lavas erupting from Nyiragongo and Nyamuragira, despite the close proximity of both edifices (15 km). The differences in composition extend to isotopic heterogeneity – Nyiragongo exhibits less radiogenic values of $^{87}Sr/^{86}Sr$, $^{207}Pb/^{204}Pb$, and $^{208}Pb/^{204}Pb$ in comparison to neighboring Nyamuragira (Chakrabarti et al., 2009a).

Mikeno. This is the oldest of the volcanoes in the Virunga Volcanic Province, and it may date to 2.6 Ma, though activity continued to ca. 0.2 Ma. The antiquity of this edifice is consistent with highly eroded profile. Lavas from this volcano are thought to be most similar to the melilite series evident on Nyiragongo (Pouclet et al., 2016).

Karisimbi. This volcano has been built of many thin flows of K-basanite and K-hawaiite, and has an earliest recorded activity dated at 0.14 Ma (± 0.06) (De Mulder et al., 1986). Karisimbi exhibits a pronounced differentiation pathway, which is a mixture of fractional crystallization and assimilation of the shallow crust (De Mulder et al., 1986; Sack et al., 1987; Rogers et al., 1992). Primitive K-basanites (those with >4% MgO) do not exhibit signs of this crustal assimilation event and have been thought to be derived from the lithospheric mantle (Rogers et al., 1992).

Bisoke (Visoke). This is the only volcano in the Virunga Volcanic Province outside of the Albert Rift that has erupted in historic times. This 1957 event manifested as two cinder cones along the volcano flank and an olivine-melilite flow (Condomines et al., 2015). This 1957 flow is thought to be derived from melting of a metasomatized garnet-bearing lherzolite (Condomines et al., 2015). U-Th and Ra isotopes reveal that the source of the 1957 lava flow resembles that of Nyamuragira, though with a much smaller degree of melting at Bisoke (Condomines et al., 2015). Flows from this edifice have been divided by Pouclet et al. (2016) into old Bisoke (K-basanite series), and new Bisoke (melilite series).

Sabinyo. This edifice is the second oldest in the province, exhibiting ages up to 0.176 Ma (± 0.03 $^{40}Ar/^{39}Ar$) (Rogers et al., 1998). The lavas from Sabinyo also are unique compositionally in comparison to other volcanoes in the province by being potassic and silica-saturated, termed 'latites' by Rogers et al. (1998). These lavas are also unusual in that they are the only ones with evidence of feldspar fractionation in the province (Rogers et al., 1998). Isotopically, Sabinyo lavas also have some unusual characteristics that have been described as either mixing of two lavas (one derived from a similar source to Nyiragongo, and another derived from a melt of Precambrian crust) (Vollmer and Norry, 1983). Alternatively, Sabinyo lavas may be derived from the assimilation of the lower crust by ponded lavas. Further work on this edifice will be necessary to resolve these competing hypotheses.

Gahinga. Lavas from this volcano follow a broadly similar differentiation trend as those from Karisimbi (Barette et al., 2017), and can be classed as following the K-basanite magma series (Rogers et al., 1998; Pouclet et al., 2016). Isotopic values of Gahinga lavas indicate some degree of assimilation is possible in the more evolved samples (Rogers et al., 1998).

Muhabura (Muhavura). Lavas from this volcano are considered to fall into the K-basanite magma series (Rogers et al., 1998; Pouclet et al., 2016). While most Muhabura lavas have relatively high SiO_2 (45-55 wt. %), another group of lavas have lower values of 43-46 wt. % (Rogers et al., 1998). The isotopic characteristics of this low-silica group trend towards K-basanites from Karisimbi, suggesting similarities in the mode of origin and are consistent with the mixing of a nephelinite and a primitive K-basanite lava (Rogers et al., 1998). It is suggested that the more evolved rocks of Muhabura and Gahinga are derived from this low-silica magma type through combined assimilation and fractional crystallization processes (Rogers et al., 1998). Radiogenic ages are between 0.033 Ma (± 0.009 $^{40}Ar/^{39}Ar$) and 0.052 Ma (± 0.019 $^{40}Ar/^{39}Ar$) (Rogers et al., 1998).

Kivu

After a hiatus in volcanism commencing at ca. 4 Ma, magmatism began once more in the Kivu volcanic province with the eruption of the 33 km long Tshibinda chain of scoria cones and associated flows between 1.9 Ma (± 0.1) and 1.6 Ma (± 0.3) (Bellon and Pouclet, 1980; Pouclet et al., 2016). The chain continues to Leymera in the north following a ca. 7 km break from the rest of the field. There is a subtle difference of ~0.5 wt. % TiO_2 between Leymera and the rest of the Tshibinda chain, perhaps suggesting heterogeneity in magmas. Volcanics interbedded with lake sediments near Bukavu are interpreted to be Quaternary, but are currently undated (Kampunzu et al., 1984). Other rocks from this region have been dated to 7.18 Ma (± 0.36) to 7.68 Ma (± 0.38) (Pouclet et al., 2016) but the variety of rocks in the area make it difficult to establish the relationship between the dated samples and those analyzed by Kampunzu et al. (1984). The most recent confirmed magmatic event in the Kivu province is a picritic lava flow dated at 0.342 Ma (± 0.10) (Ebinger, 1989a) that is interbedded with the Gisakura terrace lacustrine deposits. There may be some evidence of a magmatic event in Mwenga at 2.6 Ma (Kampunzu et al., 1998), however, the large error (± 1.6 Ma) on the measurement may place this event within the intermediate phase of activity – further study is required here. Magmas erupted in the Tshibinda chain are distinct from all those that preceded them in Kivu, and isotopically resemble magmas erupted in the contemporaneous Virunga Volcanic Province (Furman and Graham, 1999). In contrast, the single Gisakura sample analyzed, is similar to the previous Kivu magmatic events, suggesting some degree of spatial variability in the Kivu magmas during this period (Furman and Graham, 1999).

5.2.5 Geochemical composition of lavas from the Kivu Volcanic Field

Lavas at Kivu have been divided into three temporal phases (Early, Intermediate, and Modern). Very little data exists for the Early period of volcanism, but those samples are more mafic than the subsequent two phases (Fig. 21). Kivu Intermediate and Modern overlap in most elements, though the Modern period extends to lower values of TiO_2. A systematic change is evident in terms of the fractionation of MREE/HREE values, which becomes progressively less extreme with time; Early lavas exhibit the highest values of $(Tb/Yb)_{CN}$, while the Modern lavas are the lowest (Fig. 21; 22). During the Intermediate Phase a group of samples located along the eastern margin of the province that contained unusually depleted LREE concentrations were erupted (Fig. 22). These lavas, which extended from the Bugarama Graben, through Bitare, and onto S. Idjwi Islands, are tholeiitic and have been noted by prior authors (Furman and Graham, 1999; Pouclet et al., 2016). These lavas have been modelled as higher degree of partial melting of sources that are broadly similar to other more alkaline lavas in the province (Pouclet et al., 2016).

Kivu lavas exhibit consistent Type II lava patterns with pronounced depletion in K, Zr-Hf, and Ti (Fig. 23). The more enriched the incompatible trace element profile of a sample is, the larger the magnitude of the negative anomalies (Fig. 23). It should also be noted that the appearance of these anomalies is somewhat dependent on the ordering of the elements used in the primitive mantle normalized plot. For example, in the Sun and McDonough (1989) table used for primitive mantle normalized values within this work, Sm follows Nd (with F in between the two), however the primitive mantle normalized figure in that paper orders the elements Nd, Zr-Hf, Sm. How an author has ordered the elements can have a profound impact on the appearance of a Zr-Hf anomaly.

For the Early Kivu lavas, the normalized value of Nd is about 68, 29 for Sm, 17 for Zr, and 10 for Hf. Moving Sm to the other side of the Zr-Hf pair thus creates the impression of a progressive decrease in concentration from 68(Nd)-29(Sm)-17(Zr)-10(Hf). This contrasts to the

way in which the data is presented here: 68(Nd)-17(Zr)-10(Hf)-29(Sm). Similarly, some authors have arranged Gd to the left side of Ti on such plots, impacting the appearance of potential Ti anomalies. While Gd is not presented on the primitive mantle normalized figure in Sun and McDonough (1989), for mantle normalized diagrams in McDonough and Sun (1995) Gd is placed on the right side of Ti (as is the order in the original table from Sun & McDonagh, 1989). While these details may seem didactic, it is important that the reader be aware of the potential differences in patterns between primitive mantle normalized plots when considering potential anomalies.

Neither $^{87}Sr/^{86}Sr$ nor $^{143}Nd/^{144}Nd$ exhibit any correlation with MgO, suggesting a limited influence of the continental crust on magma isotopic composition (Fig. 21) (Furman and Graham, 1999). Lavas from Kivu typically plot at relatively more radiogenic values of $^{143}Nd/^{144}Nd$ and less radiogenic $^{87}Sr/^{86}Sr$ in comparison to lavas from the Rungwe Volcanic Province, except for modern lavas along the Tshibinda volcanic field. No Pb isotope data has been published on the Kivu volcanic field. Furman & Graham (1999) describe the variability in both trace element ratios and Sr-Nd isotopic values of rocks erupted in Kivu as reflecting small-scale heterogeneities in the mantle sources of these lavas, which are interpreted to be within the lithospheric mantle. The trace element composition requires the presence of amphibole in the source of Kivu lavas more broadly, but with some minor phlogopite in the source of magmas for Tshibinda (which typically resembles lavas within the adjacent Virunga Volcanic Province) (Furman and Graham, 1999). The particularly unradiogenic $^{87}Sr/^{86}Sr$ and radiogenic $^{143}Nd/^{144}Nd$ values evident in some lavas from Kivu point towards an asthenospheric influence on lavas erupted in this province (Furman and Graham, 1999). For the two samples with corresponding isotopic and trace element data, it is clear that the asthenospheric-like isotopic values correlate with less pronounced Zr-Hf anomalies, and trend towards a Type IV lava signature (Fig. 23).

These data support a model whereby asthenospheric melts are mixing with melts derived from a metasomatized lithospheric mantle (Furman and Graham, 1999).

5.2.6 Geochemical composition of lavas from the Virunga Volcanic Province

In comparison to other parts of the East African Rift, the Virunga Volcanic Province has a greater array of data collected on lavas erupted there. This wealth of data allows for a volcano-by-volcano examination of the geochemical composition of erupted lavas. The most conspicuous structures in the region are Karisimbi, followed by the recently active edifices of Nyamuragira and Nyiragongo, the three of which dominate the geochemical dataset. Existing work on the Virunga Volcanic Province identified two primary magma series – a leucite-melilite nephelinite series typified by lavas from Nyiragongo, and a leucite basanite series typified by lavas from Nyamuragira (Pouclet et al., 2016; Barette et al., 2017).

Nyiragongo, Mikeno, and younger Bisoke lavas exhibit similar compositional characteristics consistent with their common leucite-melilite lava series (Fig. 26). Notably these edifices erupted lavas that have high CaO/Al_2O_3, fractionated MREE/HREE, an enrichment in incompatible trace elements such as Nb, exhibit negative K and Zr-Hf anomalies, and possess an overall Type II lava pattern (Fig. 26; 27; 28). The negative Zr-Hf anomalies and HREE depletion results in particularly low values of Zr/Nb and elevated La/Yb for these edifices (Fig. 26). Despite similarities in the major and trace element characteristics, Nyiragongo plots at distinctly more radiogenic values of $^{143}Nd/^{144}Nd$, and unradiogenic values of $^{208}Pb/^{204}Pb$ and $^{87}Sr/^{86}Sr$ in comparison to all other lavas in the region (Fig. 29). While Bisoke and Mikeno lavas are deflected towards Nyiragongo, they overlap the field of other edifices. These observations

suggest that Nyiragongo lavas are a more pure form of the mantle endmember that melted to create lavas from this magma series.

The leucite basanite series forms the primary magmas at Nyamuragira, Karisimbi, Sabinyo, Muhavura, old Bisoke, and Gahinga (Pouclet et al., 2016). These volcanoes largely overlap in terms of major elements, trace elements, and Sr-Nd-Pb isotopes (with the exception of Sabinyo, discussed later). The primitive mantle normalized trace element patterns of lavas erupted in these edifices differ from other lavas erupted in the region and does not conform to any of the previously recognized lava types. This pattern is characterized by a somewhat flat pattern on the most incompatible side of the primitive mantle normalized figure, with small negative anomalies in U and K, and a mild depletion in Zr-Hf (Fig. 28). We classify this pattern as Type V and suggest that the type patterns for this lava are the more primitive endmembers at Nyamuragira and Bufumbira. Furman & Graham (1999) attribute this magma series to melting of a phlogopite-bearing metasome within the lithospheric mantle.

Sabinyo appears to have been significantly contaminated with crustal materials – manifesting as a progressive decrease in $^{143}Nd/^{144}Nd$ and Nb, and an increase in $^{87}Sr/^{86}Sr$ with decreasing MgO (Fig. 26). These contaminated lavas from Sabinyo help explain the unusual variation in Pb isotopes in the Virunga Volcanic Province where little difference in $^{206}Pb/^{204}Pb$ (~19.5) is recorded but an array of $^{208}Pb/^{204}Pb$ compositions (39 – 41.5) are evident (Fig. 29). Lavas in the Virunga Volcanic Province exhibit progressive contamination whereby more evolved lavas typically exhibit elevated $^{208}Pb/^{204}Pb$ values (Fig. 29). Parallel converging arrays for Karisimbi are particularly clear, while other edifices have less clear trends (Muhavura shows no clear change in the isotopic ratio with melt evolution). These data suggest contamination of the lavas with a source that has relatively radiogenic $^{206}Pb/^{204}Pb$ (~19.5) and very radiogenic $^{208}Pb/^{204}Pb$ (42+). Such high Th/Pb contaminants have been seen elsewhere in the rift, and control magma evolution at Tarosero in the NTD and Naivasha from the Kenya Rift, though the

$^{143}Nd/^{144}Nd$ value of that contaminant was markedly more radiogenic (Fig. 16; 18). The $^{143}Nd/^{144}Nd$ values of lavas from Sabinyo (nearing 0.5120) extend to some of the least radiogenic in the East African Rift and suggest the influence of old continental crust.

Existing work on the Virunga Volcanic Province has suggested the influence of a carbonatite metasomatic fluid on the magma source (Dupuy et al., 1992; Furman and Graham, 1999; Chakrabarti et al., 2009a; Pouclet et al., 2016). Much of the support for this model comes from fractionation of Zr from Hf and the overall enrichment of REE over HFSE. As noted by Ivanov et al. (1998), the depletion in Zr-Hf in lavas within the Rungwe Volcanic Province likely results from the influence of apatite. Notably, lavas from Nyiragongo, which have been highlighted as potentially having a carbonatite-metasomatized source (Pouclet et al., 2016), may also reflect the influence of apatite in their source or during fractional crystallization. There is a strong correlation between fractionated values of Zr/Hf (>50) and high P_2O_5 concentrations (>1 wt. %) in these same lavas. Excluding two outliers, no lava with <1 wt. % P_2O_5 exhibits fractionation of Zr/Hf (Fig. 26). Presuming apatite melts (i.e. it is not residual in the mantle), an apatite-based fractionation of Zr/Hf is consistent with experimental work that showed that the apatite-melt partition coefficient ratio (D_{Zr}/D_{Hf}) ranged from 2.7 to 4.6, and that mineral-melt partition coefficients for Zr and Hf were significantly lower than adjacent elements such as Sm (Prowatke and Klemme, 2006), resulting in Hf/Sm fractionation in any resulting melt.

Carbonate may be present within the metasomes that melted to form the lavas in the Virunga Volcanic Province (e.g., high CaO/Al_2O_3 and CO_2), however, the origin of this carbonate may not reflect a carbonatite metasomatic liquid, but instead could be related to subduction-related fluids. Hudgins et al. (2015) explored volatile concentrations within melt inclusions from the Virunga Volcanic Province and found that the CO_2-rich melt inclusions had Li/Yb and B/Be values that extended far beyond that typical of MORB and OIB. Hudgins et al. (2015) noted that these values were similar to a slab-fluid or recycled sediments in a subduction zone, and

suggested that metasomatism of the lithospheric mantle during the Pan-African subduction event may be responsible for these volatile additions to the lithospheric mantle. Subduction-related metasomatism, which may have overprinted older metasomes, may thus provide an alternative mechanism for the volatile and trace element enrichment of the lithosphere without the need for widespread carbonatite metasomatism.

While some recent work has hypothesized that lavas within the Virunga Volcanic Province could represent sub-lithospheric melts of a high $^{3}He/^{4}He$ mantle plume (Chakrabarti et al., 2009a; Castillo et al., 2014), the lack of elevated $^{3}He/^{4}He$ and the existence of radiogenic $^{207}Pb/^{204}Pb$ is instead supportive of a lithospheric origin for lavas erupted in the province. Further difficulties with this model center on the inability to generate magmas with the observed alkali contents without the influence of metasomatic phases that are stable only within the lithospheric mantle (Rosenthal et al., 2009). The ultimate origin of lavas from this province is thus inextricably linked with the continental lithosphere.

Rogers et al. (1998) presented a layered lithosphere model whereby volcanism in the Virunga Volcanic Province was derived from two different domains, yielding a nephelinite and a K-basanite component. The leucite-melilitite lava series evident at Nyiragongo is dominated by the nephelinite component. Lavas are typified by less radiogenic $^{87}Sr/^{86}Sr$ isotope ratios and more radiogenic $^{143}Nd/^{144}Nd$ isotope ratios. The nephelinite component is thought to derive from the lower lithosphere, which was impacted by a ca. 500 Ma metasomatic event that may be related to the Pan-African orogeny (Vollmer and Norry, 1983; Rogers et al., 1998). In contrast, the leucite basanite series that is common to the other volcanic centers is dominated by the K-basanite component. These lavas are typified by more extreme isotope ratios that are consistent with an older source. Rogers et al. (1998) suggest a ca. 1 Ga age on the basis of model ages, and reason that it is located at shallower levels within the lithospheric mantle. The 1 Ga overprint on the lithospheric mantle may relate to events surrounding the Kibaran orogeny

(Rogers et al., 1992). This 1 Ga source is described by Furman and Graham (1999) as the common lithospheric mantle component (CLM), evident in magmas more broadly across the region. In reality, lavas erupted in the province may be a mixtures of magmas derived from both sources (Rogers et al., 1998).

In addition to these two primary domains within the lithospheric mantle, variation in $^{207}Pb/^{204}Pb$ in primitive lavas from Karisimbi suggests a potential contribution from even older lithospheric mantle of likely Archean age (Rogers et al., 1992). Thus, a model of a stratified lithosphere has evolved wherein the age of the material within the lithosphere increases with decreasing depth. Thermal input from a mantle plume is thought to have destabilized the metasomes and produced magmatism within the province (Rogers et al., 1998). While no evidence currently exists that unequivocally demonstrates a plume mass contribution to lavas in the Virunga Volcanic Province, the somewhat DMM-like $^{3}He/^{4}He$ signatures seen in lavas from this province (Pik et al., 2006) could suggest some contribution from sub-lithospheric components. Significantly more work will be necessary to constrain the origin of this signature and the potential overprint of the lithosphere that is seen elsewhere in the EARS.

5.3 Toro Ankole Volcanic Province

The Toro Ankole Volcanic Province, which lies north of the Virunga Volcanic Province, is comprised of the Katwe-Kikorongo field, the Bunyaruguru field, the Katunga field, the Ndale field, and Fort Portal field (Rosenthal et al., 2009) (Fig. 25). Existing geochronological constraints point to a very young province, with no evidence of any volcanic events predating 0.050 Ma (Boven et al., 1998). The magmatic activity in the province is dominantly phreatomagmatic (e.g., Boven et al., 1998), which can result in abundant crustal, mantle, and

cumulate xenoliths within the ejected products (Davies and Lloyd, 1989; Lloyd et al., 1991; Muravyeva and Senin, 2018). Consequently, most of the erupted materials in this province are tuffs and ashes with much rarer lava flows. Magmas erupted in the province fall into the ultra-potassic classification and have thus been the subject of extensive nomenclature debates. For example, the region is known for Kamafugites (umbrella term for katungite, mafurite, and ugandite), which can be described as potassic olivine melilitite, olivine-pyroxene kalsilitite, and olivine-kalsilite leucitite to potassic nephelinite (Rosenthal et al., 2009). This debate is not new and some interesting insights on views from Bowen, Shand, and others is presented in Holmes (1937).

The origin of magmatism in this region is considered related to the destabilization of metasomes within the lithospheric mantle (Eby et al., 2009; Rosenthal et al., 2009). Based upon the composition of the potassic lavas, the melt source is likely clinopyroxene and phlogopite dominated veins containing modal carbonate, apatite, and some oxide phases (Rosenthal et al., 2009). The isotopic characteristics of the lavas suggest that the magmas may be mixtures of melts derived from different metasomatic veins: (A) An old MARID-type vein containing phlogopite, and (B) A younger carbonate-phlogopite vein system. This multi-melt model is consistent with Pb isotopic data suggesting the contribution from two distinct reservoirs (Muravyeva and Senin, 2018), and with xenocrystic phlogopite present within the lavas that show a MARID-type vein origin, and a second variety typically associated with metasomatic events in peridotite (Lloyd et al., 2002).

5.3.1 Katwe-Kirorongo

This ca. 30 km long field occurs within the rift floor adjacent to Lake Edward and is comprised of many maars and tuff cones that exhibit a NE-SW alignment (Boven et al., 1998). Carbonatite tuffs are present here but the silicate component of the field dominates, and lava flows are occasionally seen (Stoppa and Schiazza, 2013). Four lava flows are known, and are associated

with the Nabugando and Mbuga craters (Woolley, 2001). Holmes and Harwood (1932), and Holmes (1950, 1956) have described an array of potassic magma types in this region and their mineralogy (i.e., melilite, augite, kalsilite, leucite and K-rich glass). Lloyd et al. (2002) also describe the importance of Ti-bearing phlogopite in these lavas. Given the intense interest in the unusual mineralogical characteristics of the erupted materials in this region, the interested reader is directed to Lloyd et al. (1991) for an effective review of this aspect of the magmatic products in this field.

5.3.2 Bunyaruguru

This field occurs along the uplifted rift margin and is comprised of many closely space vents (Boven et al., 1998). We incorporate the isolated cone of Katunga within this field (the type locality of katungite) (Combe, 1937; Holmes, 1937). A significant amount of work has been published examining the eruptive characteristics of the vents from this region, and in particular the unusual ring structures present in the Bunyaruguru and Katwe-Kikorongo fields (Lloyd et al., 1991).

5.3.3 Ndale

Little is known about this volcanic field though the magmatic products erupted here are considered more related to the silicate volcanism to the south, in comparison to the carbonatite volcanism to the north (Barker and Nixon, 1989).

5.3.4 Fort Portal

The region is dominated by 2-6 m of lapilli tuffs of carbonatite and melilite composition, and two maar/scoria cone clusters (Fort Portal and Kasekere) containing up to 50 edifices (Barker and Nixon, 1989; Eby et al., 2009; Stoppa and Schiazza, 2013). Magma compositions erupting from these cones is interpreted as extremely fluid and the rare lava compositions are defined as calciocarbonatite (Von Knorring and Du Bois, 1961; Bailey et al., 2005; Stoppa and Schiazza,

2013). Currently models for the origin of magmatism in the field center on a common carbonated melilite magma that unmixed to form the two components erupted (Eby et al., 2009).

5.3.5 Geochemical composition of lavas from the Toro Ankole Volcanic Province

Carbonatite lavas from this region are examined in part V of the synthesis series (Rooney, 2020c); the description presented here focuses upon the silicate rocks. Lavas from the Toro Ankole Volcanic Province (Bunyaruguru and Katwe-Kikorongo) define distinctive evolutionary trends that indicate separate parental magmas. While Bunyaruguru extends to much more mafic values than that at Katwe-Kikorongo, the parallel evolution trends of MgO vs Zr and Nb suggest distinctive initial magmas in each of the fields within the Toro Ankole Volcanic Province (Fig. 6). Lavas from both fields exhibit very steep REE patterns, resulting in some of the most extreme fractionation of the LREE, MREE and HREE elements in the East African Rift (Fig. 6). The primitive mantle normalized pattern for these lavas is similar, and resembles Nyiragongo, though there is a more significant negative anomaly of P, and these lavas lack any Ti anomaly (Fig. 28). While some correlation is evident between lower $^{87}Sr/^{86}Sr$ and MgO for Bunyaruguru, the lavas remain very primitive and may reflect mixing between components rather than assimilation. The majority of data from the Toro Ankole Volcanic Province clusters just below the CLM field (Fig. 6) defined by Furman & Graham (1999). Pb isotope ratios for the more primitive samples cluster at $^{206}Pb/^{204}Pb$ 19-19.5 and $^{208}Pb/^{204}Pb$ from 39.25 to 40.25. This region is one of the few to possess Hf isotope data, which reveal an important characteristic – lavas from the Toro Ankole Volcanic Province plot below the Global Mantle Array in Nd-Hf space. Such behavior is exhibited by HIMU but also lithospheric mantle metasomes (Tappe et al., 2008; Rooney et al., 2014). Given the unusual composition of lavas in this region (ultra-potassic) it is probable that the source of these lavas lies within metasomatically enriched portions of the East African Lithospheric mantle. Unlike regions from the eastern branch of the

EARS where $Na_2O>K_2O$, suggesting amphibole as the dominant mineral in these metasomes (Späth et al., 2001), phlogopite is likely a key phase in the mantle source of rocks from this region. Existing isotopic data shows that the composition of rocks in the region is dominated by mixing of two magma types derived from two separate sources. The origin of these sources remains debated, with some supporting a mixed lithosphere-asthenosphere model (Muravyeva and Senin, 2018), while others show evidence for mixing of two melts deriving from vein systems within the lithospheric mantle. In this latter model, one vein is a phlogopite-bearing MARID-type metasome, while the other is a more recent carbonate- and phlogopite-bearing metasome.

Mixed calciocarbonatite-melilitite material from the 6000-4000 year old Fort Portal Carbonatite indicate that both carbonatite and melilitite magmas were contemporaneously liquids (Barker and Nixon, 1989; Eby et al., 2009). Eby et al. (2009) propose a model of liquid immiscibility from a parental carbonated melilite magma that was initially rich in alkalis (K in particular). The carbonatite and melilitite magma have very similar compositions in terms of incompatible trace elements and cannot be readily separated. It was noted, however, that a late stage carbonatite ocelli, which separated from the melilitite, are distinct from the carbonatite lava and lapilli – the carbonate ocelli are extremely depleted in HFSE (Eby et al., 2009), pointing to the complexity of partitioning among the different carbonatite phases.

6 Conclusions

The history of magmatism in this region reflects the progressive development of the EARS. While the precise timing of the initiation of magmatism has been difficult to establish, the events described herein exhibit a clear pattern – an initial pulse of magmatism and extension manifests in Turkana, followed by a hiatus. This pulse then extends southward and manifests as a period of magmatism and extension in the developing rift, and is followed by a waning period that is typified by more evolved volcanism. There already exists a general understanding that Turkana

is the nexus of extension from which rifting has extended to the south and north (e.g., Purcell, 2018). However, this synthesis suggests that the propagation of rifting is not a single event, and that pulsed activity has influenced the development of the rift.

The data presented herein show a lack synchronicity in magmatism and extension throughout the rift during the various phases iterated below. However, these data provide a valuable insight – the hiatuses in magmatism may be as critical as the magmatism itself; they constrain the consistent pattern of pulses of basaltic magmatism that are followed by waning activity. These observations equally extend north of Turkana, also defining the temporal development of the Main Ethiopian Rift (with some additional complexity imposed by the Red Sea System). There are three clear phases of rift development commencing in Turkana at ca. 20 Ma, 12 Ma, and 4 Ma. Each of these events has a subsequent manifestation in the Southern Kenya Rift. The relationship between these pulses of extension and the western branch of the EARS remains less clear. While it is evident that some strain must have been transmitted through the craton given the synchronicity of magmatic activity ca. 20 Ma, 12 Ma, and during the subsequent rift evolution phases, further geochronological work is needed. Magmatic activity in this region is best described using the following six temporal divisions:

The Samburu Phase (20 – 16 Ma). Within the Kenya Rift, this event manifested as large volume basaltic flows and shield development that extended southwards to the margin of the Tanzania craton. In the cratonic regions surrounding the Turkana Depression, this phase manifested as alkaline volcanoes. This phase also corresponds with the first recorded magmatic activity within the Nyanza rift, and in Kivu, which is located on the opposite side of the Tanzania craton but directly on strike with the Nyanza rift. While previous models have suggested that stress was transmitted through the craton at ca. 12 Ma, the synchronous magmatic activity along the Nyanza rift and in Kivu suggest a much earlier linkage – i.e. during the Samburu Phase.

The Flood Phonolite Phase (16 – 12 Ma). The Flood Phonolite Phase heralded the expansion of magmatic activity further to the south in comparison with the earlier Samburu Phase. These voluminous volcanic flows also followed directly from the Samburu Phase and are thus likely linked with the progression of lithospheric thinning southward into the cratonic region in the Southern Kenya Rift. While the origin of the phonolites had initially been considered the result of anatexis of the continental crust, it is increasingly clear that assimilation and fractional crystallization processes play a more critical role in magma evolution.

Mid Miocene Resurgence Phase (12 – 9 Ma). Within the Southern Kenya Rift this event is largely absent. Instead, smaller-scale phonolite flows continued from the prior Flood Phonolite Phase. Within the western branch of the EARS, this period correlates with a significant increase in volcanic activity at Kivu.

Early Rift Development Phase (9 – 4 Ma). This phase corresponds to a magmatic hiatus in Turkana but a significant phase of magmatic activity within the Kenya Rift. Initial activity during this phase manifests as a relatively widespread phonolite at ca. 9 Ma, which is followed by a period of explosive volcanism that lasted until ca. 3.5 Ma. A renewed period of effusive volcanism centered on the Southern Kenya Rift commenced ca. 6 Ma. During this Phase, large volumes of basaltic magmatism were erupted and the initial magmatic products of Mt. Kenya were emplaced. This period of effusive activity also corresponds to the first recorded magmatism in the NTD. In the western branch of the EARS, magmatic activity continued sporadically and correlated with the development of the rift in the Kivu region at 7.5 Ma, which constrained the spatial distribution of subsequent magmatism. It evident that this phase of activity is related to a pulse of extension that extended throughout the Southern Kenya Rift and western branch of the EARS.

The Stratoid Phase (4 – 0.5 Ma). While this phase has been defined on the basis of the commencement of widespread magmatism within the Turkana region after a prolonged hiatus, 4

Ma has been noted by previous authors as a critical period of rift development in the Southern Kenya Rift. The initiation of full graben morphology and eruption of thick flows of basalts and trachytes into these developing basins provides some parallels with events in Turkana, though offset in time. As with the previous phases described above, magmatism in the Southern Kenya Rift appeared to lag events to the north. Thus, rather than a synchronous 4 Ma event throughout the region, magmatism in the Southern Kenya rift and NTD exhibits a distinct pulse at ca. 3 - 2.5 Ma. Within the western branch of the EARS, there is a commencement of magmatism in the Virunga Volcanic Province, and the beginning of the intermediate phase of activity in the Rungwe Volcanic Province. Clearly the 3 – 2.5 Ma interval is a critical period of renewed period activity that is likely linked with magmatic events commencing in Turkana ca. 4 Ma.

Axial Phase (0.5 Ma – Present). Continued evolution of the western branch of the EARS and the Southern Kenya Rift/NTD has resulted in a dichotomy in modern magmatic activity. Within the more mature regions of the Southern Kenya Rift, the development of axial grabens within the larger rift valley has largely focused magmatic activity. The initial material filling these axial grabens consists of fissural flows of basalt and trachyte, on top of which erupted central silicic volcanoes and parasitic basaltic cones. Linear chains of such cones also occur between the central volcanoes. In less mature regions of the rift, particularly alkaline central volcanoes have developed, but without widespread rift-filling fissural flows (e.g., NTD, Virunga Volcanic Province, Toro Ankole Volcanic Province).

There is a clear temporal sequence in the composition of rift lavas. The initial stages of magmatism within the Southern Kenya Rift were dominated by alkaline lavas derived from the lithospheric mantle. As the rift developed, erupted lavas exhibited a hybrid composition that was formed from the mixing of sub-lithosphercially derived melts and metasome-derived melts. As the rift matured and the lithosphere thinned further, lava compositions became dominated by sub-lithospheric reservoirs. While it is evident that magmatic activity in the region results from

the interaction of a deeply-sourced mantle thermo-chemical anomaly with the continental lithosphere, it is the presence of the Tanzania craton that clearly controls the composition of erupted lavas in the Southern Kenya Rift and western branch of the EARS. The diversity of magma compositions results from the variable alkalinity of the lavas imposed by metasomes located within the sub-continental lithospheric mantle. Ultra-potassic lavas are the result of the destabilization of phlogopite-dominant metasomes (stable to greater depths), while sodic lavas result from melting of amphibole-dominant metasomes (stable at relatively shallower depths) (e.g., Rosenthal et al., 2009; Foley et al., 2012). The wide variety of accessory phases that are potentially stable within these metasomes (apatite, carbonate, Fe-Ti oxides, zircon) control much of the trace element behavior of derivative magmas. The wide isotopic diversity in lavas from this region results from the interaction with the cratonic crust (in particular for more evolved lavas), but also from ancient metasomatic domains within the lithospheric mantle. The extreme fractionation that may result from chromatographic metasomatism and the crystallization of unusual phases, when isolated within the lithospheric mantle for billions of years, can yield extreme values of many traditional isotopic tracers.

The lavas erupted within this region are thus a probe of a rich history of lithosphere-asthenosphere interaction. The layered lithosphere model that has developed in order to address observations demonstrates the potential for the lithospheric mantle as a sink for many elements over geological time scales (e.g., Brune et al., 2017). Such evidence necessitates a re-examination of global models of element cycling to account for the formerly terra incognito that is the continental lithospheric mantle in cratonic domains.

References Cited

Adams, A., Miller, J., and Accardo, N., 2018, Relationships between lithospheric structures and rifting in the East African Rift System: A Rayleigh wave tomography study: Geochemistry, Geophysics, Geosystems, v. 19, p. 3793–3810.

Adams, A., Nyblade, A., and Weeraratne, D., 2012, Upper mantle shear wave velocity structure beneath the East African plateau: evidence for a deep, plateauwide low velocity anomaly: Geophysical Journal International, v. 189, p. 123–142.

Aoki, K., and Kurasawa, H., 1984, Sr isotope study of the tephrite series from Nyamuragira volcano, Zaire: Geochemical Journal, v. 18, p. 95–100.

Aoki, K.-I., Yoshida, T., Yusa, K., and Nakamura, Y., 1985, Petrology and geochemistry of the Nyamuragira volcano, Zaire: Journal of Volcanology and Geothermal Research, v. 25, p. 1–28.

Auchapt, A., Dupuy, C., Dostal, J., and Kanika, M., 1987, Geochemistry and petrogenesis of rift-related volcanic rocks from South Kivu (Zaire): Journal of volcanology and geothermal research, v. 31, p. 33–46.

Aulbach, S., Rudnick, R., and McDonough, W., 2008, Li-Sr-Nd isotope signatures of the plume and cratonic lithospheric mantle beneath the margin of the rifted Tanzanian craton (Labait): Contributions to Mineralogy and Petrology, v. 155, p. 79–92, doi:10.1007/s00410-007-0226-4.

Bachmann, O., and Bergantz, G.W., 2008, Rhyolites and their source mushes across tectonic settings: Journal of Petrology, v. 49, p. 2277–2285.

Bailey, K., Lloyd, F., Kearns, S., Stoppa, F., Eby, N., and Woolley, A., 2005, Melilitite at Fort Portal, Uganda: another dimension to the carbonate volcanism: Lithos, v. 85, p. 15–25.

Baker, B.H., 1967, Geology of the Mt. Kenya area: Geology Report, v. 79.

Baker, B.H., 1987, Outline of the petrology of the Kenya rift alkaline province: Geological Society, London, Special Publications, v. 30, p. 293–311.

Baker, B.H., and Mitchell, J.G., 1976, Volcanic stratigraphy and geochronology of the Kedong–Olorgesailie area and the evolution of the South Kenya rift valley: Journal of the Geological Society, v. 132, p. 467–484.

Baker, B.H., Mitchell, J.G., and Williams, L.A.J., 1988, Stratigraphy, geochronology and volcano-tectonic evolution of the Kedong–Naivasha–Kinangop region, Gregory Rift Valley, Kenya: Journal of the Geological Society, v. 145, p. 107–116.

Baker, B.H., Williams, L.A.J., Miller, J.A., and Fitch, F.J., 1971, Sequence and geochronology of the Kenya rift volcanics: Tectonophysics, v. 11, p. 191–215.

Barette, F., Poppe, S., Smets, B., Benbakkar, M., and Kervyn, M., 2017, Spatial variation of volcanic rock geochemistry in the Virunga Volcanic Province: statistical analysis of an integrated database: Journal of African Earth Sciences, v. 134, p. 888–903.

Barker, D.S., and Nixon, P.H., 1989, High-Ca, low-alkali carbonatite volcanism at Fort Portal, Uganda: Contributions to Mineralogy and Petrology, v. 103, p. 166–177.

Bell, K., and Blenkinsop, J., 1987, Nd and Sr Isotopic Compositions of East-African Carbonatites - Implications for Mantle Heterogeneity: Geology, v. 15, p. 99–102.

Bellon, H., and Pouclet, A., 1980, Datations K-Ar de quelques laves du Rift-ouest de l'Afrique Centrale; implications sur l'évolution magmatique et structurale: Geologische Rundschau, v. 69, p. 49–62, doi:10.1007/bf01869023.

Bestland, E.A., Thackray, G.D., and Retallack, G.J., 1995, Cycles of Doming and Eruption of the Miocene Kisingiri Volcano, Southwest Kenya: The Journal of Geology, v. 103, p. 598–607.

Bishop, W.W., Miller, J.A., and Fitch, F.J., 1969, New potassium-argon age determinations relevant to the Miocene fossil mammal sequence in east Africa: American Journal of Science, v. 267, p. 669–699, doi:10.2475/ajs.267.6.669.

Blegen, N., Brown, F.H., Jicha, B.R., Binetti, K.M., Faith, J.T., Ferraro, J.V., Gathogo, P.N., Richardson, J.L., and Tryon, C.A., 2016, The Menengai Tuff: A 36 ka widespread tephra and its chronological relevance to Late Pleistocene human evolution in East Africa: Quaternary Science Reviews, v. 152, p. 152–168, doi:https://doi.org/10.1016/j.quascirev.2016.09.020.

Boniface, N., 2017, Crystal chemistry of pyrochlore from the Mesozoic Panda Hill carbonatite deposit, western Tanzania: Journal of African Earth Sciences, v. 126, p. 33–44.

Bosshard-Stadlin, S.A., Mattsson, H.B., and Keller, J., 2014, Magma mixing and forced exsolution of CO2 during the explosive 2007–2008 eruption of Oldoinyo Lengai (Tanzania): Journal of Volcanology and Geothermal Research, v. 285, p. 229–246.

Boven, A., Pasteels, P., Punzalan, L.E., Yamba, T.K., and Musisi, J.H., 1998, Quaternary perpotassic magmatism in Uganda (Toro-Ankole Volcanic Province): age assessment and significance for magmatic evolution along the East African Rift: Journal of African Earth Sciences, v. 26, p. 463–476.

Boynton, W.V., 1984, Cosmochemistry of the rare earth elements: meteorite studies, *in* Henderson, P. ed., Rare earth element geochemistry, Amsterdam, Elsevier, p. 63–114.

Brune, S., Williams, S.E., and Müller, R.D., 2017, Potential links between continental rifting, CO2 degassing and climate change through time: Nature Geoscience, v. 10, p. 941–946, doi:10.1038/s41561-017-0003-6.

Castillo, P.R., Hilton, D.R., and Halldórsson, S.A., 2014, Trace element and Sr-Nd-Pb isotope geochemistry of Rungwe Volcanic Province, Tanzania: implications for a Superplume source for East Africa Rift magmatism: Frontiers in Earth Science, v. 2, p. 21.

Chakrabarti, R., Basu, A.R., Santo, A.P., Tedesco, D., and Vaselli, O., 2009a, Isotopic and geochemical evidence for a heterogeneous mantle plume origin of the Virunga volcanics, Western rift, East African Rift system: Chemical Geology, v. 259, p. 273–289.

Chakrabarti, R., Sims, K.W., Basu, A.R., Reagan, M., and Durieux, J., 2009b, Timescales of magmatic processes and eruption ages of the Nyiragongo volcanics from 238U-230Th-226Ra-210Pb disequilibria: Earth and Planetary Science Letters, v. 288, p. 149–157.

Chesley, J.T., Rudnick, R.L., and Lee, C.T., 1999, Re-Os systematics of mantle xenoliths from the East African Rift: Age, structure, and history of the Tanzanian craton: Geochimica Et Cosmochimica Acta, v. 63, p. 1203–1217.

Chualaowanich, T., Sutthirat, C., Pisuttha-Arnond, V., Hauzenberger, C., Lo, C., Lee, T., and Charusiri, P., 2014, Geochemical characteristics and new eruption ages of ruby-related basalts from southeast Kenya: Journal of Earth Science, v. 25, p. 799–821, doi:10.1007/s12583-014-0482-y.

Claessens, L., Veldkamp, A., Schoorl, J.M., Wijbrans, J.R., van Gorp, W., and Macdonald, R., 2016, Large scale pantelleritic ash flow eruptions during the Late Miocene in central Kenya and evidence for significant environmental impact: Global and Planetary Change, v. 145, p. 30–41, doi:https://doi.org/10.1016/j.gloplacha.2016.08.006.

Clarke, M.C., 1990, Geological, Volcanological and Hydrogeological Controls on the Occurrence of Geothermal Activity in the Area Surrounding Lake Naivasha, Kenya: With Coloured 1: 250 000 Geological Maps: Ministry of Energy.

Cohen, R.S., O'Nions, R.K., and Dawson, J.B., 1984, Isotope geochemistry of xenoliths from East Africa: implications for development of mantle reservoirs and their interaction: Earth and Planetary Science Letters, v. 68, p. 209–220.

Cohen, A.S., Soreghan, M.J., and Scholz, C.A., 1993, Estimating the age of formation of lakes: an example from Lake Tanganyika, East African Rift system: Geology, v. 21, p. 511–514.

Combe, A.D., 1937, The Katunga Volcano, South-West Uganda: Geological Magazine, v. 74, p. 195–200, doi:10.1017/s0016756800089706.

Condomines, M., Carpentier, M., and Ongendangenda, T., 2015, Extreme radium deficit in the 1957 AD Mugogo lava (Virunga volcanic field, Africa): Its bearing on olivine-melilitite genesis: Contributions to Mineralogy and Petrology, v. 169, p. 29.

Cote, S., Kingston, J., Deino, A., Winkler, A., Kityo, R., and MacLatchy, L., 2018, Evidence for rapid faunal change in the early Miocene of East Africa based on revised biostratigraphic and radiometric dating of Bukwa, Uganda: Journal of Human Evolution, v. 116, p. 95–107, doi:https://doi.org/10.1016/j.jhevol.2017.12.001.

Crossley, R., 1979, The Cenozoic stratigraphy and structure of the western part of the Rift Valley in southern Kenya: Journal of the Geological Society, v. 136, p. 393–405.

Crossley, R., and Knight, R.M., 1981, Volcanism in the western part of the rift valley in southern Kenya: Bulletin Volcanologique, v. 44, p. 117–128.

Davies, G.R., and Lloyd, F.E., 1989, Pb–Sr–Nd isotope and trace element data bearing on the origin of the potassic subcontinental lithosphere beneath south west Uganda, *in*

Kimberlites and Related Rocks, Blackwell Scientific, Geologial Society of Australia Special Publication, v. 14, p. 784–794.

Dawson, J.B., 2008, The Gregory rift valley and Neogene-recent volcanoes of northern Tanzania, *in* Geological Society of London.

Dawson, J.B., and Smith, J.V., 1988, Metasomatized and veined upper-mantle xenoliths from Pello Hill, Tanzania - Evidence for anomalously-light mantle beneath the Tanzanian Sector of the East-African rift-valley: Contributions to Mineralogy and Petrology, v. 100, p. 510–527.

De Mulder, M., Hertogen, J., Deutsch, S., and André, L., 1986, The role of crustal contamination in the potassic suite of the Karisimbi volcano (Virunga, African Rift Valley): Chemical geology, v. 57, p. 117–136.

Deans, T., and Roberts, B., 1984, Carbonatite tuffs and lava clasts of the Tinderet foothills, western Kenya: a study of calcified natrocarbonatites: Journal of the Geological Society, v. 141, p. 563–580.

Deino, A., and Potts, R., 1990, Single-crystal 40Ar/39Ar dating of the Olorgesailie Formation, southern Kenya Rift: Journal of Geophysical Research: Solid Earth, v. 95, p. 8453–8470.

Demant, A., Lestrade, P., Lubala, R.T., Kampunzu, A.B., and Durieux, J., 1994, Volcanological and petrological evolution of Nyiragongo volcano, Virunga volcanic field, Zaire: Bulletin of Volcanology, v. 56, p. 47–61.

Ditchfield, P., Hicks, J., Plummer, T., Bishop, L.C., and Potts, R., 1999, Current research on the Late Pliocene and Pleistocene deposits north of Homa Mountain, southwestern Kenya: Journal of Human Evolution, v. 36, p. 123–150.

DRAKE, R.E., VAN COUVERING, J.A., PICKFORD, M.H., CURTIS, G.H., and HARRIS, J.A., 1988, New chronology for the Early Miocene mammalian faunas of Kisingiri, Western Kenya: Journal of the Geological Society, v. 145, p. 479–491, doi:10.1144/gsjgs.145.3.0479.

Dupuy, C., Liotard, J.M., and Dostal, J., 1992, Zr/Hf fractionation in intraplate basaltic rocks - Carbonate metasomatism in the mantle source: Geochimica Et Cosmochimica Acta, v. 56, p. 2417–2423.

Ebinger, C.J., 1989a, Geometric and kinematic development of border faults and accommodation zones, Kivu-Rusizi rift, Africa: Tectonics, v. 8, p. 117–133.

Ebinger, C.J., 1989b, Tectonic development of the western branch of the East-African rift system: Geological Society of America Bulletin, v. 101, p. 885–903.

Ebinger, C.J., Deino, A.L., Drake, R.E., and Tesha, A.L., 1989, Chronology of volcanism and rift basin propagation: Rungwe volcanic province, East Africa: Journal of Geophysical Research: Solid Earth, v. 94, p. 15785–15803.

Ebinger, C.J., Deino, A.L., Tesha, A.L., Becker, T., and Ring, U., 1993a, Tectonic controls on rift basin morphology: evolution of the Northern Malawi (Nyasa) Rift: Journal of Geophysical Research: Solid Earth, v. 98, p. 17821–17836.

Ebinger, C., Djomani, Y.P., Mbede, E., Foster, A., and Dawson, J.B., 1997, Rifting Archaean lithosphere: the Eyasi-Manyara-Natron rifts, East Africa: Journal of the Geological Society, v. 154, p. 947–960.

Ebinger, C.J., Yemane, T., WoldeGabriel, G., Aronson, J.L., and Walter, R.C., 1993b, Late Eocene-Recent volcanism and faulting in the southern main Ethiopian Rift: Journal of the Geological Society of London, v. 150, p. 99–108.

Eby, G.N., Lloyd, F.E., and Woolley, A.R., 2009, Geochemistry and petrogenesis of the Fort Portal, Uganda, extrusive carbonatite: Lithos, v. 113, p. 785–800.

Foley, S.F., 2008, Rejuvenation and erosion of the cratonic lithosphere: Nature Geoscience, v. 1, p. 503.

Foley, S.F., Link, K., Tiberindwa, J.V., and Barifaijo, E., 2012, Patterns and origin of igneous activity around the Tanzanian craton: Journal of African Earth Sciences, v. 62, p. 1–18.

Fontijn, K., Delvaux, D., Ernst, G.G., Kervyn, M., Mbede, E., and Jacobs, P., 2010a, Tectonic control over active volcanism at a range of scales: Case of the Rungwe Volcanic Province, SW Tanzania; and hazard implications: Journal of African Earth Sciences, v. 58, p. 764–777.

Fontijn, K., Elburg, M.A., Nikogosian, I.K., van Bergen, M.J., and Ernst, G.G., 2013, Petrology and geochemistry of Late Holocene felsic magmas from Rungwe volcano (Tanzania), with implications for trachytic Rungwe Pumice eruption dynamics: Lithos, v. 177, p. 34–53.

Fontijn, K., Ernst, G.G., Bonadonna, C., Elburg, M.A., Mbede, E., and Jacobs, P., 2011, The~ 4-ka Rungwe Pumice (South-Western Tanzania): a wind-still Plinian eruption: Bulletin of volcanology, v. 73, p. 1353–1368.

Fontijn, K., Ernst, G.G., Elburg, M.A., Williamson, D., Abdallah, E., Kwelwa, S., Mbede, E., and Jacobs, P., 2010b, Holocene explosive eruptions in the Rungwe Volcanic Province, Tanzania: Journal of Volcanology and Geothermal Research, v. 196, p. 91–110.

Fontijn, K., Williamson, D., Mbede, E., and Ernst, G.G., 2012, The Rungwe volcanic province, Tanzania–a volcanological review: Journal of African Earth Sciences, v. 63, p. 12–31.

Furman, T., 1995, Melting of metasomatized subcontinental lithosphere - Undersaturated mafic lavas from Rungwe, Tanzania: Contributions to Mineralogy and Petrology, v. 122, p. 97–115.

Furman, T., and Graham, D., 1994, Chemical and isotopic variations in volcanic rocks from the Rungwe Province: constraints on the development and scales of source heterogeneity beneath the African Western Rift: Mineralogical Magazine, v. 58, p. 297–298.

Furman, T., and Graham, D., 1999, Erosion of lithospheric mantle beneath the East African Rift system; geochemical evidence from the Kivu volcanic province: Lithos, v. 48, p. 237–262.

Furman, T., Nelson, W., and Elkins-Tanton, L.T., 2014, Evolution of the East African Rift: Drip Melting, Lithospheric Thinning and Mafic Volcanism, *in* p. 14–11.

Gebo, D.L., MacLatchy, L., Kityo, R., Deino, A., Kingston, J., and Pilbeam, D., 1997, A Hominoid Genus from the Early Miocene of Uganda: Science, v. 276, p. 401–404, doi:10.1126/science.276.5311.401.

Geraads, D., Lehmann, T., Peppe, D.J., and McNulty, K.P., 2016, New Rhinocerotidae from the Kisingiri localities (lower Miocene of western Kenya): Journal of Vertebrate Paleontology, v. 36, p. e1103247, doi:10.1080/02724634.2016.1103247.

Grijalva, A., Nyblade, A.A., Homman, K., Accardo, N.J., Gaherty, J.B., Ebinger, C.J., Shillington, D.J., Chindandali, P.R., Mbogoni, G., and Ferdinand, R.W., 2018, Seismic Evidence for Plume-and Craton-Influenced Upper Mantle Structure Beneath the Northern Malawi Rift and the Rungwe Volcanic Province, East Africa: Geochemistry, Geophysics, Geosystems, v. 19, p. 3980–3994.

Guibert, P., Delaloye, M., and Hunziker, J., 1975, Contribution à l'étude géologique du volcan Mikeno, chaîne des Virunga (République du Zaïre): CR Scé. Soc. Phys. Hist. Nat., Genève, ns, v. 10, p. 57–66.

Guth, A.L., 2013, Spatial and Temporal Evolution of the Volcanics and Sediments of the Kenya Rift: Michigan Technological University.

Hackman, B.D., 1988, Geology of the Baringo-Laikipia area: degree sheet 35 with coloured 1: 250,000 geological map and results of geochemical exploration: Ministry of Environment and Natural Resources, Mines and Geological Deptartment.

Halldórsson, S.A., Hilton, D.R., Scarsi, P., Abebe, T., and Hopp, J., 2014, A common mantle plume source beneath the entire East African Rift System revealed by coupled helium-neon systematics: Geophysical Research Letters, v. 41, p. 2304–2311.

Harkin, D.A., 1960, The Rungwe volcanics at the northern end of Lake Nyasa:

Harris, P.G., 1969, Basalt type and African rift valley tectonism: Tectonophysics, v. 8, p. 427–436, doi:https://doi.org/10.1016/0040-1951(69)90046-8.

Hautot, S., Tarits, P., Whaler, K., Le Gall, B., Tiercelin, J.-J., and Le Turdu, C., 2000, Deep structure of the Baringo Rift Basin (central Kenya) from three-dimensional magnetotelluric imaging: Implications for rift evolution: Journal of Geophysical Research: Solid Earth, v. 105, p. 23493–23518.

Head, E.M., Shaw, A.M., Wallace, P.J., Sims, K.W., and Carn, S.A., 2011, Insight into volatile behavior at Nyamuragira volcano (DR Congo, Africa) through olivine-hosted melt inclusions: Geochemistry, Geophysics, Geosystems, v. 12.

Hertogen, J., Vanlerberghe, L., and Namegabe, M.R., 1985, Geochemical evolution of the Nyiragongo volcano (Virunga, Western African Rift, Zaire).: Geological Society of Finland, Bulletin, v. 57, p. 21–35.

Herzberg, C., 2011, Identification of Source Lithology in the Hawaiian and Canary Islands: Implications for Origins: Journal of Petrology, v. 52, p. 113–146, doi:10.1093/petrology/egq075.

Hilton, D.R., Halldórsson, S.A., Barry, P.H., Fischer, T.P., de Moor, J.M., Ramirez, C.J., Mangasini, F., and Scarsi, P., 2011, Helium isotopes at Rungwe Volcanic Province, Tanzania, and the origin of East African Plateaux: Geophysical Research Letters, v. 38, p. doi:10.1029/2011GL049589.

Holmes, A., 1950, Petrogenesis of katungite and its associates: American Mineralogist: Journal of Earth and Planetary Materials, v. 35, p. 772–792.

Holmes, A., 1956, The ejectamenta of Katwe crater, south-west Uganda: Verhandelingen van het Koninklijk Nederlands Geologisch Mijnbouwkundig Genootschap, Geologische Serie, v. 16, p. 66.

Holmes, A., 1937, The Petrology of Katungite: Geological Magazine, v. 74, p. 200–219, doi:10.1017/s0016756800089718.

Holmes, A., and Harwood, H.F., 1932, Petrology of the volcanic fields east and south-east of Ruwenzori, Uganda: Quarterly Journal of the Geological Society, v. 88, p. 370–442.

Hudgins, T.R., Mukasa, S.B., Simon, A.C., Moore, G., and Barifaijo, E., 2015, Melt inclusion evidence for CO2-rich melts beneath the western branch of the East African Rift: implications for long-term storage of volatiles in the deep lithospheric mantle: Contributions to Mineralogy and Petrology, v. 169, p. 1–18, doi:10.1007/s00410-015-1140-9.

Huerta, A.D., Nyblade, A.A., and Reusch, A.M., 2009, Mantle transition zone structure beneath Kenya and Tanzania: more evidence for a deep-seated thermal upwelling in the mantle: Geophysical Journal International, v. 177, p. 1249–1255, doi:10.1111/j.1365-246X.2009.04092.x.

Hyndman, R.D., Currie, C.A., and Mazzotti, S.P., 2005, Subduction zone backarcs, mobile belts, and orogenic heat: GSA Today, v. 15, p. 4–10.

Ivanov, A.V., Maslovskaya, M.N., Boven, A., Andre, L., Temu, E.B., and Rasskazov, S.V., 1998, Late Cenozoic alkaline-ultrabasic and alkaline basanite magmatism of the Rungwe Province, Tanzania: Petrology, v. 6, p. 208–229.

Ivanov, A.V., Rasskazov, S.V., Boven, A., Punzalan, L., Brandt, I.S., Brandt, S.B., and Fernandez-Alonso, M., 1999, Timing and Late Cenozoic volcanic activity and rift basin formations in the Rungwe province of Tanzania substantiated by K–Ar and 40Ar/39Ar dating: Proceedings of Rifting in Intracontinental Setting: Baikal Rift System and Other Continental Rifts, p. 22–30.

Jones, W.B., and Lippard, S.J., 1979, New age determinations and the geology of the Kenya Rift-Kavirondo Rift junction, W Kenya: Journal of the Geological Society, v. 136, p. 693–704.

Kampunzu, A.B., Bonhomme, M.G., and Kanika, M., 1998, Geochronology of volcanic rocks and evolution of the Cenozoic Western Branch of the East African Rift System: Journal of African Earth Sciences, v. 26, p. 441–461.

Kampunzu, A.B., Kanika, M., Caron, J.-H., Lubala, R.T., and Velluttini, P.J., 1984, Les basaltes transitionnels dans l'évolution des rifts continentaux: Exemple de la Haute-Ruzizi dans le Rift de l'Afrique Centrale (Kivu-Zaîre): Geologische Rundschau, v. 73, p. 895–916.

Keller, J., Zaitsev, A.N., and Wiedenmann, D., 2006, Primary magmas at Oldoinyo Lengai: the role of olivine melilitites: Lithos, v. 91, p. 150–172.

King, B.C., Le Bas, M.J., and Sutherland, D.S., 1972, The history of the alkaline volcanoes and intrusive complexes of eastern Uganda and western Kenya: Journal of the Geological Society, v. 128, p. 173–205, doi:10.1144/gsjgs.128.2.0173.

Kingston, J.D., Jacobs, B.F., Hill, A., and Deino, A., 2002, Stratigraphy, age and environments of the late Miocene Mpesida Beds, Tugen Hills, Kenya: Journal of Human Evolution, v. 42, p. 95–116.

Le Bas, M.J., and Rubie, D.C., 1977, Kisingiri I: an ijolite–carbonatite–nephelinite volcanic complex in western Kenya, *in* Carbonatite–Nephelinite Volcanism, John Wiley & Sons London, p. 39–46.

Le Gall, B., Nonnotte, P., Rolet, J., Benoit, M., Guillou, H., Mousseau-Nonnotte, M., Albaric, J., and Déverchère, J., 2008, Rift propagation at craton margin.: Distribution of faulting and volcanism in the North Tanzanian Divergence (East Africa) during Neogene times: Tectonophysics, v. 448, p. 1–19.

Le Roex, A.P., Späth, A., and Zartman, R.E., 2001, Lithospheric thickness beneath the southern Kenya Rift: implications from basalt geochemistry: Contributions to Mineralogy and Petrology, v. 142, p. 89–106.

Leat, P.T., 1984, Geological evolution of the trachytic caldera volcano Menengai, Kenya Rift Valley: Journal of the Geological Society, v. 141, p. 1057–1069, doi:10.1144/gsjgs.141.6.1057.

Leat, P.T., 1991, Volcanological development of the Nakuru area of the Kenya rift valley: Journal of African Earth Sciences (and the Middle East), v. 13, p. 483–498.

Lee, C.T., and Rudnick, R., 1999, Compositionally stratified cratonic lithosphere: Petrology and geochemistry of peridotite xenoliths from the Labait Voclcano, Tanzania., *in* Gurney, J., Pascoe, M., and Richardson, S. eds., v. 503–521.

Lee, C.T., Rudnick, R.L., McDonough, W.F., and Horn, I., 2000, Petrologic and geochemical investigation of carbonates in peridotite xenoliths from northeastern Tanzania: Contributions to Mineralogy and Petrology, v. 139, p. 470–484.

Lippard, S.J., 1973, The petrology of phonolites from the Kenya Rift: Lithos, v. 6, p. 217–234.

Lloyd, F.E., Huntingdon, A.T., Davies, G.R., and Nixon, P.H., 1991, Phanerozoic volcanism of southwest Uganda: a case for regional K and LILE enrichment of the lithosphere beneath a domed and rifted continental plate, *in* Magmatism in extensional structural settings, Springer, p. 23–72.

Lloyd, F.E., Woolley, A.R., Stoppa, F., and Eby, G.N., 2002, Phlogopite-biotite parageneses from the K-mafic-carbonatite effusive magmatic association of Katwe-Kikorongo, SW Uganda: Mineralogy and Petrology, v. 74, p. 299–322, doi:10.1007/s007100200008.

MacDonald, R., Rogers, N.W., Fitton, J.G., Black, S., and Smith, M., 2001, Plume-lithosphere interactions in the generation of the basalts of the Kenya Rift, East Africa: Journal of Petrology, v. 42, p. 877–900.

MacDonald, R., and Scaillet, B., 2006, The central Kenya peralkaline province: Insights into the evolution of peralkaline salic magmas: Lithos, v. 91, p. 59–73.

Macgregor, D., 2015, History of the development of the East African Rift System: A series of interpreted maps through time: Journal of African Earth Sciences, v. 101, p. 232–252.

Maclatchy, L., Deino, A., and Kingston, J., 2006, An updated chronology for the early Miocene of NE Uganda, *in* SOC VERTEBRATE PALEONTOLOGY 60 REVERE DR, STE 500, NORTHBROOK, IL 60062 USA, v. 26, p. 93A-93A.

Mahaney, W.C., Barendregt, R.W., Villeneuve, M., Dostal, J., Hamilton, T.S., and Milner, M.W., 2011, Late Neogene volcanics and interbedded palaeosols near Mount Kenya: Geological Society, London, Special Publications, v. 357, p. 301–318.

Mana, S., Furman, T., Carr, M.J., Mollel, G.F., Mortlock, R.A., Feigenson, M.D., Turrin, B.D., and Swisher Iii, C.C., 2012, Geochronology and geochemistry of the Essimingor volcano: melting of metasomatized lithospheric mantle beneath the North Tanzanian Divergence zone (East African Rift): Lithos, v. 155, p. 310–325.

Mana, S., Furman, T., Turrin, B.D., Feigenson, M.D., and Swisher III, C.C., 2015, Magmatic activity across the East African North Tanzanian Divergence Zone: Journal of the Geological Society, v. 172, p. 368–389.

Marshall, A.S., MacDonald, R., Rogers, N.W., Fitton, J.G., Tindle, A.G., Nejbert, K., and Hinton, R.W., 2009, Fractionation of Peralkaline Silicic Magmas: the Greater Olkaria Volcanic Complex, Kenya Rift Valley: Journal of Petrology, v. 50, p. 323–359.

Mason, P., 1955, Geology of the Meru-Isiolo Area (with Coloured Geological Map): Government Printer.

Mattsson, H.B., Nandedkar, R.H., and Ulmer, P., 2013, Petrogenesis of the melilititic and nephelinitic rock suites in the Lake Natron–Engaruka monogenetic volcanic field, northern Tanzania: Lithos, v. 179, p. 175–192.

McCall, G.J.H., 1967, Geology of the Nakuru-Thomson's Falls-Lake Hannington area: Rep. Geol. Surv. Kenya, v. 78, p. 122.

McConnell, R.B., 1967, The East African Rift System: Nature, v. 215, p. 578–581, doi:10.1038/215578a0.

McDonough, W.F., and Sun, S.-S., 1995, The composition of the Earth: Chemical Geology, v. 120, p. 223–253.

Mesko, G.T., Class, C., Maqway, M.D., Boniface, N., Manya, S., and Hemming, S.R., 2014, The timing of early magmatism and extension in the southern East African rift: Tracking geochemical source variability with 40Ar/39Ar geochronology at the Rungwe Volcanic Province, SW Tanzania, *in* AGU Fall Meeting Abstracts,.

Morley, C.K., Karanja, F.M., Wescott, W.A., Stone, D.M., Harper, R.M., Wigger, S.T., and Day, R.A., 1999, AAPG Studies in Geology# 44, Chapter 2: Geology and Geophysics of the Western Turkana Basins, Kenya:

Mugisha, F., Ebinger, C.J., Strecker, M., and Pope, D., 1997, Two-stage rifting in the Kenya rift: implications for half-graben models: Tectonophysics, v. 278, p. 63–81.

Muirhead, J.D., and Kattenhorn, S.A., 2018, Activation of preexisting transverse structures in an evolving magmatic rift in East Africa: Journal of Structural Geology, v. 106, p. 1–18, doi:https://doi.org/10.1016/j.jsg.2017.11.004.

Mulibo, G.D., and Nyblade, A.A., 2013, The P and S wave velocity structure of the mantle beneath eastern Africa and the African superplume anomaly: Geochemistry, Geophysics, Geosystems, v. 14, p. 2696–2715.

Muravyeva, N.S., and Senin, V.G., 2018, Xenoliths from Bunyaruguru volcanic field: Some insights into lithology of East African Rift upper mantle: Lithos, v. 296, p. 17–36.

Nelson, W.R., Furman, T., van Keken, P.E., Shirey, S.B., and Hanan, B.B., 2012, Os-Hf isotopic insight into mantle plume dynamics beneath the East African Rift System: Chemical Geology, v. 320–321, p. 66–79.

Nelson, W.R., Hanan, B.B., Graham, D.W., Shirey, S.B., Yirgu, G., Ayalew, D., and Furman, T., 2019, Distinguishing Plume and Metasomatized Lithospheric Mantle Contributions to Post-Flood Basalt Volcanism on the Southeastern Ethiopian Plateau: Journal of Petrology, v. 60, p. 1063–1094, doi:10.1093/petrology/egz024.

Nonnotte, P., Benoit, M., Le Gall, B., Hémond, C., Rolet, J., Cotten, J., Brunet, P., and Makoba, E., 2011, Petrology and geochemistry of alkaline lava series, Kilimanjaro, Tanzania: new constraints on petrogenetic processes: Geol. Soc. Am. Spec. Pap, v. 478, p. 127–158.

Nyblade, A.A., and Brazier, R.A., 2002, Precambrian lithospheric controls on the development of the East African rift system: Geology, v. 30, p. 755–758.

Nyblade, A.A., Owens, T.J., Gurrola, H., Ritsema, J., and Langston, C.A., 2000, Seismic evidence for a deep upper mantle thermal anomaly beneath east Africa: Geology, v. 28, p. 599–602.

O'Donnell, J.P., Adams, A., Nyblade, A.A., Mulibo, G.D., and Tugume, F., 2013, The uppermost mantle shear wave velocity structure of eastern Africa from Rayleigh wave tomography: Constraints on rift evolution: Geophysical Journal International, v. 194, p. 961–978.

Opdyke, N.D., Kent, D.V., Huang, K., Foster, D.A., and Patel, J.P., 2010, Equatorial paleomagnetic time-averaged field results from 0–5 Ma lavas from Kenya and the latitudinal variation of angular dispersion: Geochemistry, Geophysics, Geosystems, v. 11.

Owens, T.J., Nyblade, A.A., Gurrola, H., and Langston, C.A., 2000, Mantle transition zone structure beneath Tanzania, East Africa: Geophysical Research Letters, v. 27, p. 827–830.

Park, Y., and Nyblade, A.A., 2006, P-Wave tomography reveals a westward dipping low velocity zone beneath the Kenya rift.: Geophysical Research Letters, v. 33, p. L07311, doi:10.1029/2005GL025605.

Paslick, C., Halliday, A., James, D., and Dawson, J.B., 1995, Enrichment of the continental lithosphere by OIB melts; isotopic evidence from the volcanic province of northern Tanzania: Earth and Planetary Science Letters, v. 130, p. 109–126.

Pasteels, P., Villeneuve, M., De Paepe, P., and Klerkx, J., 1989, Timing of the volcanism of the southern Kivu province: implications for the evolution of the western branch of the East African Rift system: Earth and Planetary Science Letters, v. 94, p. 353–363.

Pickford, M., Sawada, Y., Tayama, R., Matsuda, Y., Itaya, T., Hyodo, H., and Senut, B., 2006, Refinement of the age of the Middle Miocene Fort Ternan Beds, Western Kenya, and its implications for Old World biochronology: Comptes Rendus Geoscience, v. 338, p. 545–555.

Pik, R., Marty, B., and Hilton, D.R., 2006, How many mantle plumes in Africa? The geochemical point of view: Chemical Geology, v. 226, p. 100–114.

Pilet, S., Baker, M.B., Müntener, O., and Stolper, E.M., 2011, Monte Carlo Simulations of Metasomatic Enrichment in the Lithosphere and Implications for the Source of Alkaline Basalts: Journal of Petrology, v. 52, p. 1415–1442, doi:10.1093/petrology/egr007.

Platz, T., Foley, S.F., and André, L., 2004, Low-pressure fractionation of the Nyiragongo volcanic rocks, Virunga Province, DR Congo: Journal of Volcanology and Geothermal research, v. 136, p. 269–295.

Pouclet, A., Bellon, H., and Bram, K., 2016, The Cenozoic volcanism in the Kivu rift: Assessment of the tectonic setting, geochemistry, and geochronology of the volcanic activity in the South-Kivu and Virunga regions: Journal of African Earth Sciences, v. 121, p. 219–246.

Price, R.C., Johnson, R.W., Gray, C.M., and Frey, F.A., 1985, Geochemistry of phonolites and trachytes from the summit region of Mt. Kenya: Contributions to Mineralogy and Petrology, v. 89, p. 394–409, doi:10.1007/bf00381560.

Prowatke, S., and Klemme, S., 2006, Trace element partitioning between apatite and silicate melts: Geochimica Et Cosmochimica Acta, v. 70, p. 4513–4527, doi:https://doi.org/10.1016/j.gca.2006.06.162.

Purcell, P.G., 2018, Re-imagining and re-imaging the development of the East African Rift: Petroleum Geoscience, v. 24, p. 21–40.

Rasskazov, S.V., Logachev, N.A., Ivanov, A.V., Boven, A.A., Maslovskaya, M.N., Saranina, E.V., Brandt, I.S., and Brandt, S.B., 2003, A magmatic episode in the Western Rift of East Africa (19-17 Ma): Geologiya i Geofizika, v. 44, p. 317–324.

Rasskazov, S.V., Maslovskaya, M.N., Saranina, E.V., Ivanov, A.V., and Boven, A., 1999, Strontium isotope study of Late Cenozoic evolved volcanic rocks from the Rungwe province, Tanzania: Isochron ages of 16.1 and 463 Myr for phonolite eruption and mantle–crust differentiation event: Proceedings Rifting in Intracontinental Setting: Baikal Rift System and Other Continental Rifts, p. 22–30.

Ritsema, J., Nyblade, A.A., Owens, T.J., Langston, C.A., and VanDecar, J.C., 1998, Upper mantle seismic velocity structure beneath Tanzania, east Africa: Implications for the stability of cratonic lithosphere: Journal of Geophysical Research-Solid Earth, v. 103, p. 21201–21213.

Roberts, E.M., Stevens, N.J., O'Connor, P.M., Dirks, P., Gottfried, M.D., Clyde, W.C., Armstrong, R.A., Kemp, A.I.S., and Hemming, S., 2012, Initiation of the western branch of the East African Rift coeval with the eastern branch: Nature Geoscience, v. 5, p. 289–294.

Rogers, N., 2006, Basaltic magmatism and the geodynamics of the East African Rift System, *in* Yirgu, G., Ebinger, C., and Maguire, P. eds., The Afar Volcanic Province within the East African Rift System, London, The Geological Society Special Publications, v. 259, p. 77–93.

Rogers, N.W., Demulder, M., and Hawkesworth, C.J., 1992, An enriched mantle source for potassic basanites - Evidence from Karisimbi Volcano, Virunga volcanic province, Rwanda: Contributions to Mineralogy and Petrology, v. 111, p. 543–556.

Rogers, N.W., James, D., Kelley, S.P., and de Mulder, M., 1998, The generation of potassic lavas from the eastern Virunga Province, Rwanda: Journal of Petrology, v. 39, p. 1223–1247.

Rogers, N., Macdonald, R., Fitton, J.G., George, R., Smith, M., and Barreiro, B., 2000, Two mantle plumes beneath the East African Rift system; Sr, Nd and Pb isotope evidence from Kenya Rift basalts: Earth and Planetary Science Letters, v. 176, p. 387–400.

Rogers, N.W., Thomas, L.E., Macdonald, R., Hawkesworth, C.J., and Mokadem, F., 2006, U-238-Th-230 disequilibrium in recent basalts and dynamic melting beneath the Kenya rift: Chemical Geology, v. 234, p. 148–168, doi:DOI 10.1016/j.chemgeo.2006.05.002.

Rooney, T.O., 2020a, The Cenozoic Magmatism of East Africa: Part II–Rifting of the mobile belt: Lithos, p. In Press, doi:10.1016/j.lithos.2019.105291.

Rooney, T.O., 2020b, The Cenozoic Magmatism of East Africa: Part IV – The Terminal Stages of Rifting Preserved in the Northern East African Rift System: Lithos, p. In Review.

Rooney, T.O., 2020c, The Cenozoic magmatism of East Africa: Part V–Magma sources and processes in the East African Rift: Lithos, p. In Press, doi:10.1016/j.lithos.2019.105296.

Rooney, T.O., 2017, The Cenozoic magmatism of East-Africa: Part I–Flood basalts and pulsed magmatism: Lithos, v. 286, p. 264–301.

Rooney, T.O., Hart, W.K., Hall, C.M., Ayalew, D., Ghiorso, M.S., Hidalgo, P., and Yirgu, G., 2012a, Peralkaline magma evolution and the tephra record in the Ethiopian Rift: Contributions to Mineralogy and Petrology, v. 164, p. 407–426, doi:DOI: 10.1007/s00410-012-0744-6.

Rooney, T.O., Herzberg, C., and Bastow, I.D., 2012b, Elevated mantle temperature beneath East Africa: Geology, v. 40, p. 27–30, doi:10.1130/g32382.1.

Rooney, T.O., Nelson, W.R., Ayalew, D., Hanan, B., Yirgu, G., and Kappelman, J., 2017, Melting the lithosphere: Metasomes as a source for mantle-derived magmas: Earth and Planetary Science Letters, v. 461, p. 105–118, doi:http://dx.doi.org/10.1016/j.epsl.2016.12.010.

Rooney, T.O., Nelson, W.R., Dosso, L., Furman, T., and Hanan, B., 2014, The role of continental lithosphere metasomes in the production of HIMU-like magmatism on the northeast African and Arabian plates: Geology, v. 42, p. 419–422, doi:10.1130/g35216.1.

Rosenthal, A., Foley, S.F., Pearson, D.G., Nowell, G.M., and Tappe, S., 2009, Petrogenesis of strongly alkaline primitive volcanic rocks at the propagating tip of the western branch of the East African Rift: Earth and Planetary Science Letters, v. 284, p. 236–248, doi:10.1016/j.epsl.2009.04.036.

Rudnick, R.L., Ireland, T.R., Gehrels, G., Irving, A.J., Chesley, J.T., and Hanchar, J.M., 1998, Dating mantle metasomatism: U-Pb geochronology of zircons in cratonic mantle xenoliths from Montana and Tanzania, *in* v. 7, p. 754–756.

Rudnick, R.L., McDonough, W.F., and Chappell, B.W., 1993, Carbonatite metasomatism in the Northern Tanzanian mantle - Petrographic and geochemical characteristics: Earth and Planetary Science Letters, v. 114, p. 463–475.

Sack, R.O., Walker, D., and Carmichael, I.S.E., 1987, Experimental petrology of alkalic lavas - Constraints on cotectics of multiple saturation in natural basic liquids: Contributions to Mineralogy and Petrology, v. 96, p. 1–23.

Saggerson, E.P., 1991, Geology of the Nairobi area: Mines & Geological Department.

Simonetti, A., and Bell, K., 1993, Isotopic disequilibrium in clinopyroxenes from nephelinitic lavas, Napak volcano, eastern Uganda: Geology, v. 21, p. 243–246.

Simonetti, A., and Bell, K., 1995, Nd, Pb and Sr isotopic data from the Mount Elgon volcano, eastern Uganda-western Kenya: implications for the origin and evolution of nephelinite lavas: Lithos, v. 36, p. 141–153.

Simonetti, A., and Bell, K., 1994, Nd, Pb and Sr isotopic data from the Napak carbonatite-nephelinite centre, eastern Uganda: an example of open-system crystal fractionation: Contributions to Mineralogy and Petrology, v. 115, p. 356–366.

Smith, M., 1994, Stratigraphic and structural constraints on mechanisms of active rifting in the Gregory Rift, Kenya: Tectonophysics, v. 236, p. 3–22.

Späth, A., Le Roex, A.P., and Opiyo-Akech, N., 2001, Plume-lithosphere interaction and the origin of continental rift-related alkaline volcanism; the Chyulu Hills volcanic province, southern Kenya: Journal of Petrology, v. 42, p. 765–787.

Stoppa, F., and Schiazza, M., 2013, An overview of monogenetic carbonatitic magmatism from Uganda, Italy, China and Spain: volcanologic and geochemical features: Journal of South American Earth Sciences, v. 41, p. 140–159.

Stracke, A., and Bourdon, B., 2009, The importance of melt extraction for tracing mantle heterogeneity: Geochimica et Cosmochimica Acta, v. 73, p. 218–238.

Sun, S. s-, and McDonough, W.F., 1989, Chemical and isotopic systematics of oceanic basalts: Implications for mantle composition and processes., *in* Saunders, A.D. ed., Magmatism in the ocean basins, Geological Society of London Special Publication 42, p. 313–345.

Tappe, S., Foley, S.F., Kjarsgaard, B.A., Romer, R.L., Heaman, L.M., Stracke, A., and Jenner, G.A., 2008, Between carbonatite and lamproite—Diamondiferous Torngat ultramafic lamprophyres formed by carbonate-fluxed melting of cratonic MARID-type metasomes: Geochimica Et Cosmochimica Acta, v. 72, p. 3258–3286.

Tiberi, C. et al., 2018, Lithospheric modification by extension and magmatism at the craton-orogenic boundary: North Tanzania Divergence, East Africa: Geophysical Journal International, v. 216, p. 1693–1710, doi:10.1093/gji/ggy521.

Truckle, P.H., 1977, The geology of the area to the south of Lokori, South Turkana, Kenya.:

Van Couvering, J.A., and Miller, J.A., 1969, Miocene Stratigraphy and Age Determinations, Rusinga Island, Kenya: Nature, v. 221, p. 628, doi:10.1038/221628a0.

Veldkamp, A., Schoorl, J.M., Wijbrans, J.R., and Claessens, L., 2012, Mount Kenya volcanic activity and the Late Cenozoic landscape reorganisation in the upper Tana fluvial system: Geomorphology, v. 145–146, p. 19–31, doi:https://doi.org/10.1016/j.geomorph.2011.10.026.

Vollmer, R., and Norry, M.J., 1983, Possible origin of K-rich volcanic rocks from Virunga, East Africa, by metasomatism of continental crustal material: Pb, Nd and Sr isotopic evidence: Earth and Planetary Science Letters, v. 64, p. 374–386.

Von Knorring, O., and Du Bois, C.G.B., 1961, Carbonatitic lava from Fort Portal area in western Uganda: Nature, v. 192, p. 1064.

Wauthier, C., Cayol, V., Poland, M., Kervyn, F., d'Oreye, N., Hooper, A., Samsonov, S., Tiampo, K., and Smets, B., 2013, Nyamulagira's magma plumbing system inferred from 15 years of InSAR: Geological Society, London, Special Publications, v. 380, p. 39–65.

Weeraratne, D.S., Forsyth, D.W., Fischer, K.M., and Nyblade, A.A., 2003, Evidence for an upper mantle plume beneath the Tanzanian craton from Rayleigh wave tomography: Journal of Geophysical Research-Solid Earth, v. 108, p. doi:10.1029/2002JB002273.

White, J.C., Espejel-García, V.V., Anthony, E.Y., and Omenda, P., 2012, Open System evolution of peralkaline trachyte and phonolite from the Suswa volcano, Kenya rift: Lithos, v. 152, p. 84–104, doi:https://doi.org/10.1016/j.lithos.2012.01.023.

Wichura, H., Bousquet, R., Oberhänsli, R., Strecker, M.R., and Trauth, M.H., 2011, The Mid-Miocene East African Plateau: a pre-rift topographic model inferred from the emplacement of the phonolitic Yatta lava flow, Kenya: Geological Society, London, Special Publications, v. 357, p. 285–300.

Wölbern, I., Rümpker, G., Link, K., and Sodoudi, F., 2012, Melt infiltration of the lower lithosphere beneath the Tanzania craton and the Albertine rift inferred from S receiver functions: Geochemistry, Geophysics, Geosystems, v. 13.

Woolley, A.R., 2001, Alkaline Rocks and Carbonatites of the World: Africa (Pt. 3): Austin: University of Texas Press, 384 p.

Acknowledgements

I would like to thank all the authors I contacted who provided more details and answers to my queries on their work – there were many and I am not able to mention them all here. This work is a synthesis of all the hard work put in by the persons cited herein and the contributions from these persons should be acknowledged. Peter Purcell is thanked for providing the digital files for the rift maps used in the accompanying maps. Alex Steiner is given thanks for his assistance in collating GIS aspects of the project. I thank Benoît Smets for interactions on the Virunga Volcanic Province. Karen Fontijn is thanked for providing the base GIS files for the Rungwe Province. Thanks is provided to the MSU Library and in particular Kathleen Weessies at the Map Library and the interlibrary loans group – they tried to obtain the requests I placed, and most always succeeded. I am grateful for the formal peer review comments by Ray MacDonald and an anonymous reviewer. I am indebted to Andrew Kerr for his tireless editorial handling of this synthesis series. This work was supported by US National Science Foundation Grants: EAR

1551872 and EAR 1850606. Lastly, I acknowledge the NSF GeoPRISMS program which was part of the motivation for undertaking this synthesis.

Figures

Figure 1: Map showing the generalized distribution of Precambrian rocks in East Africa, the distribution of Cenozoic volcanism, and the footprint of Cenozoic rifting. Outcrop shapes are derived from the USGS Surficial Geology of Africa (geo7_2ag), rifts are from Purcell (2018), the extent of the craton is taken from Foley et al. (2012).

Figure 2: Map showing the distribution of lavas erupted during the Samburu and Flood Phonolite Phases throughout southern East Africa. Note that this map shows distribution both on the craton and mobile belt. Units/names are derived from Guth (2013), and the Smithsonian Volcano database. Units include: Samburu Formation (20-16 Ma), consisting of: (Nachola, Kapcherat, Chembalo, Samburu) – Kenya Rift, (Lower Kalokol, lower Irile Member, Nakoret, Muranasigar) – Turkana. Flood Phonolites consist of: upper Nachola, Aka Aiteputh, Elgeyo Formation, Chof phonolite, Sidekh phonolite, Uasin Gishu phonolite, Tiiim phonolite, Rumruti phonolites, and Jarigole Volcanics.

Figure 3: XY plots for various elements and isotopes vs MgO (A though F). Element ratio plots also shown (G, H). Data are for the Southern Kenya Rift associated with the Craton. Units include: Samburu (Simbara), Flood Phonolite Series (Lisudwa, Yatta), Early Rift Development Phase (Laikipian-Sattima, Ol Esakut, Ol Esayeti, Turasha), Stratoid Series (Kirikiti Basalts, Kordjya, Lenderut, Limuru Trachyte, Magadi-Plateau Trachyte, Marigat Trachyte, Ngong Volcanics, Ol Keju, Ol Tepesi, Olorgesailie, Sambu, Shombole, Singaraini Basalts), and the

Axial Phase (Eburru, Longonot, Menengai, Nakuru, Olkaria, Suswa). In addition, lavas from the eastern plateau are shown (Mt. Kenya, and Chyulu Hills).

Figure 4: Chondrite normalized diagram (Boynton, 1984) for more mafic samples (MgO > 5 wt. %). Units include: Samburu (Simbara), Flood Phonolite Series (Lisudwa, Yatta), Early Rift Development Phase (Laikipian-Sattima, Ol Esakut, Ol Esayeti, Turasha), Stratoid Series (Kirikiti Basalts, Kordjya, Lenderut, Limuru Trachyte, Magadi-Plateau Trachyte, Marigat Trachyte, Ngong Volcanics, Ol Keju, Ol Tepesi, Olorgesailie, Sambu, Shombole, Singaraini Basalts), and the Axial Phase (Eburru, Longonot, Menengai, Nakuru, Olkaria, Suswa). In addition, lavas from the eastern plateau are shown (Mt. Kenya, and Chyulu Hills). Background field is the data extremes for the dataset presented in this figure. Note that missing data have been interpolated between points and are shown as a lower weight line connecting the datapoints. The interpolation is a weighted linear average which can result in curved artifacts in log space. The background data is a field showing the data limits for all samples in the plot.

Figure 5: Primitive Mantle normalized diagram (Sun and McDonough, 1989) for more mafic samples (MgO > 5 wt. %). Units include: Samburu (Simbara), Flood Phonolite Series (Lisudwa, Yatta), Early Rift Development Phase (Laikipian-Sattima, Ol Esakut, Ol Esayeti, Turasha), Stratoid Series (Kirikiti Basalts, Kordjya, Lenderut, Limuru Trachyte, Magadi-Plateau Trachyte, Marigat Trachyte, Ngong Volcanics, Ol Keju, Ol Tepesi, Olorgesailie, Sambu, Shombole, Singaraini Basalts), and the Axial Phase (Eburru, Longonot, Menengai, Nakuru, Olkaria, Suswa). In addition, lavas from the eastern plateau are shown (Mt. Kenya, and Chyulu Hills). Background field is the data extremes for the dataset presented in this figure.

Figure 6: XY plots for various elements and isotopes vs MgO (A though F). Isotope ratio plots also shown (G, H). Data are for the Toro Ankole Volcanic Province (Bunyaruguru and Katwe-Kikorongo fields), and Eastern Uganda (Elgon, Budeda, Napak, and Tororo Hill).

Figure 7: Sr-Nd and Pb isotopic plots of carbonatites from East Africa. Data are: Eastern Uganda (Tinderet, Napak, Bukusu, Kisingiri, Sukulu Hill, Tororo Hill); Homa Bay (Homa Mountain and Ruri); Shombole/Kerimasi; Oldoinyo Lengai; Toro Ankole Volcanic Province (Fort Portal, Katwe-Kikorongo, Bunyaruguru). The EACL is the East Africa Carbonatite Line (Bell and Blenkinsop, 1987).

Figure 8: Isotopic variation plots for Sr, Nd and Pb isotopes. Units include: Samburu (Simbara), Flood Phonolite Series (Lisudwa, Yatta), Early Rift Development Phase (Laikipian-Sattima, Ol Esakut, Ol Esayeti, Turasha), Stratoid Series (Kirikiti Basalts, Kordjya, Lenderut, Limuru Trachyte, Magadi-Plateau Trachyte, Marigat Trachyte, Ngong Volcanics, Ol Keju, Ol Tepesi, Olorgesailie, Sambu, Shombole, Singaraini Basalts), and the Axial Phase (Eburru, Longonot, Menengai, Nakuru, Olkaria, Suswa). In addition, lavas from the eastern plateau are shown (Mt. Kenya, and Chyulu Hills).

Figure 9: Map showing the distribution of lavas erupted during the Early Rift Development Phase and the Stratoid Phase throughout southern East Africa. Note that this map shows distribution both on the craton and mobile belt. Units and names are derived from Guth (2013), and the Smithsonian Volcano database. Pyroclastic formations are not shown on this map.

Figure 10: Map showing the distribution of lavas erupted during the Axial Phase within the southern Eastern Branch of the East African Rift and Northern Tanzania Divergence (NTD). The two primary types of magma are those erupted on the plateau and that erupted within the rift basin. Units and names are derived from Guth (2013), the Smithsonian Volcano database, and Dawson (2008). Where the volcanic products of volcanoes are unmapped, I have labelled the major volcanic centers.

Figure 11: XY plots for the Northern Tanzania Divergence showing various elements and isotopes vs MgO (A though F). Element ratio plots also shown (G, H). Units include: Phase 1 (Sadiman, Essimingor, Lemagrut, and Engelosin), Phase 1-2 (where lavas could not be assigned definitively to either period), Phase 2-3 (Elanairobi, Olmoti, Loolmalasin, Ngorongoro, Oldeani, Tarosero, Monduli, Ketumbeine, Gelai, Shira & Mawenzi on Kilimanjaro, and Mosonik), Phase 4 (Meru, Oldoinyo Lengai, Kerimasi, Burko, Kwaraha, Hanang, and Kibo on Kilimanjaro).

Figure 12: Chondrite normalized diagram (Boynton, 1984) for the Northern Tanzania Divergence showing more mafic samples (MgO > 4 wt. %). Units include: Phase 1 (Sadiman, Essimingor, Lemagrut, and Engelosin), Phase 1-2 (where lavas could not be assigned definitively to either period), Phase 2-3 (Elanairobi, Olmoti, Loolmalasin, Ngorongoro, Oldeani, Tarosero, Monduli, Ketumbeine, Gelai, Shira & Mawenzi on Kilimanjaro, and Mosonik), Phase 4 (Meru, Oldoinyo Lengai, Kerimasi, Burko, Kwaraha, Hanang, and Kibo on Kilimanjaro). Background field is the data extremes for the dataset presented in this figure. Note that missing data have been interpolated between points and are shown as a lower weight line connecting the datapoints. The interpolation is a weighted linear average which can result in curved artifacts in log space. The background data is a field showing the data limits for all samples in the plot.

Figure 13: Primitive mantle normalized diagram (Sun and McDonough, 1989) for the Northern Tanzania Divergence showing more mafic samples (MgO > 4 wt. %). Units include: Phase 1 (Sadiman, Essimingor, Lemagrut, and Engelosin), Phase 1-2 (where lavas could not be assigned definitively to either period), Phase 2-3 (Elanairobi, Olmoti, Loolmalasin, Ngorongoro, Oldeani, Tarosero, Monduli, Ketumbeine, Gelai, Shira & Mawenzi on Kilimanjaro, and Mosonik), Phase 4 (Meru, Oldoinyo Lengai, Kerimasi, Burko, Kwaraha, Hanang, and Kibo on Kilimanjaro). Background field is the data extremes for the dataset presented in this figure.

Figure 14: Isotopic variation plots for the Northern Tanzania Divergence showing Sr, Nd and Pb isotopes. Units include: Phase 1 (Sadiman, Essimingor, Lemagrut, and Engelosin), Phase 1-2 (where lavas could not be assigned definitively to either period), Phase 2-3 (Elanairobi, Olmoti, Loolmalasin, Ngorongoro, Oldeani, Tarosero, Monduli, Ketumbeine, Gelai, Shira & Mawenzi on Kilimanjaro, and Mosonik), Phase 4 (Meru, Oldoinyo Lengai, Kerimasi, Burko, Kwaraha, Hanang, and Kibo on Kilimanjaro).

Figure 15: XY plots for Phase 1 volcanoes from the Northern Tanzania Divergence showing various elements and isotopes vs MgO (A though F). Isotope ratio plots are also shown (G, H). Units include: Phase 1 (Sadiman, Essimingor, Lemagrut).

Figure 16: XY plots for Phase 1-2 and 2-3 volcanoes from the Northern Tanzania Divergence showing various elements and isotopes vs MgO (A though F). Isotope ratio plots are also shown (G, H). Volcanoes shown are: Gelai, Ketumbeine, Loolmalasin, Monduli, Mosonik, Ngorongoro, Oldeani, Olmoti-Embagai, Tarosero.

Figure 17: XY plots for Phase 1-2 and 2-3 volcanoes from the Northern Tanzania Divergence showing various elements and isotopes vs MgO (A though F). Isotope ratio plots are also shown (G, H). Volcanoes shown are: Burko, inter-volcano cindercones, Hanang, Kwaraha, Meru, Oldoinyo Lengai, Kilimanjaro (all phases).

Figure 18: Pb and Sr isotopic variation for lavas from the Northern Tanzania Divergence. The data has been divided on the basis of 4% MgO to highlight the impact of crustal assimilation.

Figure 19: Primitive Mantle normalized diagram (Sun and McDonough, 1989) for carbonatites from East Africa. Data are: Oldoinyo Lengai and Toro Ankole Volcanic Province (Fort Portal).

Figure 20: Location map for the Rungwe Volcanic Province. Geological units are from Fontijn et al., (2012); rift basin outlines are from Purcell (2018).

Figure 21: XY plots for the Rungwe and Kivu volcanic provinces showing various elements and isotopes vs MgO (A though F). Element ratio plots also shown (G, H). Data are for Rungwe Phase 1 (Tukuyu); Rungwe Phase 2 (Kyejo, Mbaka older, Mbeya older, Ngozi), Rungwe Phase 3 (Mbaka, Mbeya old, Ngozi, Porotos, Tukuyu), Rungwe Phase 4 (Possible Kyejo, cinder cones, Kyejo, Mbeya recent, Ngozi, Porotos, Rungwe), Kivu Early (North Idjwi), Kivu Intermediate (Bakavu, South Idjwi, Mwenga-Kamituga), Kivu Modern (Tshibinda, Bukavu).

Figure 22: Chondrite normalized diagram (Boynton, 1984) for more mafic samples (MgO > 5 wt. %) of the Rungwe, Kivu, and older lavas of the Virunga volcanic provinces. Data are for Rungwe Phase 1 (Tukuyu); Rungwe Phase 2 (Kyejo, Mbaka older, Mbeya older, Ngozi), Rungwe Phase 3 (Mbaka, Mbeya old, Ngozi, Porotos, Tukuyu), Rungwe Phase 4 (Possible Kyejo, cinder cones, Kyejo, Mbeya recent, Ngozi, Porotos, Rungwe), Kivu Early (North Idjwi), Kivu Intermediate (Bakavu, South Idjwi, Mwenga-Kamituga), Kivu Modern (Tshibinda, Bukavu), Virunga Intermediate aged. Background field is the data extremes for the dataset presented in this figure. Note that missing data have been interpolated between points and are shown as a lower weight line connecting the datapoints. The interpolation is a weighted linear average which can result in curved artifacts in log space. The background data is a field showing the data limits for all samples in each column – the first column shows the limit of Rungwe Volcanic Province data, while the second column shows the limit of Kivu/Virunga data.

Figure 23: Primitive Mantle normalized diagram (Sun and McDonough, 1989) for more mafic samples (MgO > 5 wt. %) of the Rungwe, Kivu, and older lavas of Virunga volcanic provinces. Data are for Rungwe Phase 1 (Tukuyu); Rungwe Phase 2 (Kyejo, Mbaka older, Mbeya older, Ngozi), Rungwe Phase 3 (Mbaka, Mbeya old, Ngozi, Porotos, Tukuyu), Rungwe Phase 4 (Possible Kyejo, cinder cones, Kyejo, Mbeya recent, Ngozi, Porotos, Rungwe). Kivu Early (North Idjwi), Kivu Intermediate (Bakavu, South Idjwi, Mwenga-Kamituga), Kivu Modern

(Tshibinda, Bukavu), Virunga Intermediate aged. Background field is the data extremes for the dataset presented in this figure.

Figure 24: Isotopic variation plots for the Rungwe and Kivu volcanic provinces showing Sr, Nd and Pb isotopes. Data are for Rungwe Phase 1 (Tukuyu); Rungwe Phase 2 (Kyejo, Mbaka older, Mbeya older, Ngozi), Rungwe Phase 3 (Mbaka, Mbeya old, Ngozi, Porotos, Tukuyu), Rungwe Phase 4 (Possible Kyejo, cinder cones, Kyejo, Mbeya recent, Ngozi, Porotos, Rungwe), Kivu Early (North Idjwi), Kivu Intermediate (Bakavu, South Idjwi, Mwenga-Kamituga), Kivu Modern (Tshibinda, Bukavu).

Figure 25: Map showing the distribution of the major volcanic edifices in the Kivu, Virunga, and Toro Ankole volcanic provinces. Fields shown are that of Pouclet et al. (2016); rift basins are from Purcell (2018).

Figure 26: XY plots for modern magmatism in the Virunga volcanic province showing various elements and isotopes vs MgO (A though F). Element ratio plots also shown (G, H). Data are for Nyiragongo, Nyamuragira, Karisimbi, Muhavura, Bufumbira, Mikeno, Sabinyo, Gahinga, and Bisoke.

Figure 27: Chondrite normalized diagram (Boynton, 1984) for more mafic samples (MgO > 4 wt. %) of the Virunga Volcanic Province. Data are for Nyiragongo, Nyamuragira, Karisimbi, Muhavura, Bufumbira, Mikeno, Sabinyo, Gahinga, and Bisoke. Background field is the data extremes for the dataset presented in this figure. Note that missing data have been interpolated between points and are shown as a lower weight line connecting the datapoints. The interpolation is a weighted linear average which can result in curved artifacts in log space. The background data is a field showing the data limits for all samples.

Figure 28: Primitive Mantle normalized diagram (Sun and McDonough, 1989) for more mafic samples (MgO > 4 wt. %) of the Virunga Volcanic Province. Data are for Nyiragongo,

Nyamuragira, Karisimbi, Muhavura, Bufumbira, Mikeno, Sabinyo, Gahinga, and Bisoke. Fields for Bunyaruguru and Katwe-Kikorongo from the Toro Ankole Volcanic Province are also shown. Background field is the data extremes for the Virunga dataset presented in this figure.

Figure 29: Isotopic variation plots for the Rungwe and Kivu volcanic provinces showing Sr, Nd and Pb isotopes. Data are for Nyiragongo, Nyamuragira, Karisimbi, Muhavura, Bufumbira, Mikeno, Sabinyo, Gahinga, and Bisoke.

Figure 1

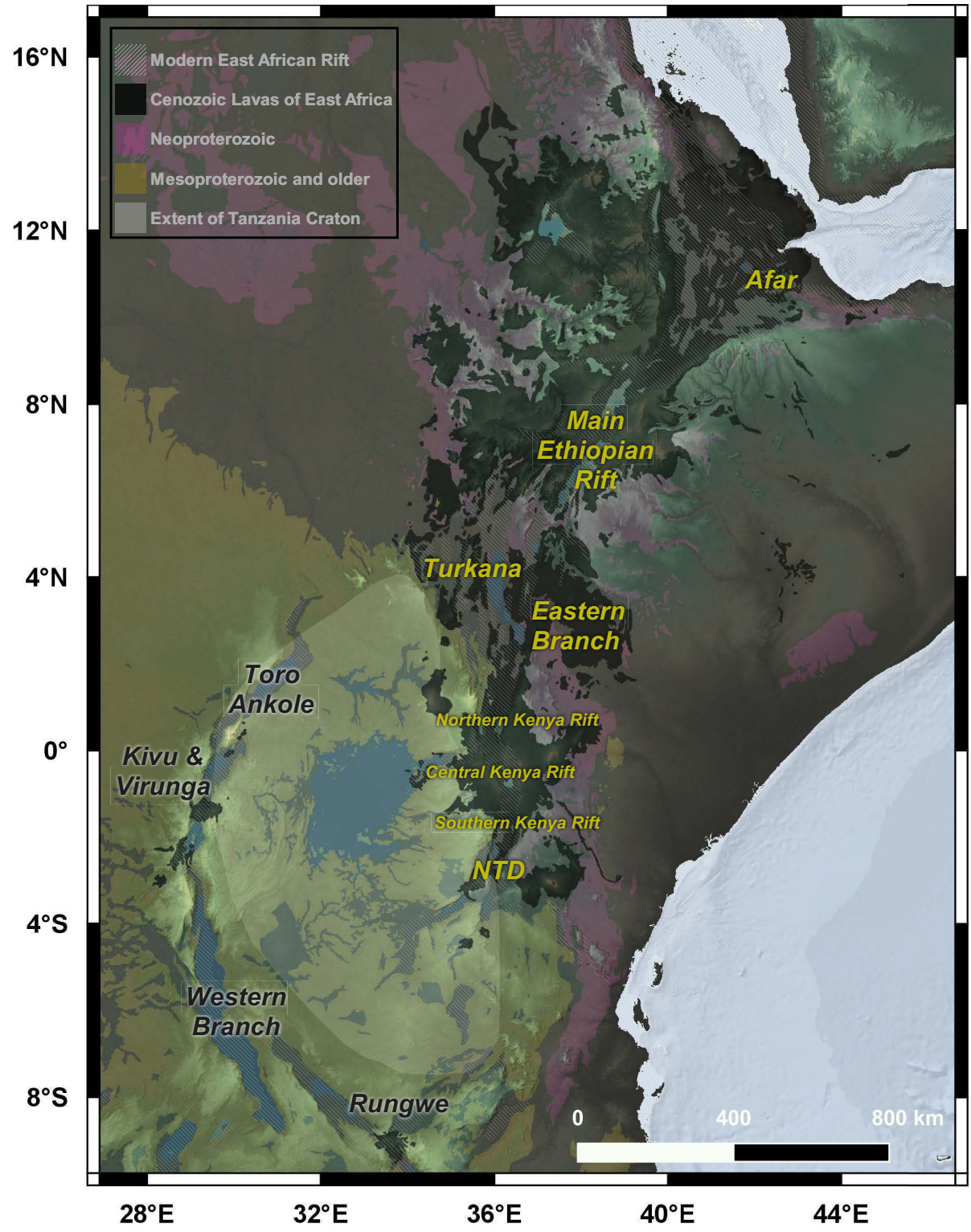
Modern East African Rift
Cenozoic Lavas of East Africa
Neoproterozoic
Mesoproterozoic and older
Extent of Tanzania Craton
16°N
12°N
8°N
4°N
0°
4°S
8°S
28°E
32°E
36°E
40°E
44°E
Afar
Main Ethiopian Rift
Turkana
Eastern Branch
Toro Ankole
Northern Kenya Rift
Kivu & Virunga
Central Kenya Rift
Southern Kenya Rift
NTD
Western Branch
Rungwe
0
400
800 km

Figure 2

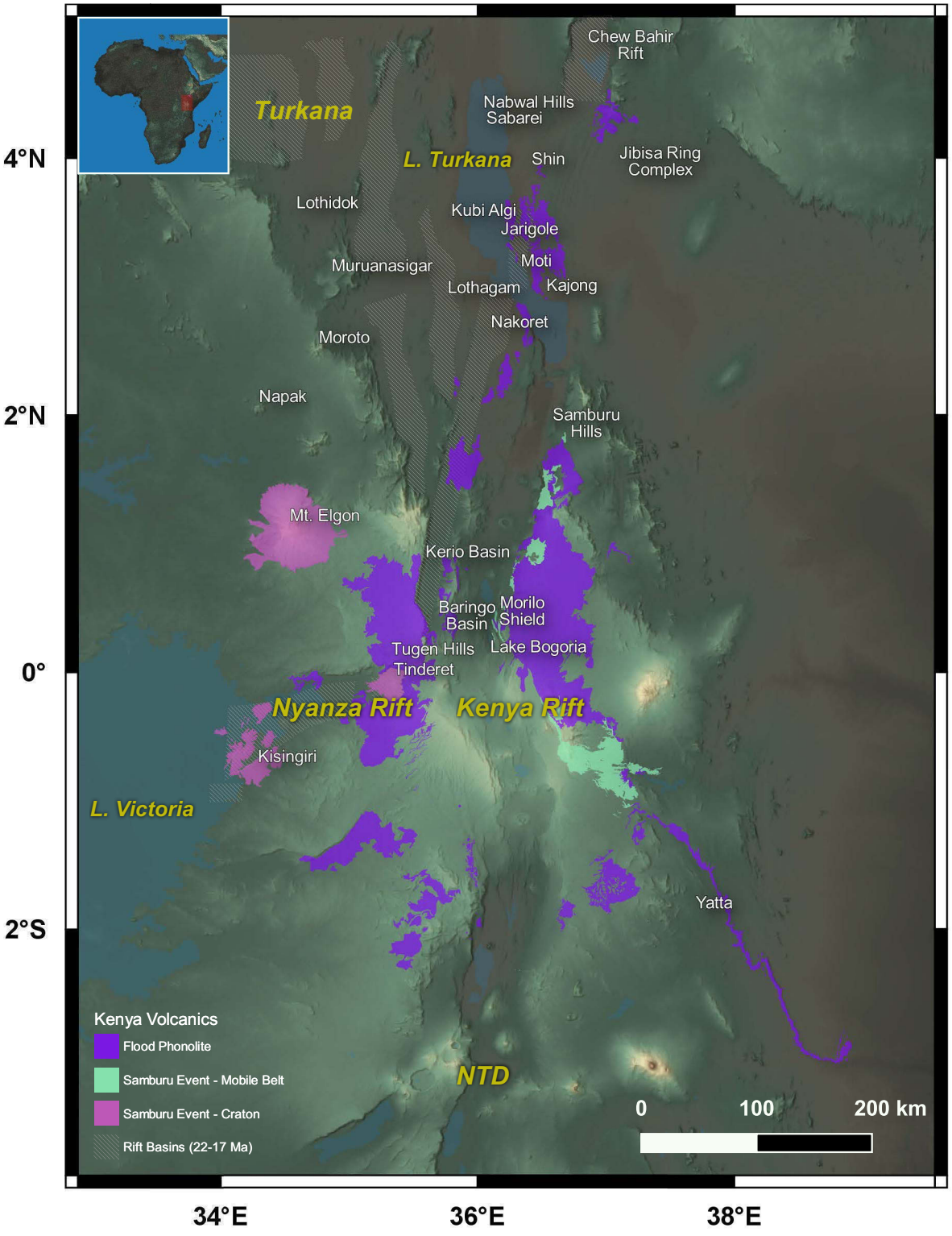
Chew Bahir Rift
Turkana
Nabwal Hills Sabarei
L. Turkana
Shin
Jibisa Ring Complex
Lothidok
Kubi Algi
Jarigole
Muruanasigar
Moti
Lothagam
Kajong
Nakoret
Moroto
Napak
Samburu Hills
Mt. Elgon
Kerio Basin
Baringo Basin
Morilo Shield
Tugen Hills
Lake Bogoria
Tinderet
Nyanza Rift
Kenya Rift
Kisingiri
L. Victoria
Yatta
NTD
Kenya Volcanics
Flood Phonolite
Samburu Event - Mobile Belt
Samburu Event - Craton
Rift Basins (22-17 Ma)
0
100
200 km
4°N
2°N
0°
2°S
34°E
36°E
38°E

Figure 3

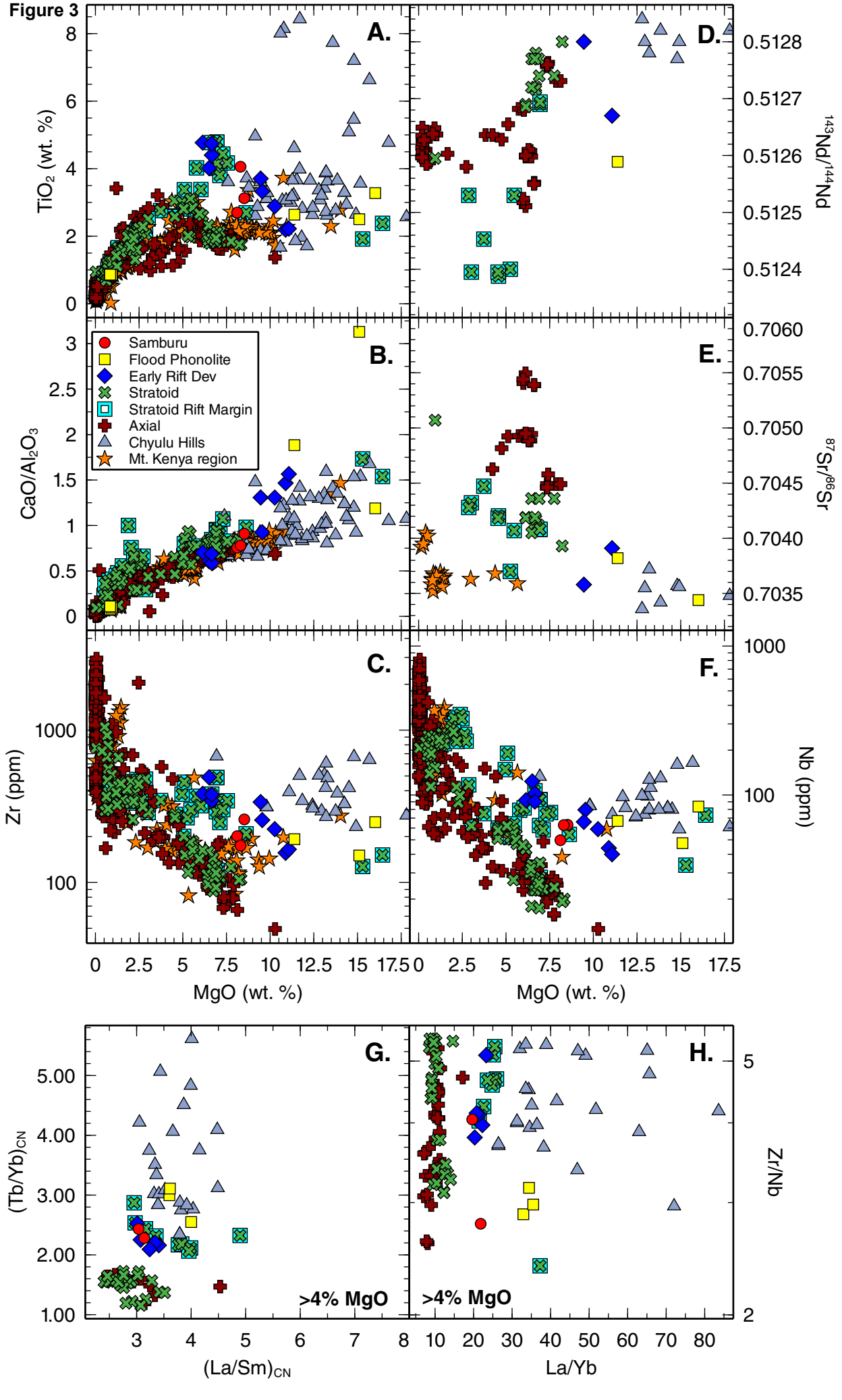
A.
B.
C.
D.
E.
F.
G.
H.
TiO2 (wt. %)
CaO/Al2O3
Zr (ppm)
143Nd/144Nd
87Sr/86Sr
Nb (ppm)
MgO (wt. %)
MgO (wt. %)
(Tb/Yb)CN
(La/Sm)CN
La/Yb
Zr/Nb
>4% MgO
>4% MgO
Samburu
Flood Phonolite
Early Rift Dev
Stratoid
Stratoid Rift Margin
Axial
Chyulu Hills
Mt. Kenya region

Figure 4

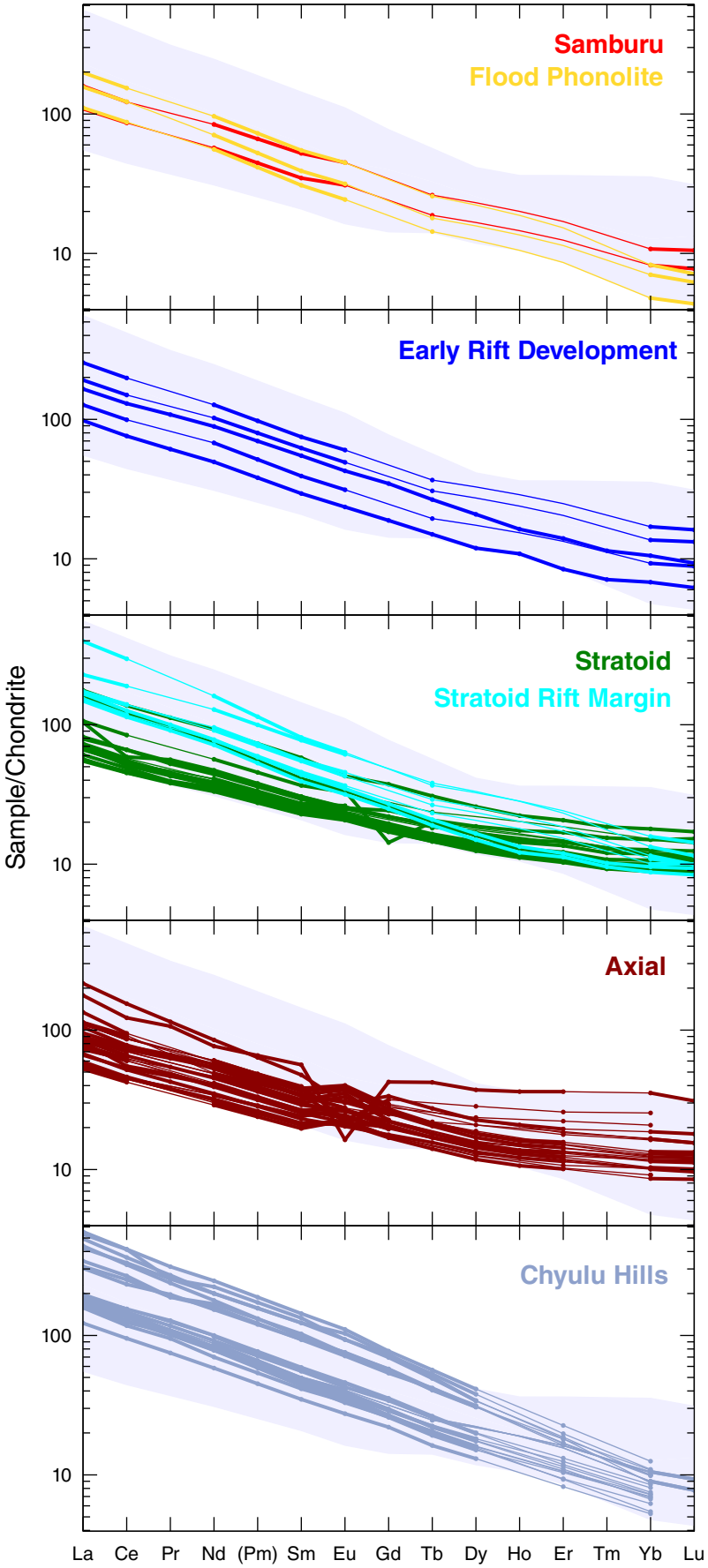
Samburu
Flood Phonolite
Early Rift Development
Stratoid
Stratoid Rift Margin
Axial
Chyulu Hills
Sample/Chondrite
100
10
La
Ce
Pr
Nd
(Pm)
Sm
Eu
Gd
Tb
Dy
Ho
Er
Tm
Yb
Lu

Figure 5

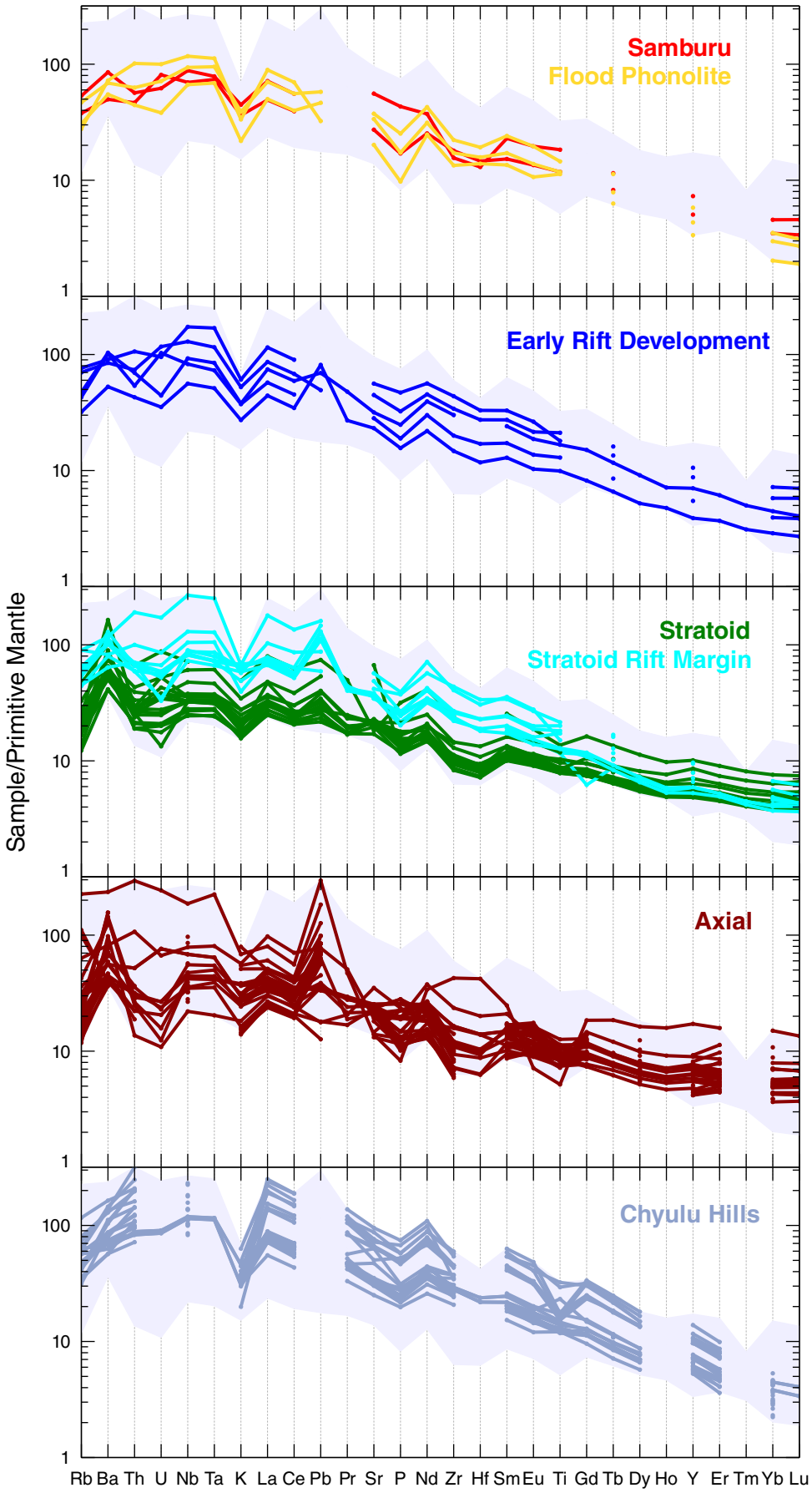
Samburu
Flood Phonolite
Early Rift Development
Stratoid
Stratoid Rift Margin
Axial
Chyulu Hills
Sample/Primitive Mantle
100
10
1
Rb Ba Th U Nb Ta K La Ce Pb Pr Sr P Nd Zr Hf Sm Eu Ti Gd Tb Dy Ho Y Er Tm Yb Lu

Figure 6

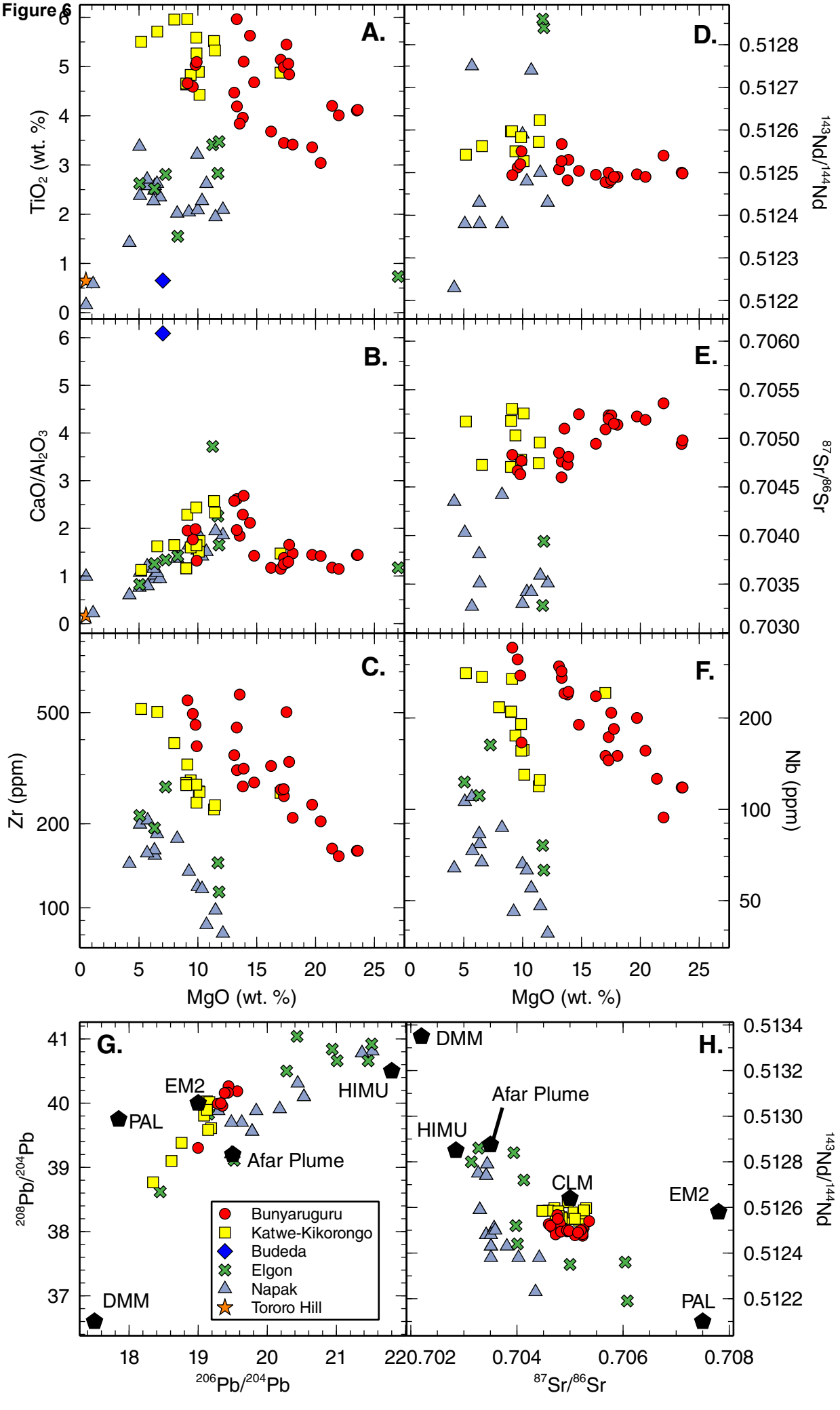
A.
B.
C.
D.
E.
F.
G.
H.
TiO2 (wt. %)
CaO/Al2O3
Zr (ppm)
143Nd/144Nd
87Sr/86Sr
Nb (ppm)
MgO (wt. %)
MgO (wt. %)
208Pb/204Pb
206Pb/204Pb
87Sr/86Sr
143Nd/144Nd
EM2
HIMU
PAL
Afar Plume
DMM
CLM
Bunyaruguru
Katwe-Kikorongo
Budeda
Elgon
Napak
Tororo Hill

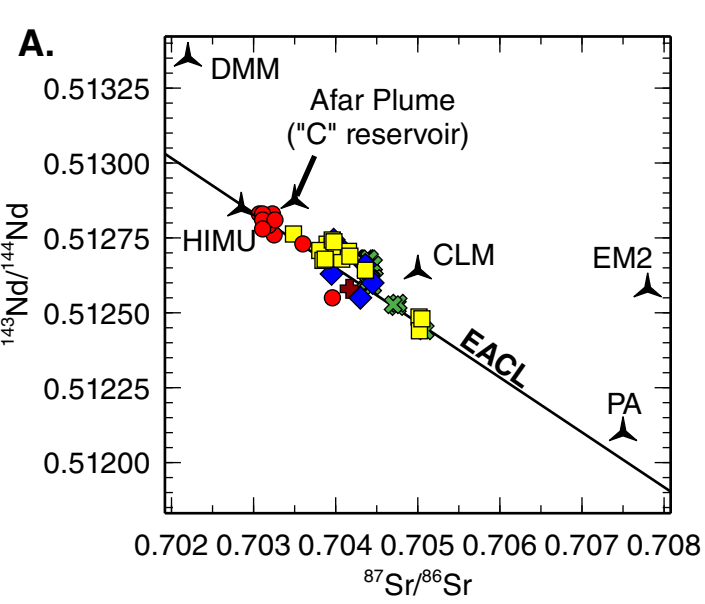
A.
DMM
Afar Plume
("C" reservoir)
HIMU
CLM
EM2
EACL
PA
0.51325
0.51300
0.51275
0.51250
0.51225
0.51200
143Nd/144Nd
0.702 0.703 0.704 0.705 0.706 0.707 0.708
87Sr/86Sr

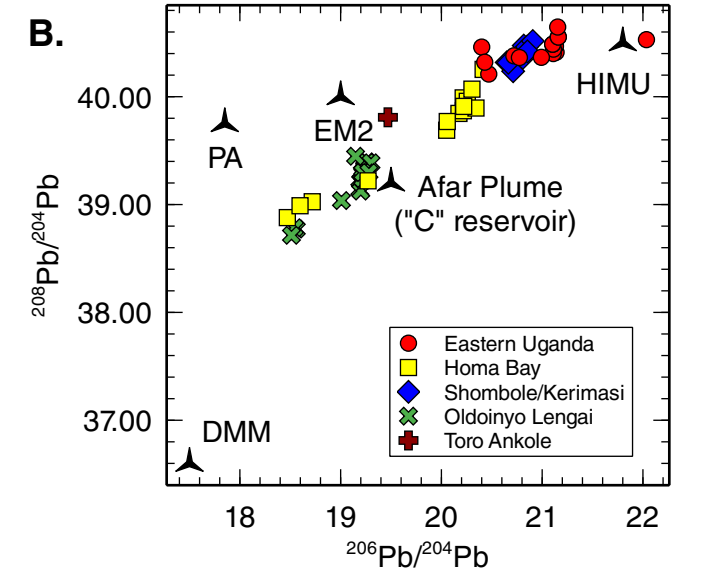
B.
HIMU
EM2
PA
Afar Plume
("C" reservoir)
DMM
40.00
39.00
38.00
37.00
208Pb/204Pb
18 19 20 21 22
206Pb/204Pb
Eastern Uganda
Homa Bay
Shombole/Kerimasi
Oldoinyo Lengai
Toro Ankole

Figure 8

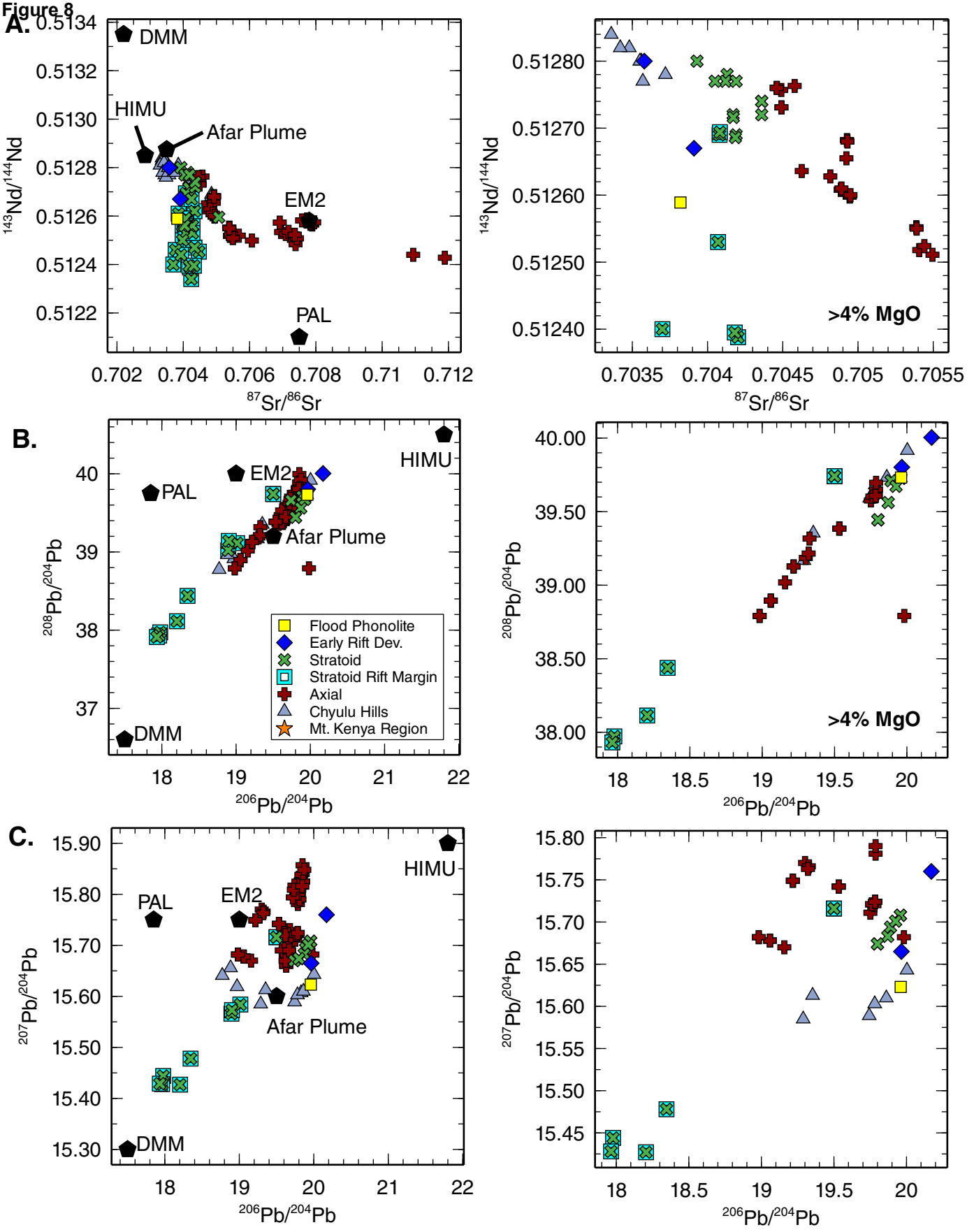
A.
DMM
HIMU
Afar Plume
EM2
PAL
$^{143}Nd/^{144}Nd$
$^{87}Sr/^{86}Sr$
>4% MgO
B.
HIMU
EM2
PAL
Afar Plume
DMM
Flood Phonolite
Early Rift Dev.
Stratoid
Stratoid Rift Margin
Axial
Chyulu Hills
Mt. Kenya Region
$^{208}Pb/^{204}Pb$
$^{206}Pb/^{204}Pb$
>4% MgO
C.
HIMU
EM2
PAL
Afar Plume
DMM
$^{207}Pb/^{204}Pb$
$^{206}Pb/^{204}Pb$

Figure 9

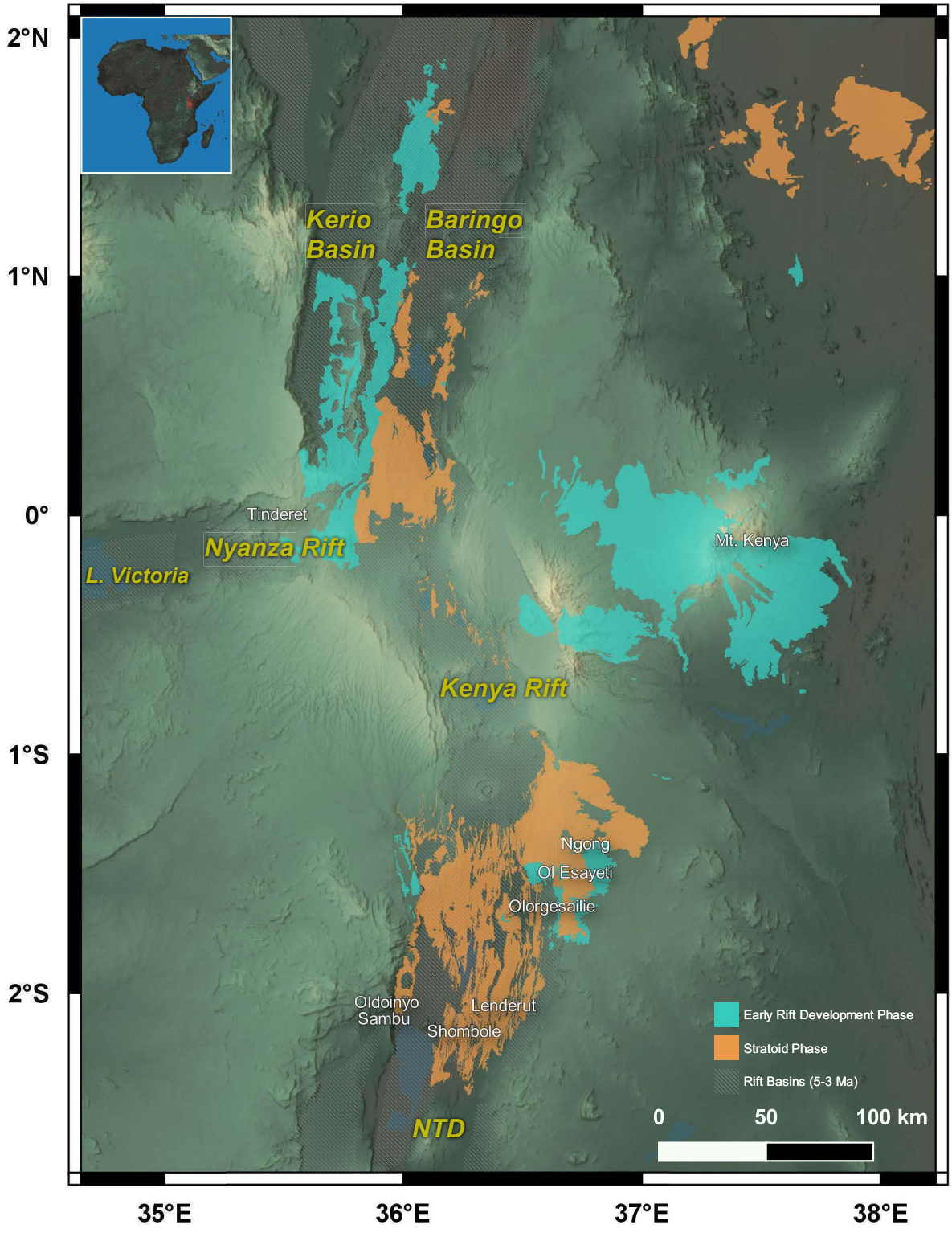
2°N
1°N
0°
1°S
2°S
35°E
36°E
37°E
38°E
Kerio Basin
Baringo Basin
Tinderet
Nyanza Rift
L. Victoria
Mt. Kenya
Kenya Rift
Ngong
Ol Esayeti
Olorgesailie
Oldoinyo Sambu
Lenderut
Shombole
NTD
Early Rift Development Phase
Stratoid Phase
Rift Basins (5-3 Ma)
0
50
100 km

Figure 10

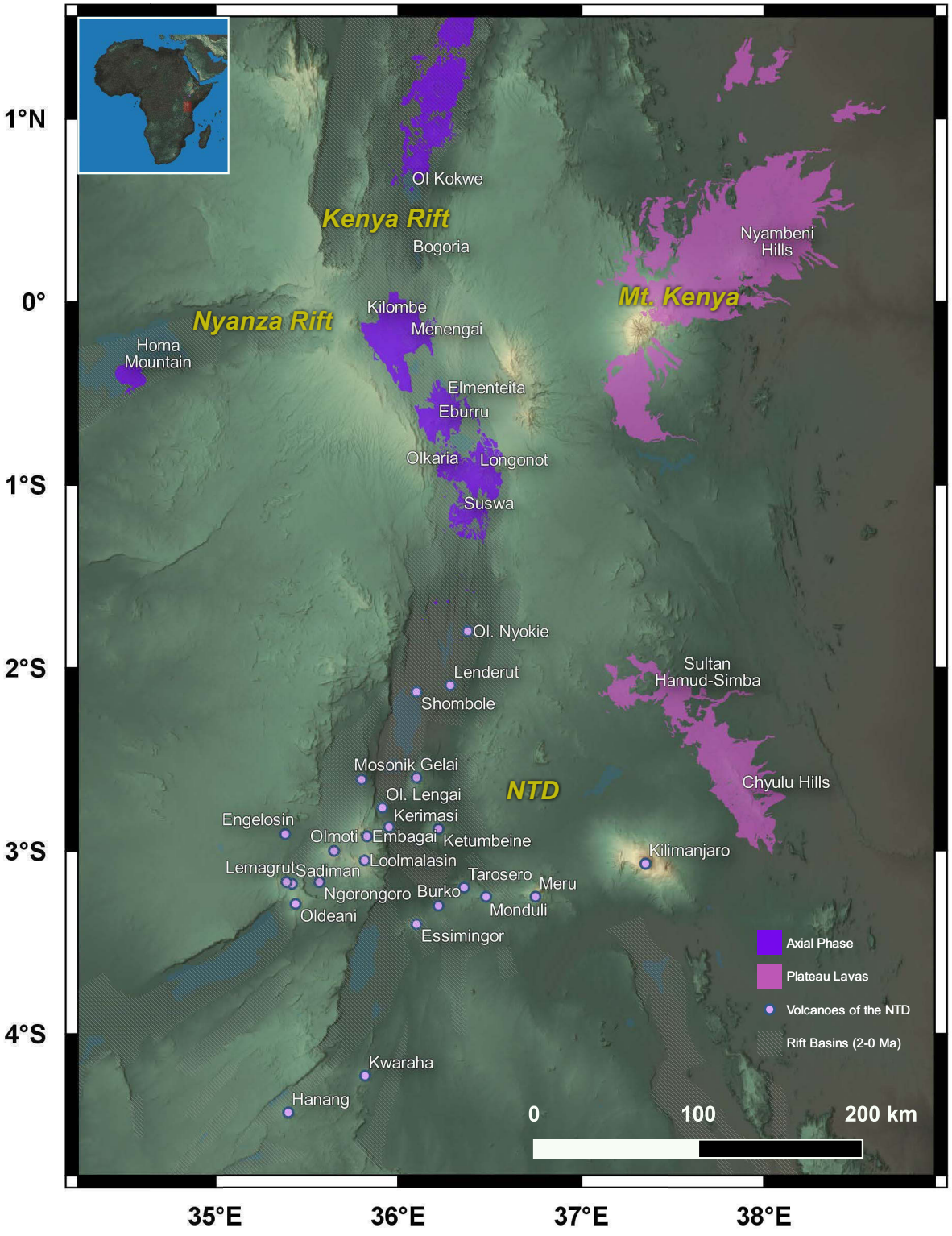
1°N
0°
1°S
2°S
3°S
4°S
35°E
36°E
37°E
38°E
Ol Kokwe
Kenya Rift
Bogoria
Nyambeni Hills
Mt. Kenya
Nyanza Rift
Kilombe
Menengai
Homa Mountain
Elmenteita
Eburru
Olkaria
Longonot
Suswa
Ol. Nyokie
Lenderut
Shombole
Sultan Hamud-Simba
Mosonik Gelai
Ol. Lengai
NTD
Chyulu Hills
Kerimasi
Engelosin
Olmoti
Embagai
Ketumbeine
Kilimanjaro
Loolmalasin
Lemagrut
Sadiman
Tarosero
Meru
Ngorongoro
Burko
Monduli
Oldeani
Essimingor
Axial Phase
Plateau Lavas
Volcanoes of the NTD
Rift Basins (2-0 Ma)
Kwaraha
Hanang
0
100
200 km

Figure 11

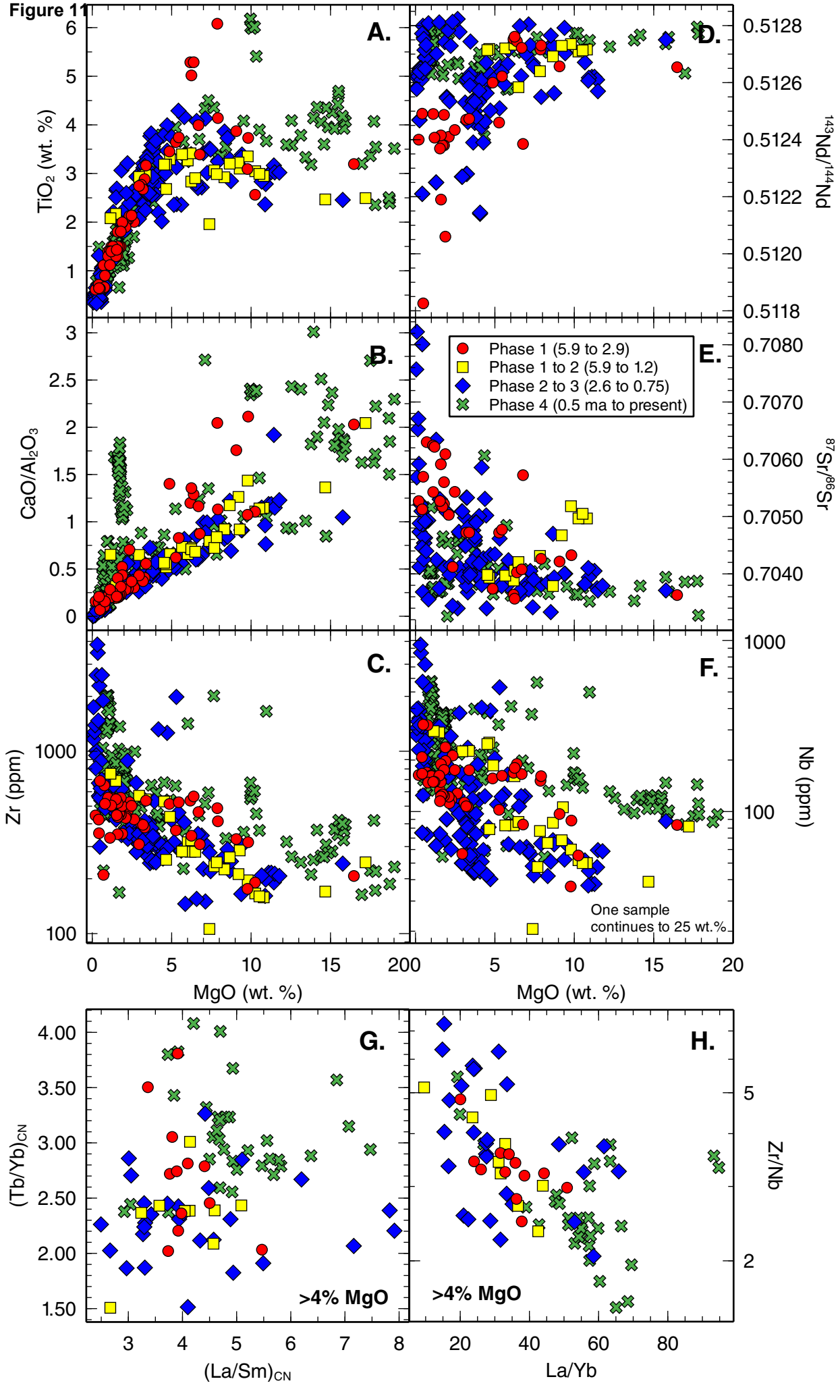
A.
B.
C.
D.
E.
F.
G.
H.
TiO2 (wt. %)
CaO/Al2O3
Zr (ppm)
143Nd/144Nd
87Sr/86Sr
Nb (ppm)
MgO (wt. %)
MgO (wt. %)
Phase 1 (5.9 to 2.9)
Phase 1 to 2 (5.9 to 1.2)
Phase 2 to 3 (2.6 to 0.75)
Phase 4 (0.5 ma to present)
One sample
continues to 25 wt.%
(Tb/Yb)CN
(La/Sm)CN
>4% MgO
La/Yb
Zr/Nb
>4% MgO

Figure 12

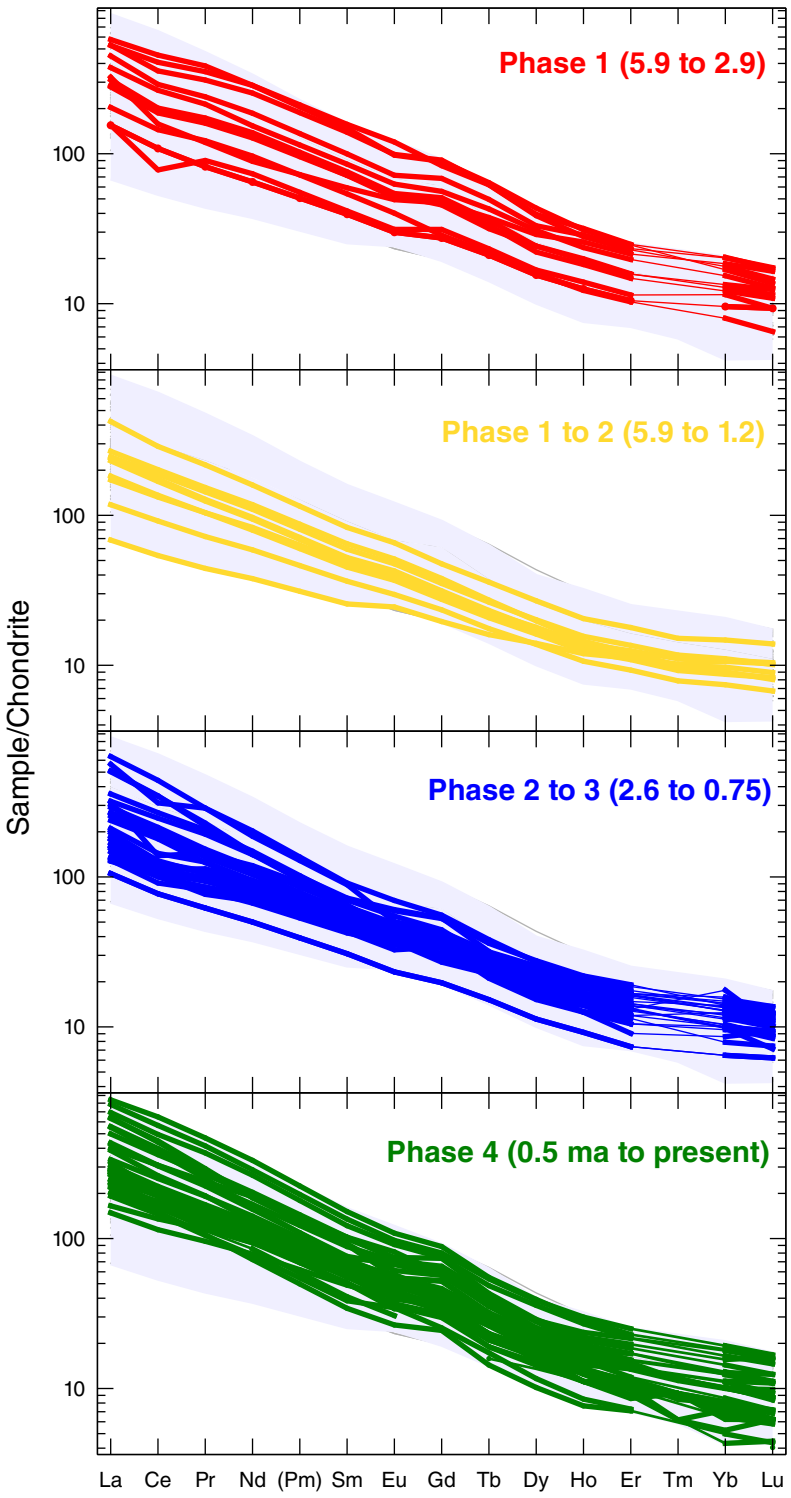
Phase 1 (5.9 to 2.9)
Phase 1 to 2 (5.9 to 1.2)
Phase 2 to 3 (2.6 to 0.75)
Phase 4 (0.5 ma to present)
Sample/Chondrite
100
10
La Ce Pr Nd (Pm) Sm Eu Gd Tb Dy Ho Er Tm Yb Lu

Figure 13

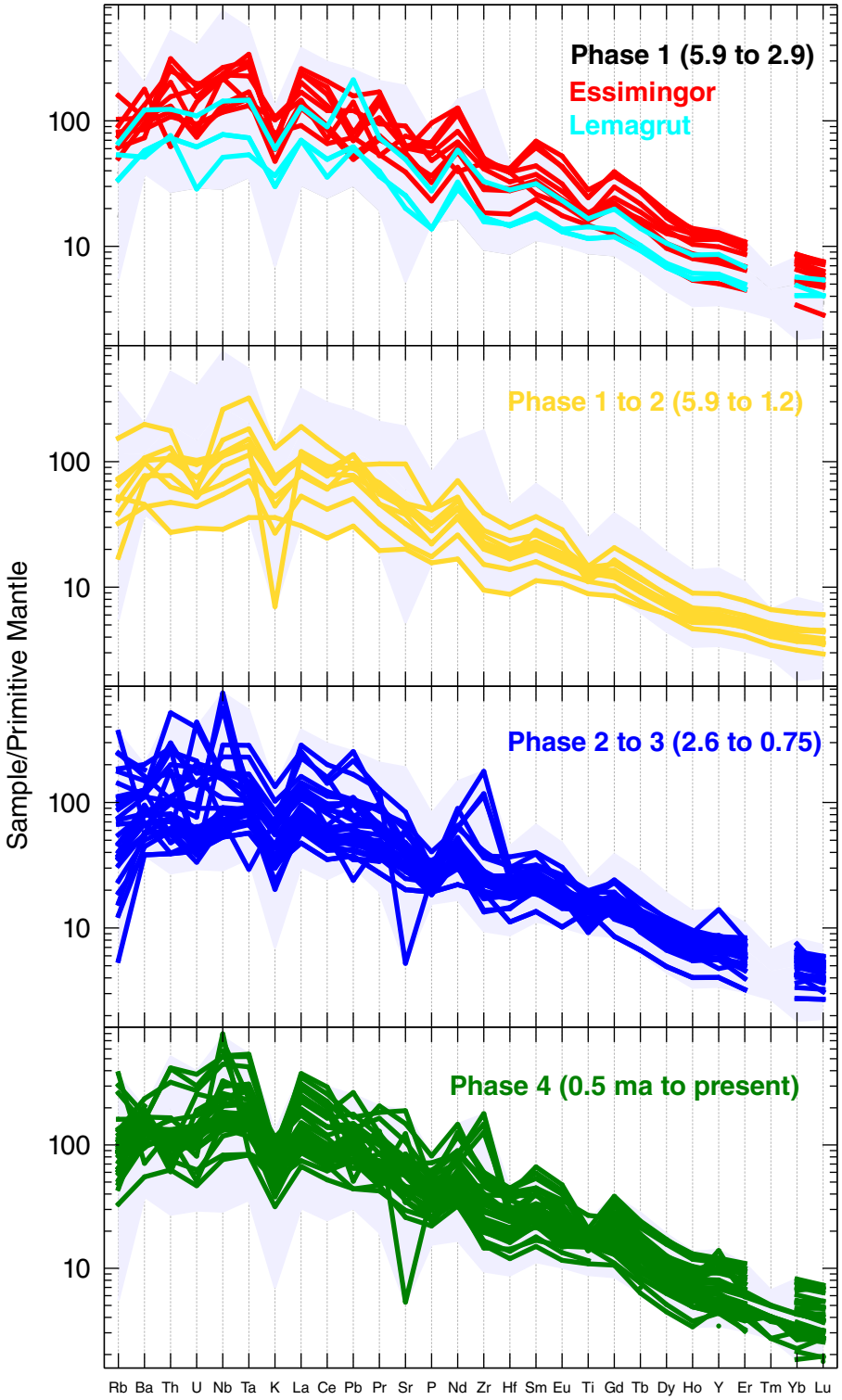
Phase 1 (5.9 to 2.9)
Essimingor
Lemagrut
Phase 1 to 2 (5.9 to 1.2)
Phase 2 to 3 (2.6 to 0.75)
Phase 4 (0.5 ma to present)
Sample/Primitive Mantle
100
10
Rb Ba Th U Nb Ta K La Ce Pb Pr Sr P Nd Zr Hf Sm Eu Ti Gd Tb Dy Ho Y Er Tm Yb Lu

Figure 14

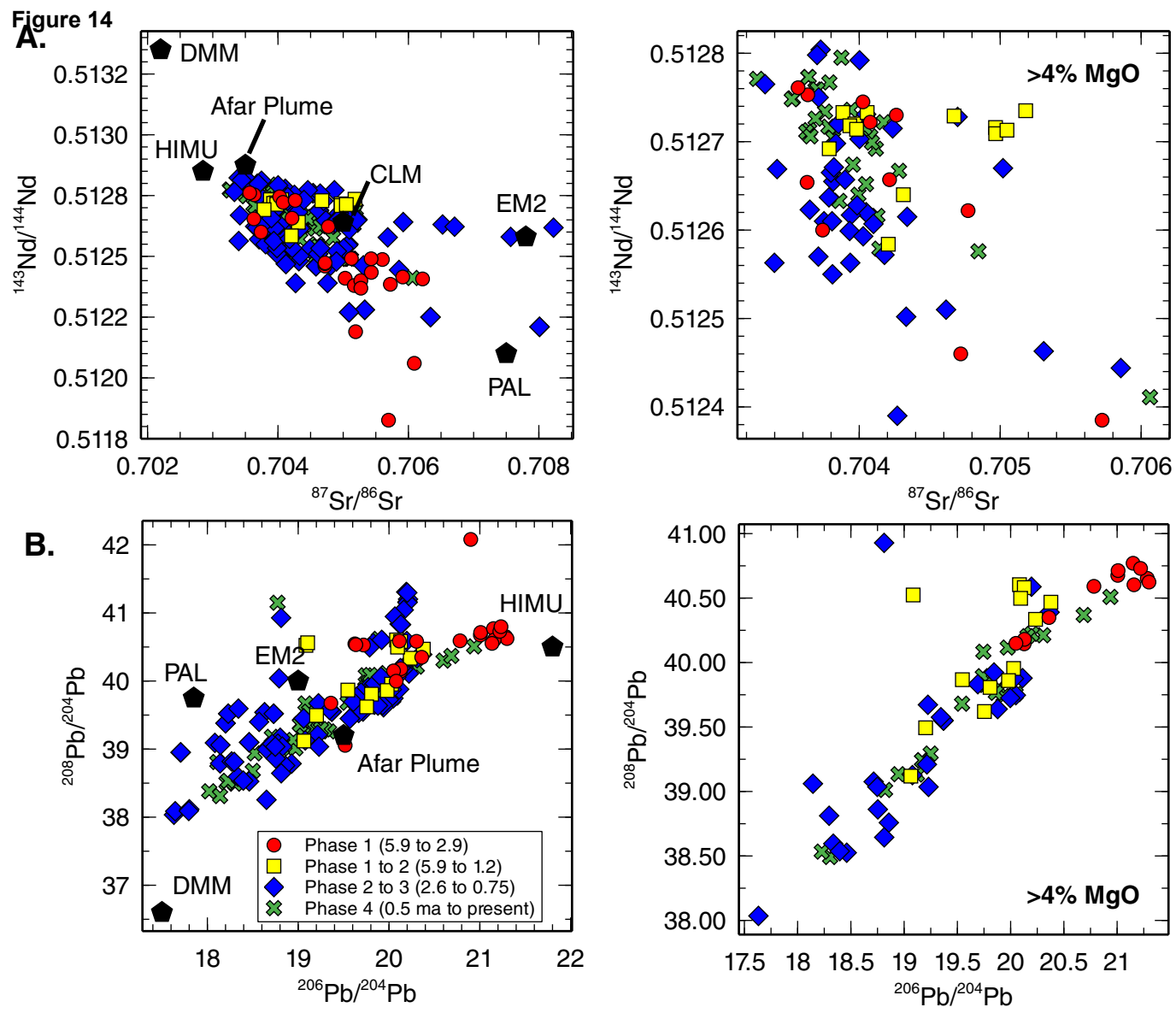
A.
DMM
Afar Plume
HIMU
CLM
EM2
PAL
0.5132
0.5130
0.5128
0.5125
0.5122
0.5120
0.5118
0.702
0.704
0.706
0.708
143Nd/144Nd
87Sr/86Sr
>4% MgO
0.5128
0.5127
0.5126
0.5125
0.5124
0.704
0.705
0.706
B.
HIMU
EM2
PAL
Afar Plume
DMM
42
41
40
39
38
37
18
19
20
21
22
208Pb/204Pb
206Pb/204Pb
Phase 1 (5.9 to 2.9)
Phase 1 to 2 (5.9 to 1.2)
Phase 2 to 3 (2.6 to 0.75)
Phase 4 (0.5 ma to present)
41.00
40.50
40.00
39.50
39.00
38.50
38.00
17.5
18
18.5
19
19.5
20
20.5
21
>4% MgO

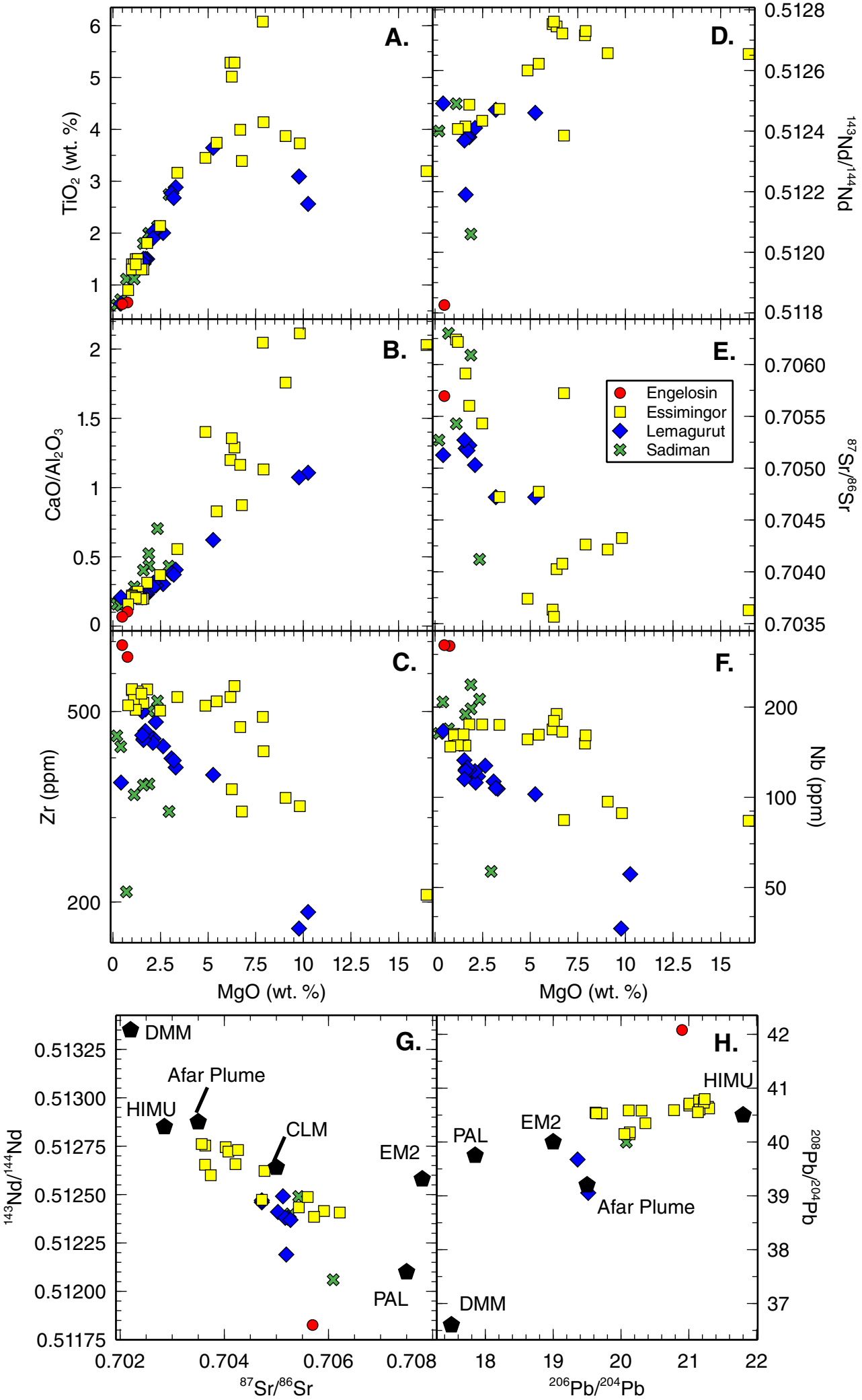
A.
B.
C.
D.
E.
F.
G.
H.
TiO2 (wt. %)
CaO/Al2O3
Zr (ppm)
143Nd/144Nd
87Sr/86Sr
Nb (ppm)
MgO (wt. %)
MgO (wt. %)
Engelosin
Essimingor
Lemagurut
Sadiman
DMM
Afar Plume
HIMU
CLM
EM2
PAL
87Sr/86Sr
143Nd/144Nd
206Pb/204Pb
208Pb/204Pb

Figure 16

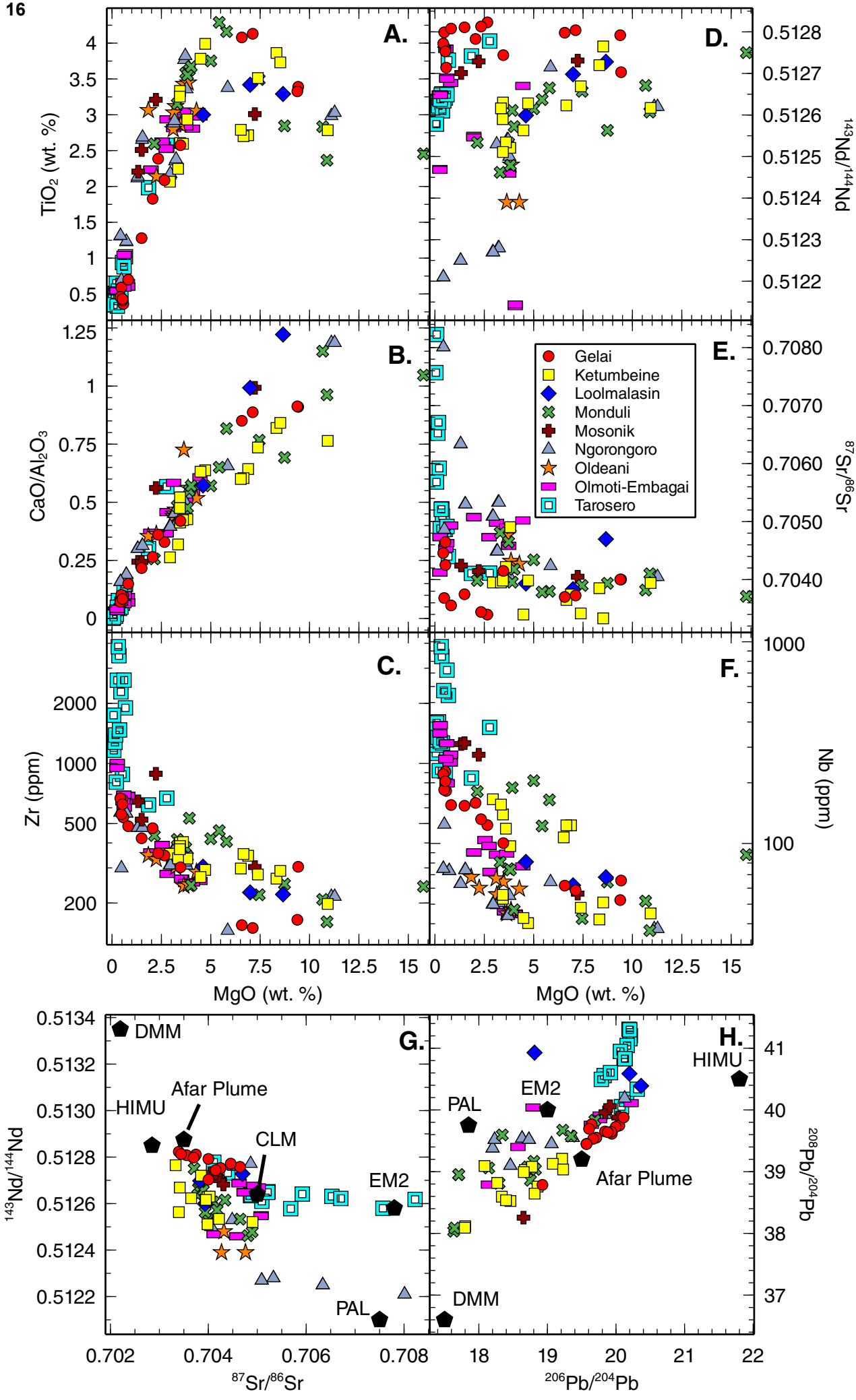
A.
B.
C.
D.
E.
F.
G.
H.
TiO2 (wt. %)
CaO/Al2O3
Zr (ppm)
143Nd/144Nd
87Sr/86Sr
Nb (ppm)
MgO (wt. %)
MgO (wt. %)
Gelai
Ketumbeine
Loolmalasin
Monduli
Mosonik
Ngorongoro
Oldeani
Olmoti-Embagai
Tarosero
DMM
Afar Plume
HIMU
CLM
EM2
PAL
87Sr/86Sr
206Pb/204Pb
208Pb/204Pb

Figure 17

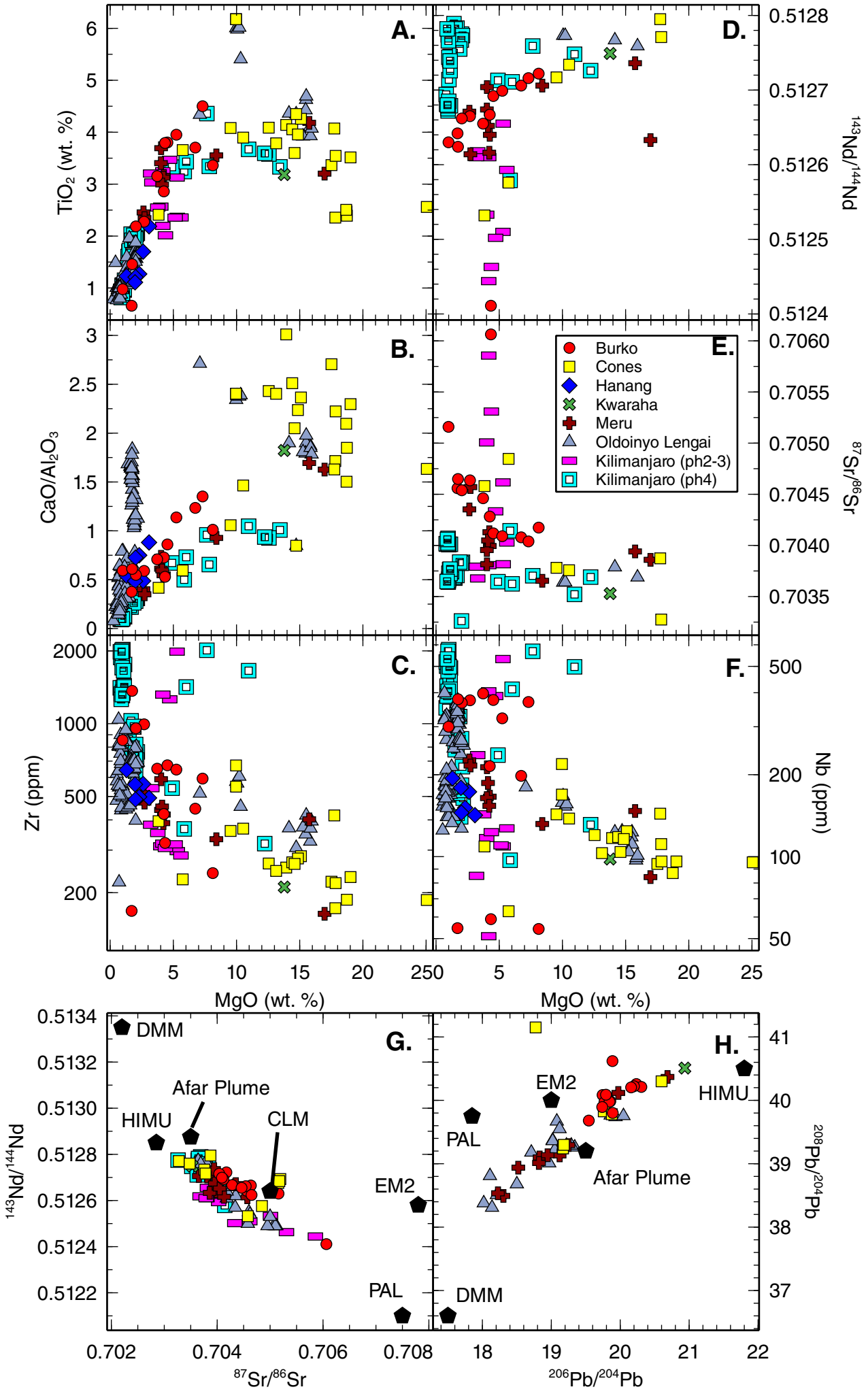
A.
B.
C.
D.
E.
F.
G.
H.
TiO2 (wt. %)
CaO/Al2O3
Zr (ppm)
143Nd/144Nd
87Sr/86Sr
Nb (ppm)
MgO (wt. %)
MgO (wt. %)
Burko
Cones
Hanang
Kwaraha
Meru
Oldoinyo Lengai
Kilimanjaro (ph2-3)
Kilimanjaro (ph4)
DMM
Afar Plume
HIMU
CLM
EM2
PAL
DMM
EM2
HIMU
PAL
Afar Plume
DMM
87Sr/86Sr
206Pb/204Pb
208Pb/204Pb

Figure 18

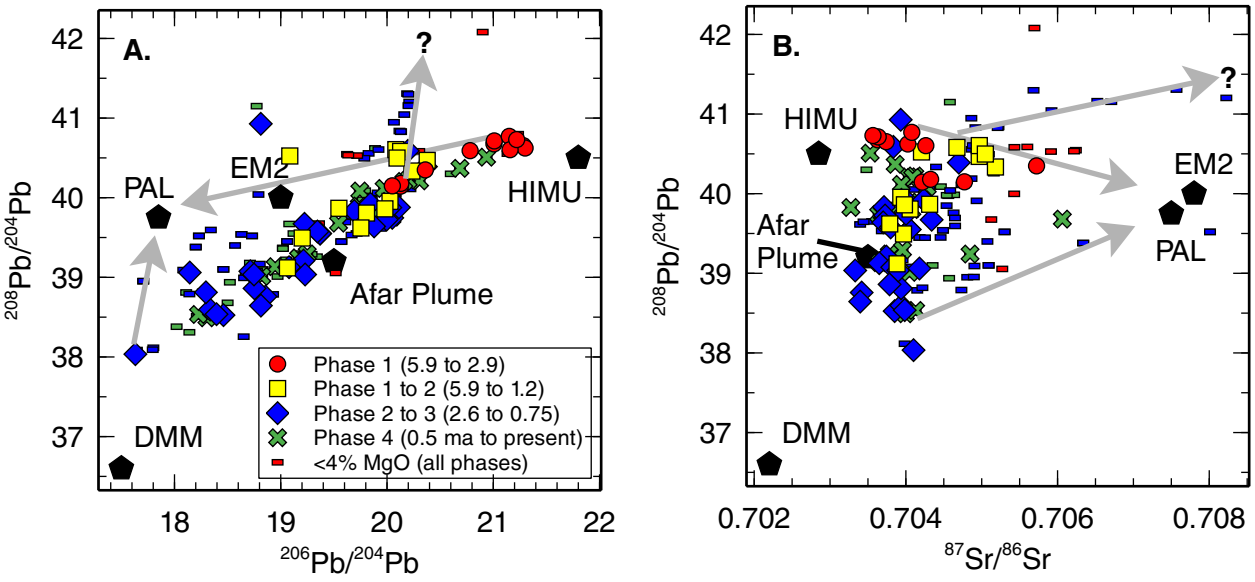
A.
?
EM2
PAL
HIMU
Afar Plume
DMM
Phase 1 (5.9 to 2.9)
Phase 1 to 2 (5.9 to 1.2)
Phase 2 to 3 (2.6 to 0.75)
Phase 4 (0.5 ma to present)
<4% MgO (all phases)
208Pb/204Pb
206Pb/204Pb
42
41
40
39
38
37
18
19
20
21
22
B.
?
HIMU
EM2
Afar
Plume
PAL
DMM
208Pb/204Pb
87Sr/86Sr
0.702
0.704
0.706
0.708

Figure 19

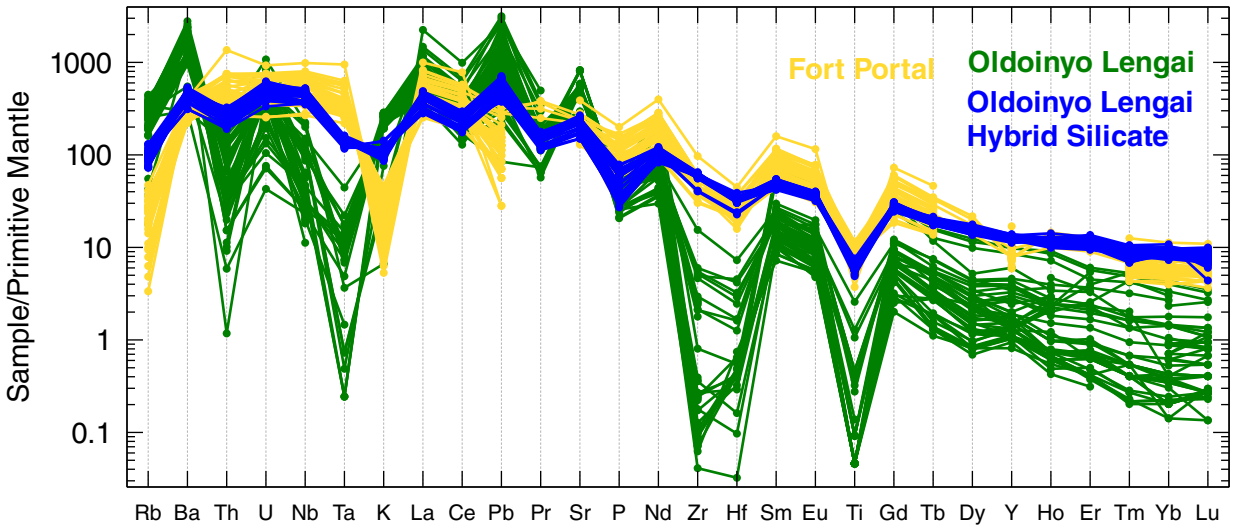
Sample/Primitive Mantle
1000
100
10
1
0.1
Rb Ba Th U Nb Ta K La Ce Pb Pr Sr P Nd Zr Hf Sm Eu Ti Gd Tb Dy Y Ho Er Tm Yb Lu
Fort Portal
Oldoinyo Lengai
Oldoinyo Lengai
Hybrid Silicate

Figure 20

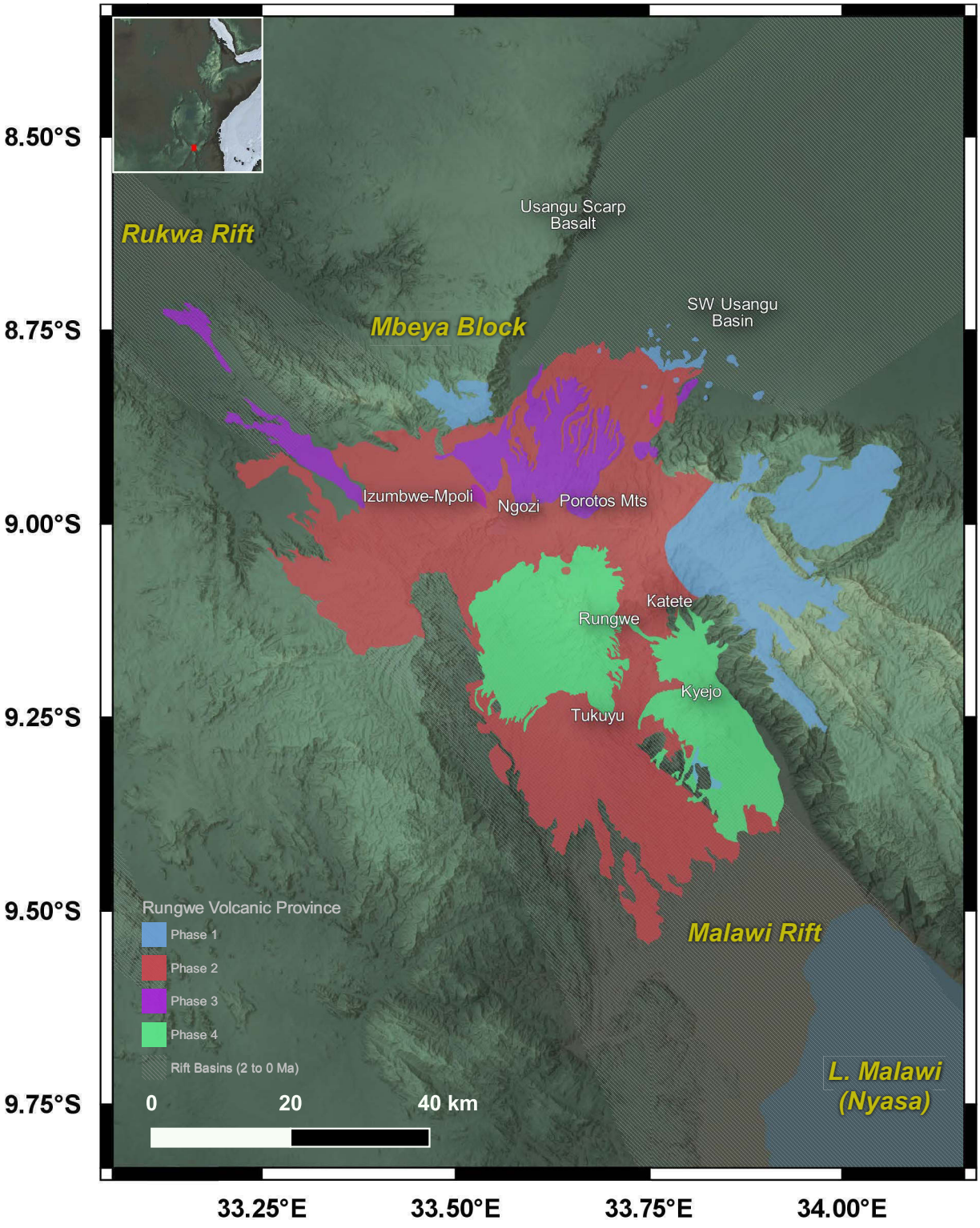
8.50°S
8.75°S
9.00°S
9.25°S
9.50°S
9.75°S
33.25°E
33.50°E
33.75°E
34.00°E
Rukwa Rift
Usangu Scarp Basalt
SW Usangu Basin
Mbeya Block
Izumbwe-Mpoli
Ngozi
Porotos Mts
Katete
Rungwe
Kyejo
Tukuyu
Malawi Rift
L. Malawi (Nyasa)
Rungwe Volcanic Province
Phase 1
Phase 2
Phase 3
Phase 4
Rift Basins (2 to 0 Ma)
0
20
40 km

Figure 21

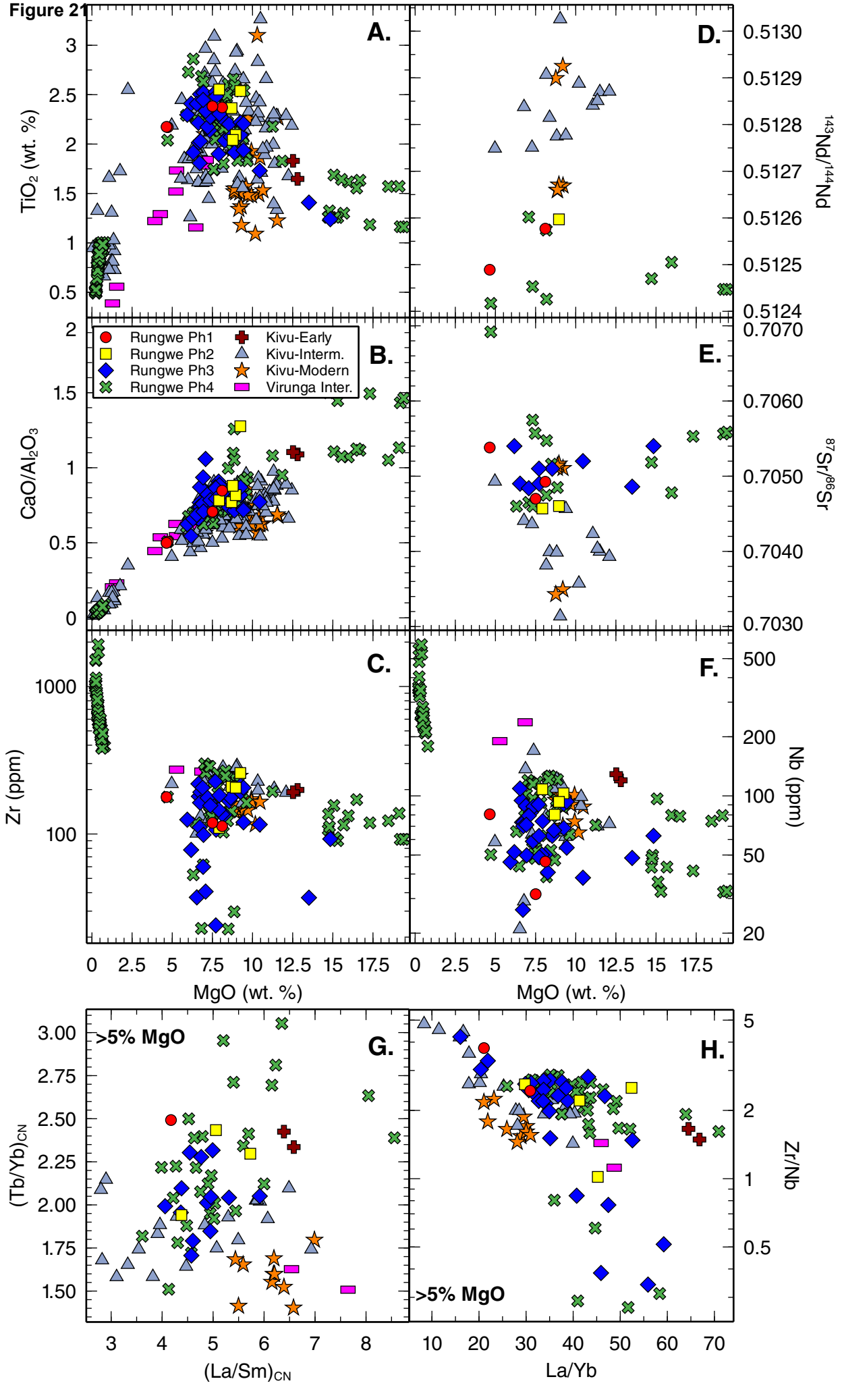
A.
B.
C.
D.
E.
F.
G.
H.
TiO2 (wt. %)
CaO/Al2O3
Zr (ppm)
143Nd/144Nd
87Sr/86Sr
Nb (ppm)
MgO (wt. %)
MgO (wt. %)
Rungwe Ph1
Rungwe Ph2
Rungwe Ph3
Rungwe Ph4
Kivu-Early
Kivu-Interm.
Kivu-Modern
Virunga Inter.
>5% MgO
>5% MgO
(Tb/Yb)CN
(La/Sm)CN
La/Yb
Zr/Nb

Figure 22

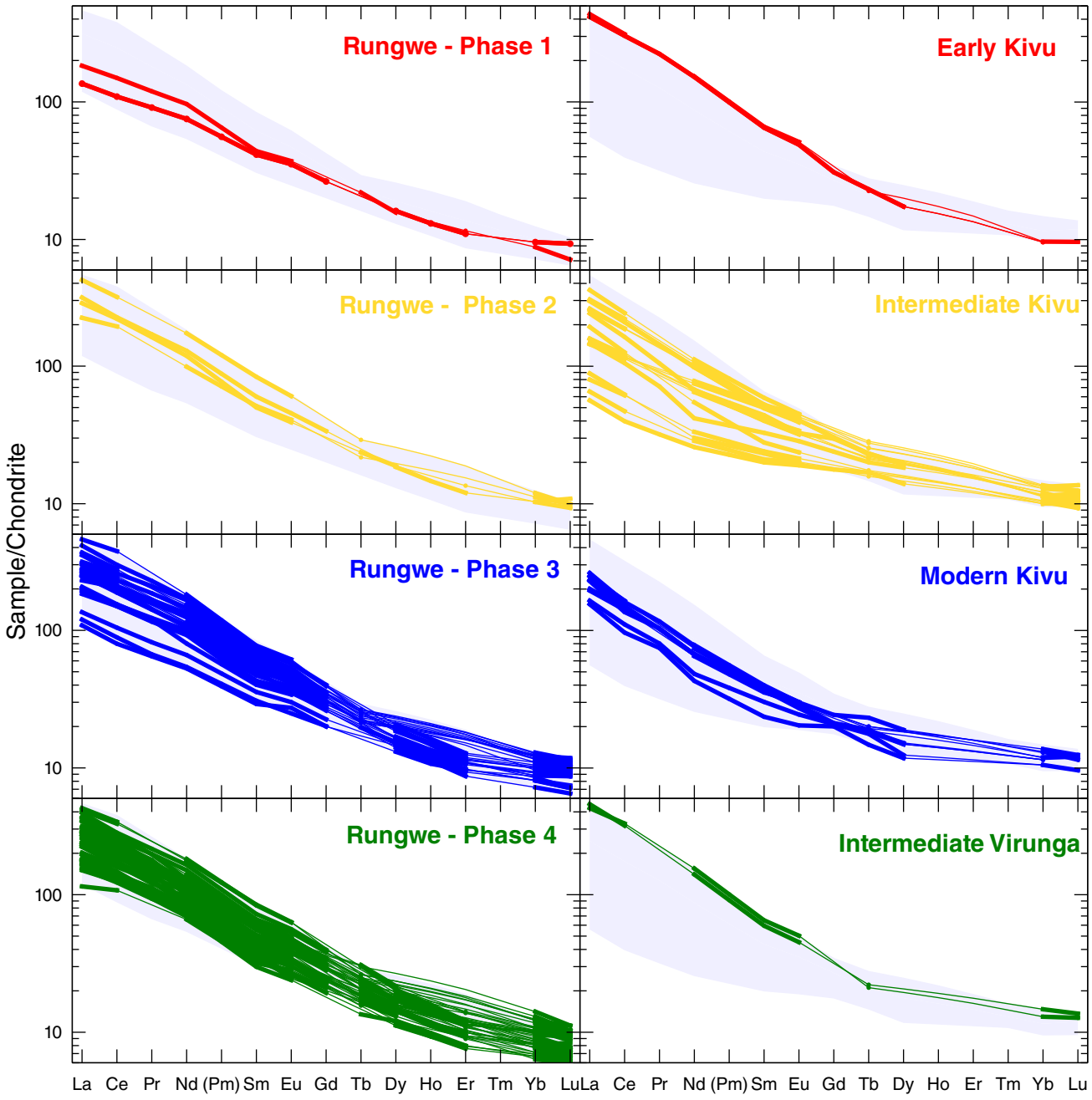
Rungwe - Phase 1
Early Kivu
Rungwe - Phase 2
Intermediate Kivu
Rungwe - Phase 3
Modern Kivu
Rungwe - Phase 4
Intermediate Virunga
Sample/Chondrite
100
10
La Ce Pr Nd (Pm) Sm Eu Gd Tb Dy Ho Er Tm Yb Lu

Figure 23

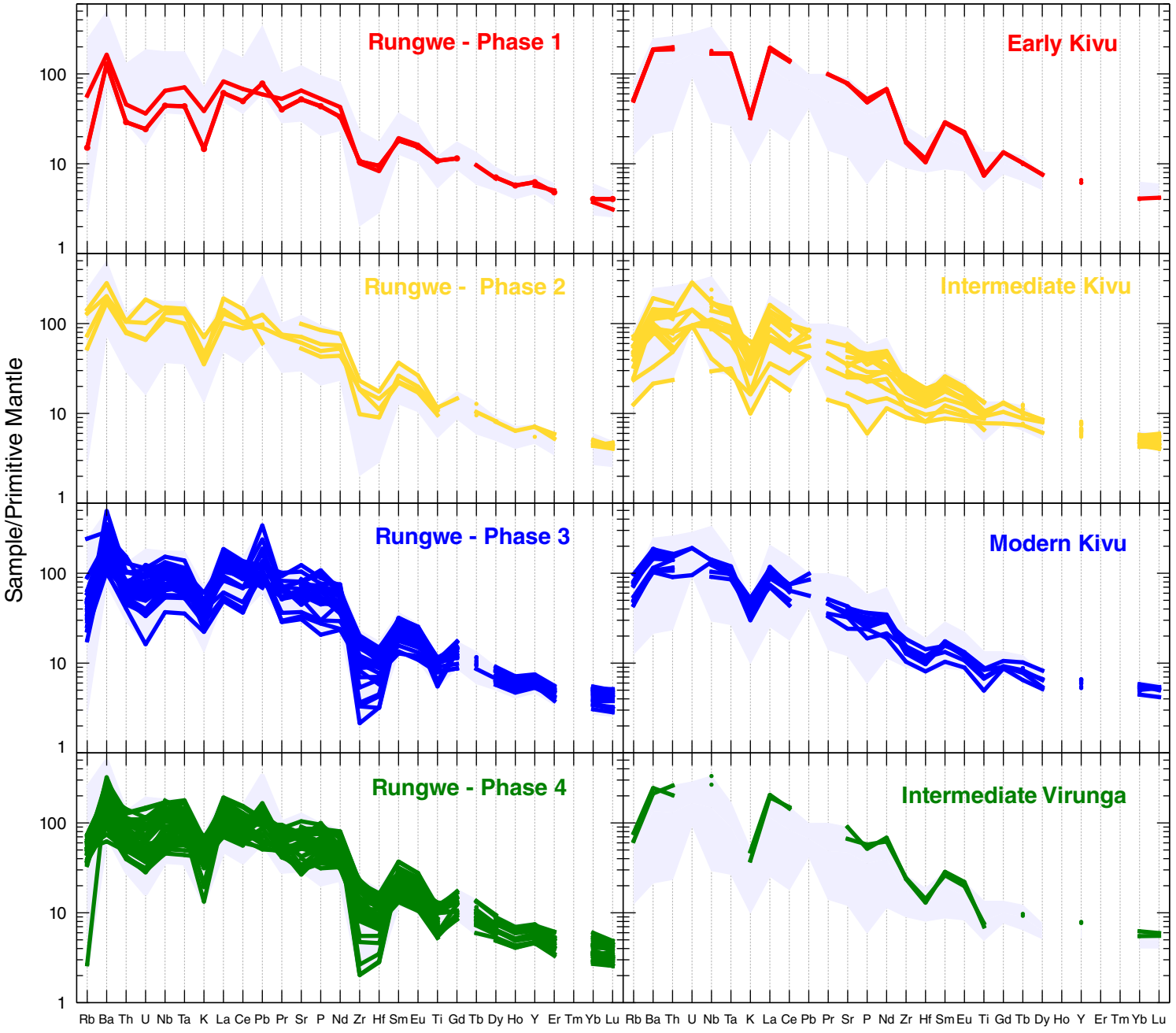
Rungwe - Phase 1
Early Kivu
Rungwe - Phase 2
Intermediate Kivu
Rungwe - Phase 3
Modern Kivu
Rungwe - Phase 4
Intermediate Virunga
Sample/Primitive Mantle
100
10
1
Rb Ba Th U Nb Ta K La Ce Pb Pr Sr P Nd Zr Hf Sm Eu Ti Gd Tb Dy Ho Y Er Tm Yb Lu
Rb Ba Th U Nb Ta K La Ce Pb Pr Sr P Nd Zr Hf Sm Eu Ti Gd Tb Dy Ho Y Er Tm Yb Lu

Figure 24

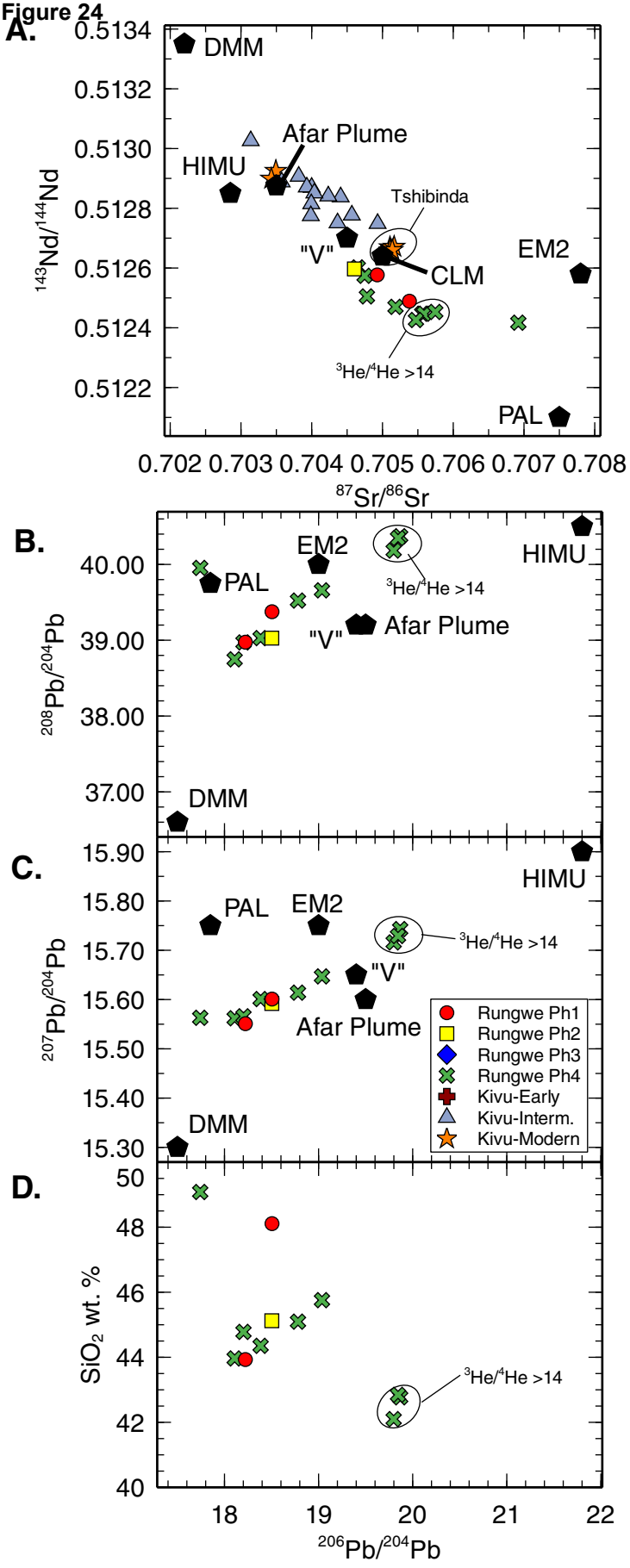
A.
DMM
Afar Plume
HIMU
Tshibinda
"V"
CLM
EM2
PAL
$^{3}He/^{4}He$ >14
$^{143}Nd/^{144}Nd$
$^{87}Sr/^{86}Sr$
B.
EM2
HIMU
PAL
$^{3}He/^{4}He$ >14
"V"
Afar Plume
DMM
$^{208}Pb/^{204}Pb$
C.
HIMU
PAL
EM2
$^{3}He/^{4}He$ >14
"V"
Afar Plume
DMM
Rungwe Ph1
Rungwe Ph2
Rungwe Ph3
Rungwe Ph4
Kivu-Early
Kivu-Interm.
Kivu-Modern
$^{207}Pb/^{204}Pb$
D.
$^{3}He/^{4}He$ >14
SiO_2 wt. %
$^{206}Pb/^{204}Pb$

Figure 25

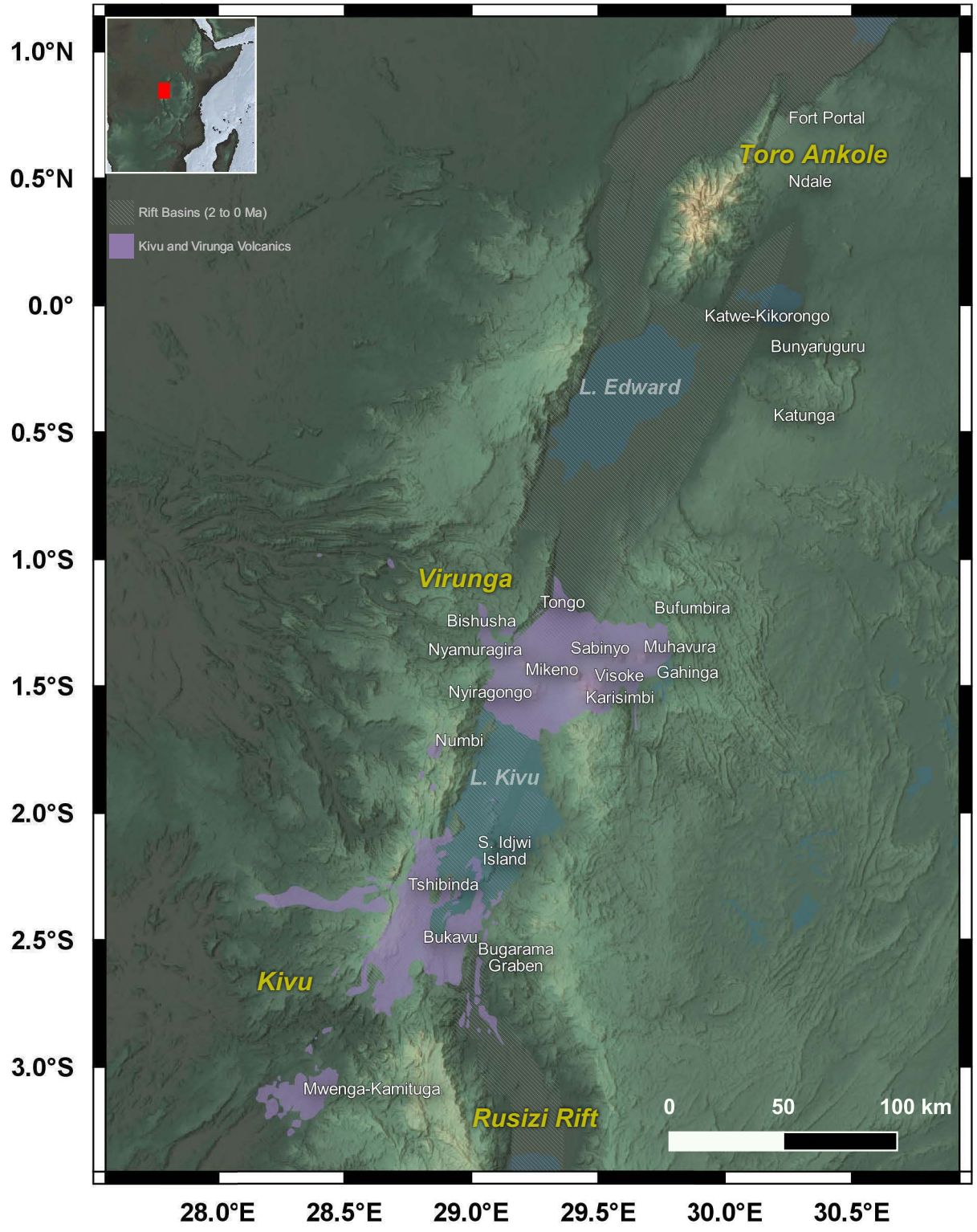
1.0°N
0.5°N
0.0°
0.5°S
1.0°S
1.5°S
2.0°S
2.5°S
3.0°S
28.0°E
28.5°E
29.0°E
29.5°E
30.0°E
30.5°E
Rift Basins (2 to 0 Ma)
Kivu and Virunga Volcanics
Fort Portal
Toro Ankole
Ndale
Katwe-Kikorongo
Bunyaruguru
L. Edward
Katunga
Virunga
Tongo
Bufumbira
Bishusha
Nyamuragira
Sabinyo
Muhavura
Mikeno
Visoke
Gahinga
Nyiragongo
Karisimbi
Numbi
L. Kivu
S. Idjwi Island
Tshibinda
Bukavu
Bugarama Graben
Kivu
Mwenga-Kamituga
Rusizi Rift
0
50
100 km

Figure 26

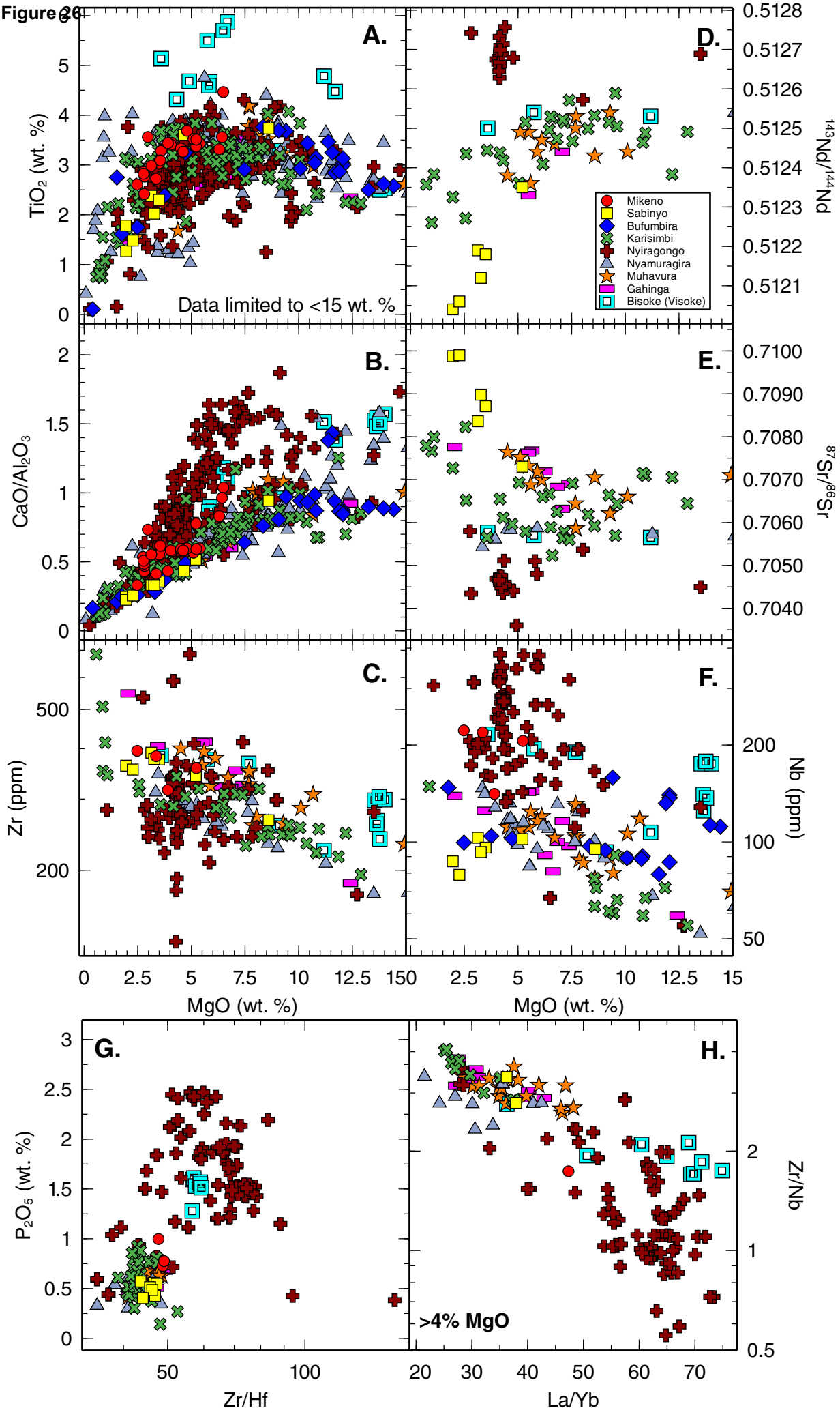
A.
B.
C.
D.
E.
F.
G.
H.
TiO2 (wt. %)
CaO/Al2O3
Zr (ppm)
143Nd/144Nd
87Sr/86Sr
Nb (ppm)
P2O5 (wt. %)
Zr/Nb
MgO (wt. %)
MgO (wt. %)
Zr/Hf
La/Yb
Data limited to <15 wt. %
>4% MgO
Mikeno
Sabinyo
Bufumbira
Karisimbi
Nyiragongo
Nyamuragira
Muhavura
Gahinga
Bisoke (Visoke)

Figure 27

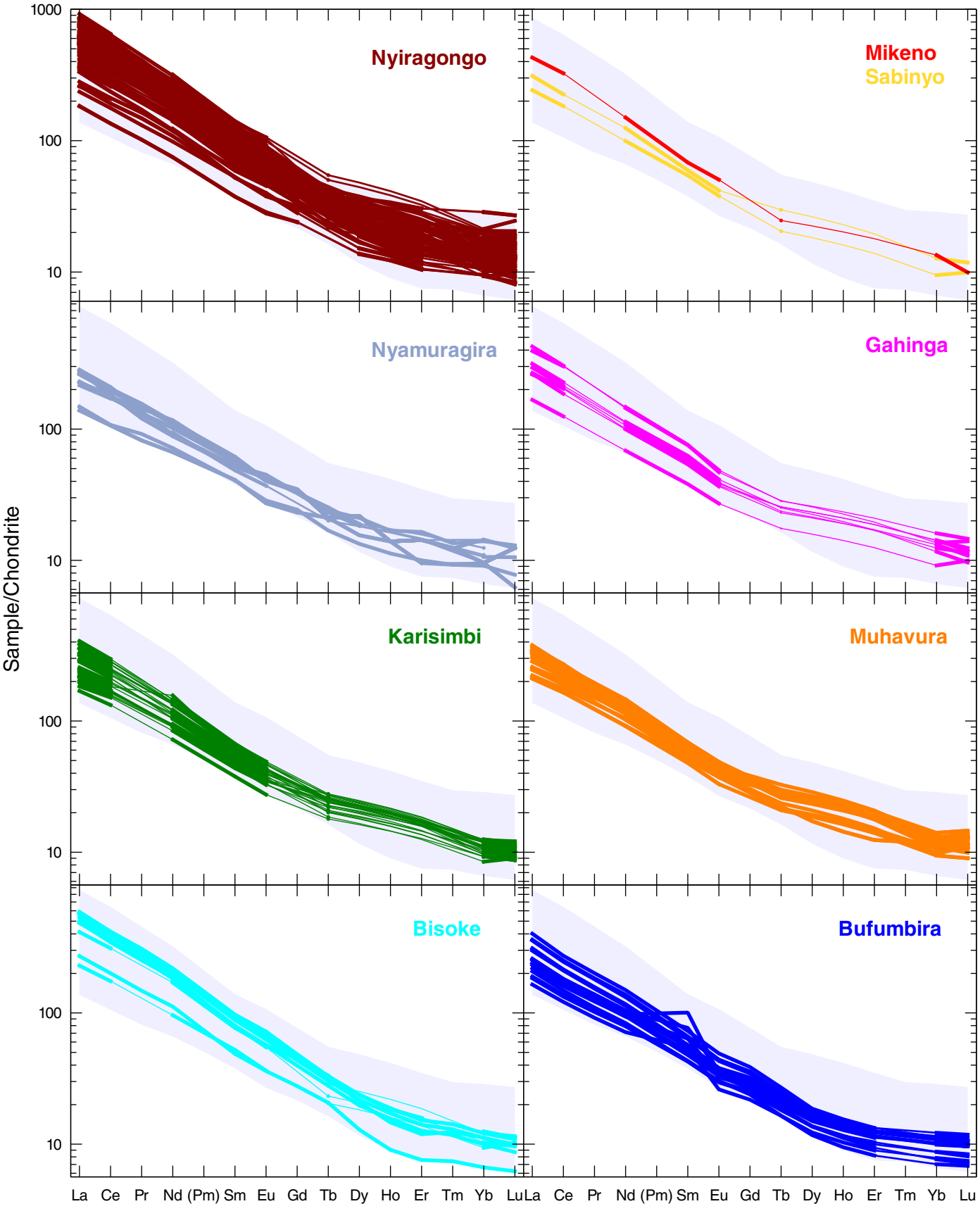
Nyiragongo
Mikeno
Sabinyo
Nyamuragira
Gahinga
Karisimbi
Muhavura
Bisoke
Bufumbira
Sample/Chondrite
1000
100
10
La Ce Pr Nd (Pm) Sm Eu Gd Tb Dy Ho Er Tm Yb Lu

Figure 28

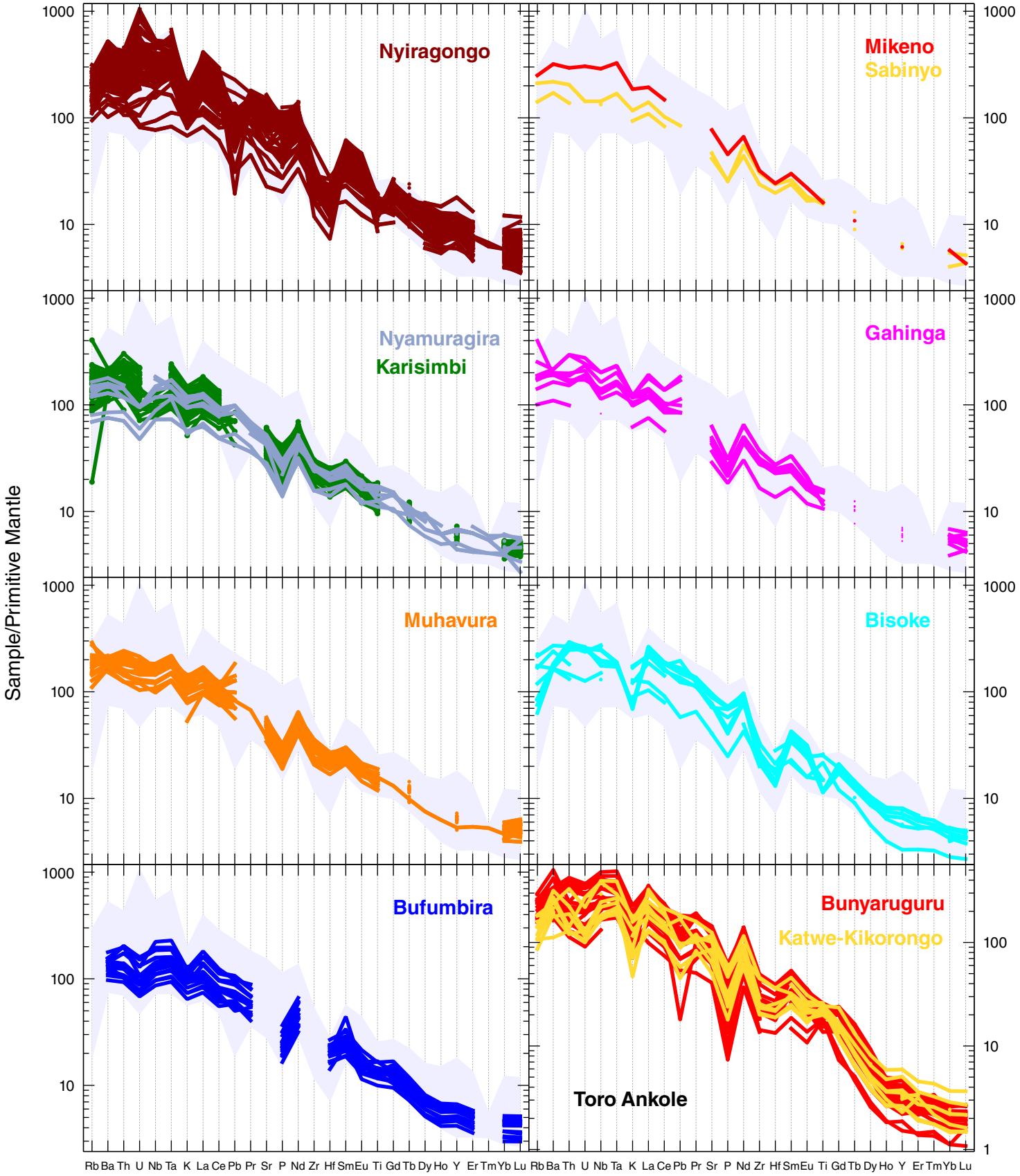
Nyiragongo
Mikeno
Sabinyo
Nyamuragira
Karisimbi
Gahinga
Muhavura
Bisoke
Bufumbira
Bunyaruguru
Katwe-Kikorongo
Toro Ankole
Sample/Primitive Mantle
1000
100
10
1
Rb Ba Th U Nb Ta K La Ce Pb Pr Sr P Nd Zr Hf Sm Eu Ti Gd Tb Dy Ho Y Er Tm Yb Lu

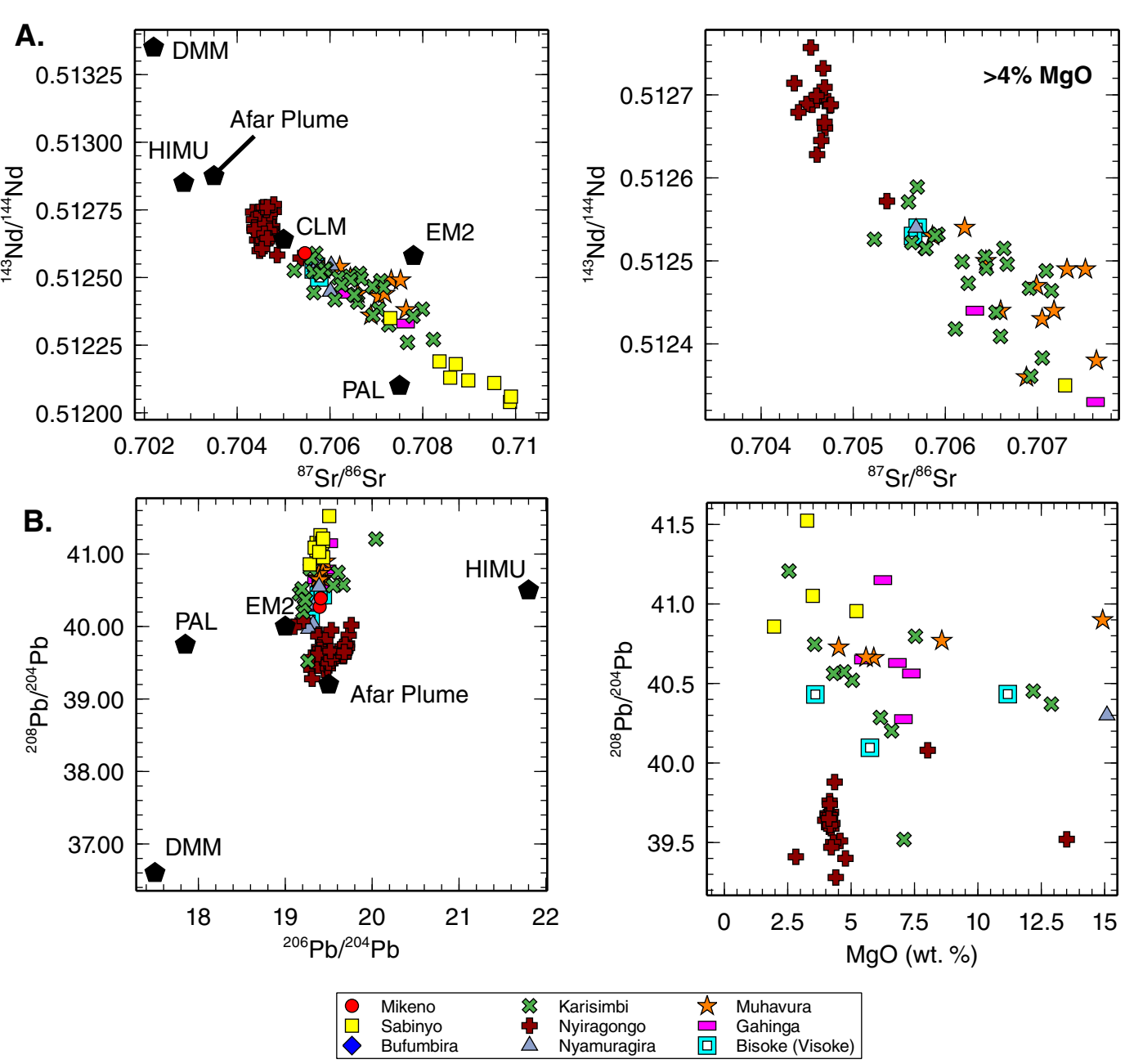
A.
DMM
Afar Plume
HIMU
CLM
EM2
PAL
0.51325
0.51300
0.51275
0.51250
0.51225
0.51200
143Nd/144Nd
0.702
0.704
0.706
0.708
0.71
87Sr/86Sr
>4% MgO
0.5127
0.5126
0.5125
0.5124
0.704
0.705
0.706
0.707
87Sr/86Sr
B.
HIMU
EM2
PAL
Afar Plume
DMM
41.00
40.00
39.00
38.00
37.00
208Pb/204Pb
18
19
20
21
22
206Pb/204Pb
41.5
41.0
40.5
40.0
39.5
208Pb/204Pb
0
2.5
5
7.5
10
12.5
15
MgO (wt. %)
Mikeno
Sabinyo
Bufumbira
Karisimbi
Nyiragongo
Nyamuragira
Muhavura
Gahinga
Bisoke (Visoke)

Table 2

Time Window	Name	Characteristics in this Region
20 – 16 Ma	The Samburu Phase	Large volume basaltic flows and shield development in the Kenya Rift, extending southwards to the margin of the Tanzania craton. In the cratonic regions surrounding the Turkana Depression, this phase manifested as alkaline volcanoes. Activity is recorded in Nyanza Rift and at Kivu in the Western Branch of the East African Rift.
16 – 12 Ma	The Flood Phonolite Phase	Widespread silicic lavas that erupted in the same regions as the prior Samburu Phase. Magmatic activity expanded further southward within the Eastern Branch of the East African Rift.
12 – 9 Ma	Mid-Miocene Resurgence Phase	Primarily manifests in this region within the Western Branch of the East African Rift. Largely basaltic flows seen in the Kivu area. Smaller-scale silicic lavas continued within the Eastern Branch.
9 – 4 Ma	Early Rift Development Phase	Explosive silicic activity in the evolving rift dominates this phase of magmatism. A large volume of basaltic material is also erupted in the region in addition to the initiation of Mt. Kenya. This phase represents the first activity in northern Tanzania.
4 – 0.5 Ma	The Stratoid Phase	In the Eastern Branch, this phase manifests as thick flows of basalts and trachytes erupting into developing rift basins. In the Western Branch, magmatism within the Virunga province commences.
0.5 Ma – Present	The Axial Phase	In more developed portions of the Eastern Branch, rift grabens and focused axial magmatism dominates the system. Elsewhere (including the Western Branch), alkaline central volcanoes dominate the system.

Table 2: Summary of magmatic events presented in this contribution. The characteristics of these events as described relate only to how these events manifest within the craton-influenced region of the East African Rift System. For details of these same Phases and their impact on the Mobile Belt, please see Part II of the synthesis series (Rooney 2020a).

Table 1

Magma Type	Characteristics	Origin
I – Incompatible element depleted family of magmas	Extreme depletions in most elements forming a relatively flat incompatible trace element normalized pattern. Subtype Ia exhibits positive anomalies in LILE (e.g. Ba).	Associated with Eocene and Oligocene Flood basalts and remains of uncertain origin.
II – OIB Family of magmas	Exhibits a typical OIB-like pattern in a primitive mantle normalized diagram. Type IIa extend to MgO-rich compositions and are less silica undersaturated. Type IIb have lower SiO_2 and elevated CaO and incompatible trace elements	Origin of Type IIa is controversial and may be associated with material within the Afar plume, lithospheric material metasomatized by the plume, or delaminated. Type IIb are likely derived from melting of lithospheric mantle metasomses.
III – The Moderate Family of Magmas	Typified by a distinctive Ba peak, a U-Th trough, and a Nb-Ta peak. The slope of the REE are controlled by the depth and degree of melting.	The most common magma type within the East African Rift and is interpreted to be a melt of a plume-influenced upper mantle.
IV – Intermediate Composition	Typified by a pattern that is a simple mix of Type II and Type III magma	Contamination of a Type III magma as it passes through the lithosphere and either assimilates a metasome or mixes with a Type II melt.
V – Potassic Metasomes	Typified by a relatively flat pattern in the most incompatible trace elements within the primitive mantle normalized figure, with small negative anomalies in U and K, and a mild depletion in Zr-Hf.	Melts derived from a phlogopite-bearing lithospheric mantle metasome. Well-developed within the Virunga Province in the Western Branch.
VI – Depleted Source	Typified by extreme depletion in the most incompatible trace elements that resemble MORB, but with unusual positive anomalies in LILE	Uncertain – may be a plume component but more work needed.

Table 1: Classification of magma types erupting in the East African Rift. This classification adds to that presented in Rooney (2017) and is presented in more detail in Part V of the synthesis series. These magma types are predominantly identified on the basis of commonalities in patterns in primitive mantle normalized incompatible trace element diagrams. Other magma groups may emerge as further work is undertaken in the region and this list should therefore be viewed as preliminary and subject to addition in the future.